Synchronization and Coding in Wireless Communication Systems

A DISSERTATION

SUBMITTED TO THE FACULTY OF THE GRADUATE SCHOOL

OF THE UNIVERSITY OF MINNESOTA

BY

Te-Lung Kung

IN PARTIAL FULFILLMENT OF THE REQUIREMENTS

FOR THE DEGREE OF

Doctor of Philosophy

Professor Keshab K. Parhi, Advisor

September, 2013

Acknowledgements

First of all, I wish to thank my advisor, Professor Keshab K. Parhi, for his continuing encouragement, tremendous guidance, and financial support throughout my entire Ph.D. study at the University of Minnesota. It has been a privilege and a pleasure to work with Professor Parhi. The valuable lessons I have learnt from him will certainly be a lifetime benefit for me. If not for his enthusiasts, patience, and dedication of his precious time, this work can never be done. Therefore, I would like to deliver my greatest thankfulness to Professor Parhi, for his help and all those insightful discussions.

I would also like to thank Professor Zhi-Quan Luo, Professor Nikos D. Sidiropoulos, and Professor Paul Garrett for their support as members of my Ph.D. committee. Their comments and suggestions helped me to improve my thesis.

My thanks also go to the members of our research group. I would like to thank Dr. Aaron E. Cohen and Dr. Jian-Hung Lin for their guidance and assistance. Also, I am grateful to Yingbo Ho, Lan Luo, Bo Yuan, Meng Yang, and Yingjie Lao for their support in my Ph.D. life.

Finally, I owe an enormous debt of gratitude to my parents, Ling-Huei Kung and Pi-Chu Han, and especially my wife, Yi-Chun Chen. Without their unending support, love, and encouragement during my Ph.D. studies, I would not have been able to finish my degree. My wife the most influential and important person in my life has sacrificed so much to support me. Words cannot express how grateful I am to her. I am also grateful to the rest of my family for their support.

Dedication

To my grandmother Fang-Hua Sun, who is unable to share the joy of this accomplishment with me

Abstract

In the information age, modern communication systems and network applications have been growing rapidly to provide us with more versatile and higher bit rate services such as multimedia on demand (MOD), wireless local area network (LAN), 3G networks, and high-speed internet. In order to maintain the qualities of services, how to design a robust transceiver is a crucial issue. Symbol timing offset and channel response are two important parameters for signal reconstruction. A nonzero symbol timing offset at the receiver affects the baseband signal processing unit to process the sequence in a wrong order; therefore, errors occur during the decoding process, and the original information needs to be retransmitted.

In this thesis, two timing synchronization and channel estimation methods are first proposed for single-input training-sequence-based wireless communication systems. One is the frequency-domain approach, and the other is the time-domain approach. Then, we extend the time-domain approach to solve the same problem in communication systems with multiple transmit antennas. After these two synchronization methods are discussed, two variable transmission rate (VTR) orthogonal frequency division multiplexing (OFDM) based communication systems using network source coding are presented.

First, a new semiblind frequency-domain timing synchronization and channel estimation scheme based on unit vectors is proposed. Compared to conventional methods, the proposed approach has excellent timing synchronization performance under several channel models at signal-to-noise ratio (SNR) smaller than 6dB. In addition, for a low-density parity-check (LDPC) coded single-input single-output (SISO) OFDM-based communication system, our proposed approach has better bit-error-rate (BER) performance than conventional approaches for SNR varying from 5dB to 8dB.

Second, a novel joint timing synchronization and channel estimation algorithm for wireless communication systems based on the time-domain training sequence arrangement is proposed. From the simulation results, the proposed approach has excellent timing synchronization performance under several channel models at low SNR which is smaller than 1dB. Moreover, for an LDPC coded 1x2 single-input multiple-output OFDM-based communication system with maximum ratio combining, a comparison BER of less than 10^{-5} can be achieved using our proposed approach when SNR exceeds 1dB.

Third, a joint timing synchronization and channel estimation scheme for communication systems with multiple transmit antennas based on a well-designed training sequence arrangement is proposed. Simulation results show that the proposed approach has excellent timing synchronization performance under several channel models at SNR smaller than 1dB. Furthermore, the proposed approach has excellent channel estimation performance in 2×2 and 3×3 multiple-input multiple-output systems.

Finally, two VTR OFDM-based communication systems that exploit network source coding schemes are proposed, and the system performance characteristics of these two proposed VTR OFDM-based communication systems are evaluated. The proposed 3-stage encoder in the VTR SISO OFDM-based communication system provides three different coding rates from 0.5 to 0.8. As for the proposed VTR multi-band OFDM-based communication system, two correlated sources are encoded by different coding rates from 0.25 to 0.5. Furthermore, compared with a traditional uncoded OFDM system, the proposed VTR OFDM-based communication systems have at least 1 to 4 dB gain in SNR to achieve the same symbol error rate in an additive white Gaussian noise channel.

Contents

List of Tables

List of Figures

Chapter 1

Introduction

1.1 Introduction

The rapid growth of communication systems for video, voice, and cellular telephone has led to a significant increase in demand for mobile multimedia. These multimedia services will require high-data-rate transmission over broadband radio channels. For the fifth-generation (5G) telecom technologies, we expect that a high-definition video file should be completely downloaded within 1 or 2 seconds [1]. Due to the limited spectral resource, it is impractical to increase the bandwidth for data transmission. In case of wired networks, high-data-rate services are limited by the wired channel characteristic; however, high-data-rate transmission in wireless communication networks require additional technical considerations [2, 3, 4]. Moreover, further development of the advanced network technologies is constrained by the amount of information that

can be sent through the corresponding networks.

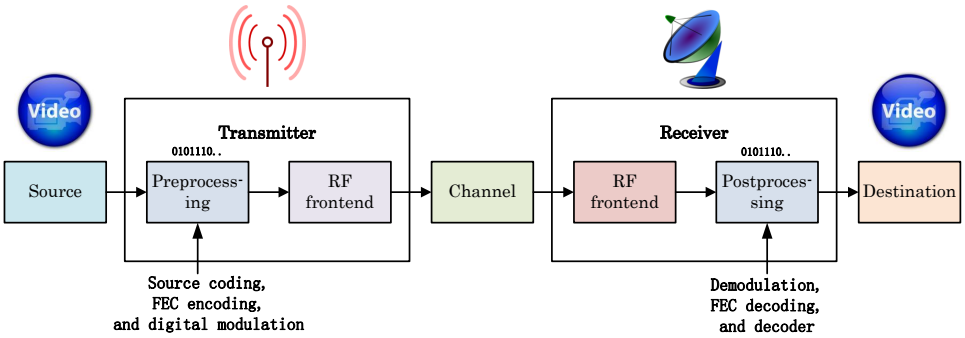

Figure 1.1: A simple block diagram of modern communication systems.

In Fig. 1.1, any simplified communication system consists of five parts: the source, the transmitter, the noisy channel, the receiver, and the destination. The preprocessing unit at the transmitter converts the source file to a sequence of bits via source coding schemes [5, 6], protects the digital data using channel coding schemes [7, 8, 9], and efficiently utilizes the spectral resources based on different modulation schemes [2]. Moreover, the decoding and demodulation processes are executed in the postprocessing unit at the receiver. The overall system performance depends on the channel characteristics. Channel estimation plays a crucial role in providing the channel information to the soft decoder and compensating the signal before the demodulation process [10]. In addition, in order to reconstruct the original file without any loss, timing offset is also an important parameter in the postprocessing unit. Without the knowledge of

timing offset and channel information at the receiver, the system will have poor performance during the entire data transmission. If there exists a nonzero timing offset at the receiver, the postprocessing unit decodes the sequence in a wrong order. Therefore, errors occur during the decoding process, and the original file can not be retrieved at the destination.

The rest of the chapter is organized as follows. Orthogonal frequency division multiplexing (OFDM) based communication systems are reviewed in Section 1.2. In Section 1.3, effects of symbol timing offset in OFDM systems are discussed. Network source coding is introduced in Section 1.4. Our contributions are summarized in Section 1.5. Finally, outlines of this thesis are listed in Section 1.6.

1.2 Orthogonal Frequency Division Multiplexing Systems

High-data-rate wireless communications are limited not only by noise but also by the inter-symbol interference (ISI) from the dispersion of the wireless communications channel. OFDM systems as shown in Fig. 1.2 have been adopted in various wireless communications applications such as digital video and audio broadcasting [11, 12], digital subscriber line [13, 14], wireless networks [15, 16, 17], and the fourth-generation mobile network [18]. Fig. 1.2 shows a traditional coded OFDM system architecture, where

$$\begin{aligned} y_l[n] &= x_l[n] * h_l[n] + w_l[n] \\ &= \sum_{m=0}^{\infty} h_l[m] x_l[n-m] + w_l[n], \end{aligned} \tag{1.1}$$

$y_l[n]$ is the lth received symbol, $x_l[n]$ is the lth transmitted symbol, $h_l[n]$ is the channel impulse response (CIR), and $w_l[n]$ is the complex additive white Gaussian noise (AWGN).

Due to the high spectrum efficiency and robustness against the frequency selective fading channels, OFDM is a prominent technique suitable for high-data-rate transmission in multicarrier communication systems [2, 4, 11, 19, 20, 21, 22, 23, 24, 25, 26]. In OFDM systems, a wideband channel is converted to a set of narrowband subchannels, and the data is transmitted using some subchannels. If the bandwidth of each subchannel is smaller than the coherent bandwidth in fading channels, the channel effect can be easily compensated by a one-tap equalizer in the frequency-domain. In addition, the postfix or prefix in each OFDM symbol is used to eliminate the ISI between OFDM symbols. In general, the duration of postfix or prefix should be greater than the maximum delay spread in the multipath fading channel. In Fig. 1.2, in order to avoid the direct current (DC) effect and reduce the power on out-of-band subcarriers, virtual carrier arrangement is introduced in OFDM systems. Furthermore, the windowing block at the transmitter is utilized to mitigate the interference to the adjacent bands.

Multi-band OFDM (MB-OFDM) systems group all subchannels into multiple subbands, and then transmit data in different subbands simultaneously [27, 28]. Hence, multi-band signal processing techniques can be viewed as either a multiple access scheme that allocates subbands to transmit different users' data at the same time or an approach to employ the frequency diversities for data transmission in order to improve the system

performance.

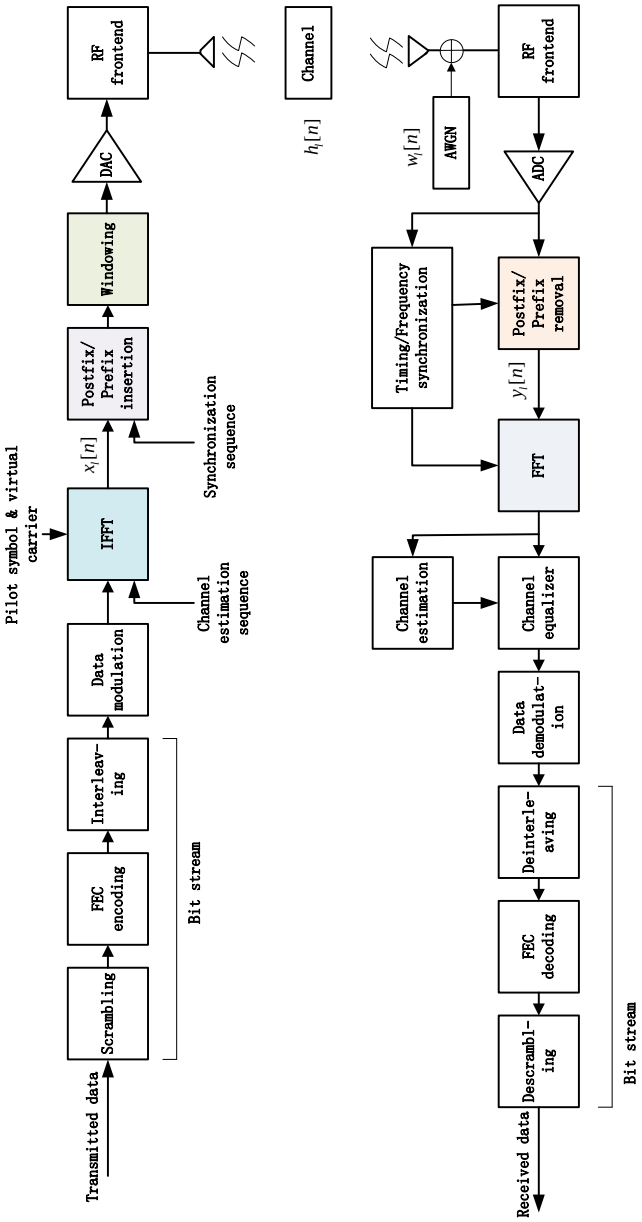

Figure 1.2: Block diagram of a traditional coded OFDM transceiver.

1.3 Effects of Symbol Timing Offset in OFDM Systems

In OFDM systems, synchronization errors can destroy the orthogonality among the subcarriers and result in performance degradation [2, 4, 22, 24, 26, 29, 30]. Thus, timing synchronization in OFDM systems is much more challenging due to the increase in the amount of inter-carrier interference (ICI) and ISI. Although the soft decoders employing error correction code can improve the system performance at low signal-to-noise ratio (SNR), perfect timing synchronization is necessary for the decoder to operate correctly. Therefore, in order to improve the system performance, it is important to find the actual delayed timing in multipath fading channels at the receiver. Depending on the location of the estimated starting position of OFDM symbol, effects of symbol timing offset (STO) are different. Four different cases are shown in Fig. 1.3.

First, let ε denote the STO. From Equation (1.1), the received signal under the presence of STO can be expressed as

$$\begin{aligned} y_l[n] &= IDFT\{Y_l[k]\} = IDFT\{H_l[k]X_l[k] + W_l[k]\} \\ &= \frac{1}{N}\sum_{k=0}^{N-1} H_l[k]X_l[k]e^{\frac{j2\pi k(n+\varepsilon)}{N}} + w_l[n], \end{aligned} \tag{1.2}$$

where N represents the number of subcarriers in the OFDM system, $w_l[n] = IDFT\{W_l[k]\}$, and $IDFT\{\cdot\}$ means the operation of inverse discrete Fourier transform.

Consider $h_l[n] = \sum_{k=0}^{\tau_{max}-1} \alpha(k)\delta[n-k]$ in Equation (1.2), where τ_{max} is the maximum delay spread in the channel and $\alpha(k)$ is the kth tap CIR. Furthermore, let us focus on the interference from $x_l[n]$, $x_{l-1}[n]$, and $x_{l+1}[n]$, and assume perfect channel information

is available at the receiver. In addition, assume there is no AWGN in Equation (1.2). In Fig. 1.3(a), Case 1 represents the case when the estimated starting position of the lth OFDM symbol coincides with the exact timing offset. Therefore, the orthogonality among subcarriers is preserved. In this case, there is neither ISI nor ICI.

In Case 2, the estimated starting position of the lth OFDM symbol is after the exact point which indicates that the estimated STO is later than the actual timing offset. For this case, the received signal within the fast Fourier transform (FFT) interval consists of two parts,

$$y_l[n] = \begin{cases} x_l[n+\varepsilon] \ \forall n, \ 0 \leq n \leq N-1-\varepsilon \\ \\ x_{l+1}[n+\varepsilon-N_{CP}] \ \forall n, \ N-\varepsilon \leq n \leq N-1, \end{cases} \tag{1.3}$$

where N_{CP} is the length of cyclic prefix. Then, taking the FFT of Equation (1.3), we

have

$$
\begin{aligned}
Y_l[k] &= FFT\{y_l[n]\} \\
&= \sum_{n=0}^{N-1-\varepsilon} x_l[n+\varepsilon] e^{\frac{-j2\pi nk}{N}} + \sum_{n=N-\varepsilon}^{N-1} x_{l+1}[n+\varepsilon-N_{CP}] e^{\frac{-j2\pi nk}{N}} \\
&= \sum_{n=0}^{N-1-\varepsilon} (\frac{1}{N} \sum_{p=0}^{N-1} X_l[p] e^{\frac{j2\pi(n+\varepsilon)p}{N}}) e^{\frac{-j2\pi nk}{N}} \\
&+ \sum_{n=N-\varepsilon}^{N-1} (\frac{1}{N} \sum_{p=0}^{N-1} X_{l+1}[p] e^{\frac{j2\pi(n+\varepsilon-N_{CP})p}{N}}) e^{\frac{-j2\pi nk}{N}} \\
&= \frac{1}{N} \sum_{p=0}^{N-1} X_l[p] e^{\frac{j2\pi p\varepsilon}{N}} \sum_{n=0}^{N-1-\varepsilon} e^{\frac{j2\pi(p-k)n}{N}} \\
&+ \frac{1}{N} \sum_{p=0}^{N-1} X_{l+1}[p] e^{\frac{j2\pi p(\varepsilon-N_{CP})}{N}} \sum_{n=N-\varepsilon}^{N-1} e^{\frac{j2\pi(p-k)n}{N}} \\
&= \frac{N-\varepsilon}{N} X_l[k] e^{\frac{j2\pi k\varepsilon}{N}} + \underbrace{\frac{1}{N} \sum_{p=0, p\neq k}^{N-1} X_l[p] e^{\frac{j2\pi p\varepsilon}{N}} \sum_{n=0}^{N-1-\varepsilon} e^{\frac{j2\pi(p-k)n}{N}}}_{\textbf{ICI}} \\
&+ \underbrace{\frac{1}{N} \sum_{p=0}^{N-1} X_{l+1}[p] e^{\frac{j2\pi p(\varepsilon-N_{CP})}{N}} \sum_{n=N-\varepsilon}^{N-1} e^{\frac{j2\pi(p-k)n}{N}}}_{\textbf{ISI, ICI}},
\end{aligned}
\tag{1.4}
$$

where

$$
\begin{aligned}
\sum_{n=0}^{N-1-\varepsilon} e^{\frac{j2\pi(p-k)n}{N}} &= e^{\frac{j\pi(p-k)(N-1-\varepsilon)}{N}} \times \frac{sin[(N-\varepsilon)\pi(k-p)/N]}{sin[\pi(k-p)/N]} \\
&= \begin{cases} N-\varepsilon, \ p=k \\ Nonzero, \ p\neq k, \end{cases}
\end{aligned}
\tag{1.5}
$$

and

$$\sum_{n=N-\varepsilon}^{N-1} e^{\frac{j2\pi(p-k)n}{N}} = \begin{cases} \varepsilon, \ p = k \\ Nonzero, \ p \neq k. \end{cases} \tag{1.6}$$

From Equation (1.4), both ISI and ICI occur in Case 2.

In Fig. 1.3(b), in Case 3, the estimated starting position of the lth OFDM symbol is not only before the exact timing offset but also after the end of channel response to the $(l-1)$th OFDM symbol. Consider the received signal in the frequency-domain by taking the FFT of the time-domain received samples $\{x_l[n+\varepsilon]\}$. Then, we have

$$\begin{aligned} Y_l[k] &= \sum_{n=0}^{N-1} x_l[n+\varepsilon] e^{\frac{-j2\pi nk}{N}} \\ &= \frac{1}{N} \sum_{n=0}^{N-1} \{ \sum_{p=0}^{N-1} X_l[p] e^{\frac{j2\pi(n+\varepsilon)p}{N}} \} e^{\frac{-j2\pi nk}{N}} \\ &= \frac{1}{N} \sum_{p=0}^{N-1} X_l[p] e^{\frac{j2\pi\varepsilon p}{N}} \sum_{n=0}^{N-1} e^{\frac{j2\pi(p-k)n}{N}} \\ &= X_l[k] e^{\frac{j2\pi\varepsilon k}{N}}, \end{aligned} \tag{1.7}$$

where

$$\begin{aligned} \sum_{n=0}^{N-1} e^{\frac{j2\pi(p-k)n}{N}} &= e^{\frac{j\pi(p-k)(N-1)}{N}} \times \frac{sin[\pi(k-p)]}{sin[\frac{\pi(k-p)}{N}]} \\ &= \begin{cases} N, \ k = p \\ 0, \ k \neq p. \end{cases} \end{aligned} \tag{1.8}$$

Therefore, from Equation (1.7), there exists a phase offset proportional to the STO δ and subcarrier index k in Case 3. In addition, there is neither ISI nor ICI in this case.

In Fig. 1.3(c), in Case 4, the estimated starting position of the lth OFDM symbol is before the end of channel response to the $(l-1)$th OFDM symbol. Therefore, in this case, the symbol timing is too early to avoid the ISI from the previous symbol. In addition, the orthogonality among subcarriers is also destroyed by ISI, and furthermore, ICI occurs in this case.

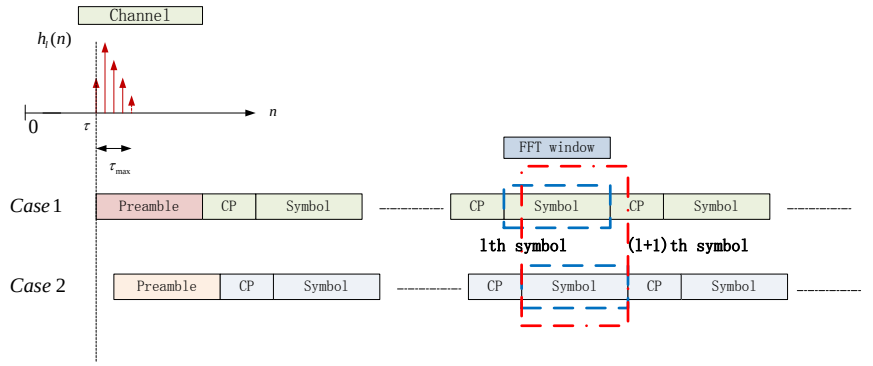

(a)

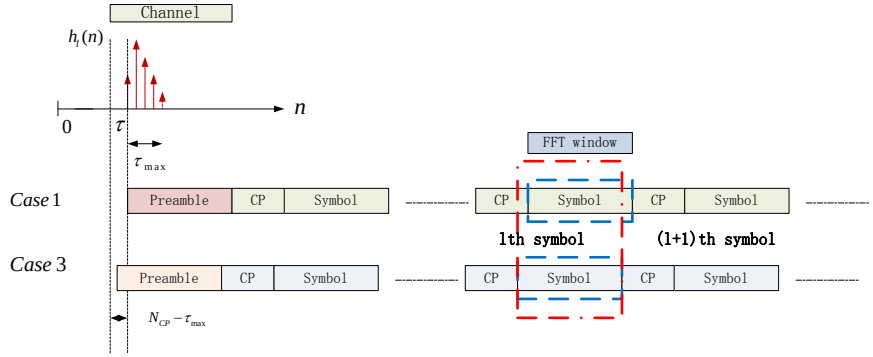

(b)

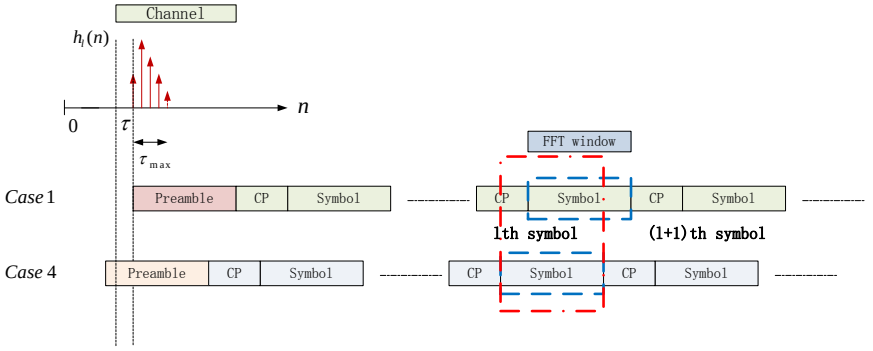

(c)

Figure 1.3: Four different cases of OFDM symbol starting point subject to the symbol timing offset.

1.4 Network Source Coding

In a wired or wireless network, where the bandwidth is strictly limited, it is imperative to use efficient data representations or source codes for optimizing network system performance [31, 32]. In order to transmit data stream over communication networks with limited bandwidth, network source coding can be used to solve this problem. Network source coding expands the data compression problem for networks beyond the point-to-point network introduced by Shannon [33]. These include networks with multiple transmitters, multiple receivers, side information, intermediate nodes, and any combination of these features. Thus, network source coding attempts to bridge the gap between point-to-point network and recent complicated network environments. Moreover, network source coding is a promising technique that provides many advantages as shown in Fig. 1.4, including source dependence, functional demands, and resource sharing [34, 35, 36, 37, 38, 39, 40, 41].

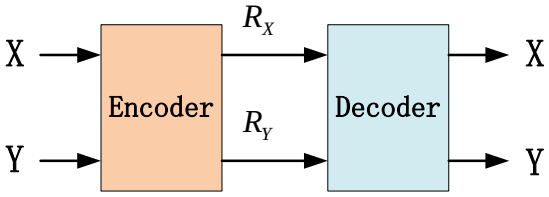

(a) Source dependence.

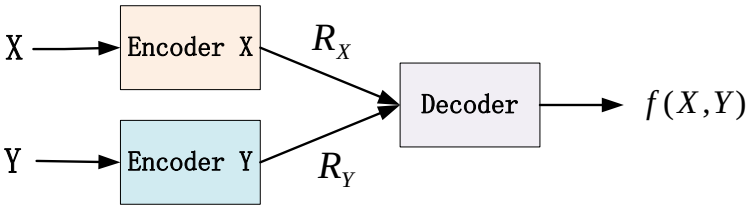

(b) Functional demands.

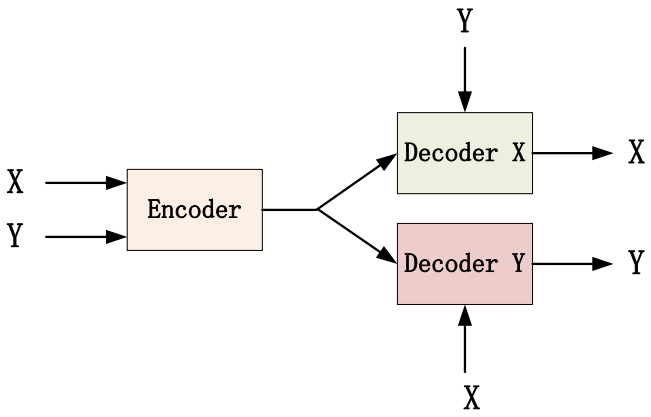

(c) Resource sharing.

Figure 1.4: Three network source coding advantages.

By utilizing network source coding, the system performance can be improved by using correlated sources. This leads to an adjustable transmission rate scheme, and the input data streams share the entire network resource during the transmission. If decoders have the information about the relation of transmitted data sources, the input data sources can be reconstructed without any loss in a noiseless channel.

In Fig. 1.5, the information X is conveyed from a source node to the destination node in different transmission rates, where W, Y, and Z are the side information, and R_i (bits/sample) is the rate of Node i. We can employ the network source coding schemes in Node 1, Node 2, and Destination Node to adjust the transmission rate in different stages. In modern communication networks, a reconfigurable transmission rate scheme is needed in order to route the packet from the source node to the destination node. Therefore, the use of network source coding schemes takes advantage of the network topology and is able to maximally compress data before the transmission.

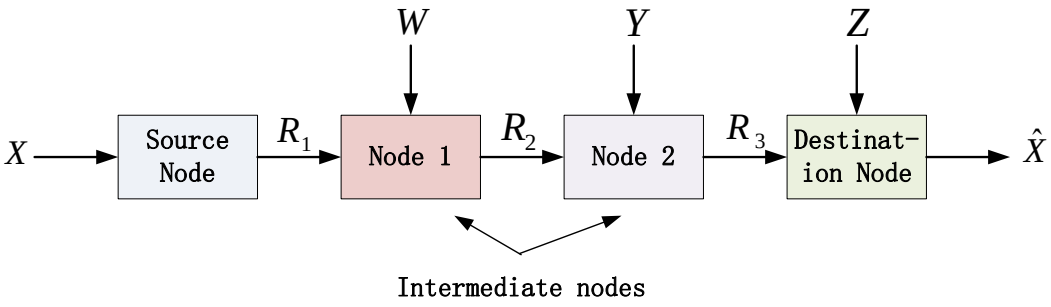

Figure 1.5: A source coding problem for a network with intermediate nodes.

1.5 Summary of Contributions

As described in Section 1.1 and Section 1.3, timing offset and channel estimate are two important parameters at the receiver in a coded OFDM system. Therefore, we focus on how to obtain better estimates of these two parameters. In this thesis, two different timing synchronization and channel estimation schemes for single-input training-sequence-based communication systems are proposed, including the frequency-domain approach and the time-domain approach. Then, we extend the time-domain approach to deal with the timing synchronization and channel estimation problem in communication systems with multiple transmit antennas. Finally, two variable transmission rate (VTR) OFDM-based communication systems using network source coding are presented.

1.5.1 Semiblind Frequency-Domain Timing Synchronization and Channel Estimation

We propose unit vectors in the high dimensional Cartesian coordinate system as the preamble, and then propose a semiblind timing synchronization and channel estimation scheme for OFDM systems [42, 43]. Due to the lack of useful information in the time-domain, a frequency-domain timing synchronization algorithm is proposed. The proposed semiblind approach consists of three stages. In the first stage, a coarse timing estimate related to the delayed timing of the path with the maximum gain in multipath fading channels is obtained. Then, a fine time adjustment algorithm is performed to find

the actual delayed timing in channels. Finally, the channel response in the frequency-domain is obtained based on the final timing estimate. Although the computational complexity in the proposed algorithm is higher than those in conventional methods, the simulation results show that the proposed approach has excellent timing synchronization performance under several channel models at SNR smaller than 6dB. In addition, for a low-density parity-check (LDPC) coded single-input single-output (SISO) OFDM system, our proposed approach has better bit-error-rate (BER) performance than conventional approaches for SNR varying from 5dB to 8dB.

1.5.2 Optimized Joint Timing Synchronization and Channel Estimation

This work addresses training-sequence-based joint timing synchronization and channel estimation for single-input OFDM systems [44]. The proposed approach consists of three stages. First, a coarse timing estimate is obtained. Then, an advanced timing, relative timing indices, and CIR estimates are obtained by maximum-likelihood (ML) estimation based on a sliding observation vector (SOV). Finally, the fine time adjustment based on the minimum mean squared error (MMSE) criterion is performed. Simulation results show that the proposed approach has excellent timing synchronization performance under several channel models at low SNR which is smaller than 1dB. Moreover, for an LDPC coded 1x2 single-input multiple-output (SIMO) OFDM system with maximum ratio combining (MRC), a comparison BER of less than 10^{-5} can be achieved using our

proposed approach when SNR exceeds 1dB.

1.5.3 Optimized Joint Timing Synchronization and Channel Estimation with Multiple Transmit Antennas

A joint timing synchronization and channel estimation scheme for communication systems with multiple transmit antennas based on a well-designed training sequence arrangement is proposed [45]. In addition, a generalized ML channel estimation scheme is presented, and this one-shot scheme is applied to obtain all CIRs from different transmit antennas. The proposed approach consists of three stages at each receive antenna. First, coarse timing and frequency estimates are obtained. Then, an advanced timing, relative timing indices, and the corresponding CIR estimates at the second stage are obtained using the generalized ML estimation based on the SOV. Finally, the fine time adjustment based on the MMSE criterion is performed. From the simulation results, the proposed approach has excellent timing synchronization performance under several channel models at SNR smaller than 1dB. Furthermore, the proposed approach has excellent channel estimation performance in 2×2 and 3×3 multiple-input multiple-output (MIMO) systems.

1.5.4 Variable Transmission Rate Communication Systems via Network Source Coding

Studies related to the network source coding have addressed rate-distortion analysis in both noiseless and noisy channels. However, to the best of the author's knowledge, no prior work has studied network source coding in the context of OFDM systems. In addition, the system performance using network source coding schemes also remains unknown. In this work [46], two variable transmission rate (VTR) OFDM-based communication systems that exploit network source coding schemes are proposed, and the system performance characteristics of these two proposed VTR-OFDM systems are evaluated. For the proposed VTR SISO-OFDM system, we employ the concept of a network with intermediate nodes to develop a 3-stage encoder/decoder, and the proposed encoder provides three different coding rates from 0.5 to 0.8. As for the proposed VTR MB-OFDM system, two correlated sources are simultaneously transmitted using the multiterminal source coding schemes, and two sources are encoded by different coding rates from 0.25 to 0.5. Compared with a traditional uncoded OFDM system, the proposed VTR-OFDM systems have at least 1 to 4 dB gain in SNR to achieve the same symbol error rate (SER) in an AWGN channel.

1.6 Thesis Outline

This thesis is organized as follows. Chapter 2 introduces a semiblind timing synchronization and channel estimation method for single-input communication systems. In this chapter, unit vectors in the high dimensional Cartesian coordinate system are utilized to be the preamble, and a frequency-domain timing synchronization algorithm is proposed.

Chapter 3 addresses joint timing synchronization and channel estimation for single-input training-sequence-based communication systems. In this chapter, a time-domain joint timing synchronization and channel estimation algorithm is proposed. The proposed approach consists of three stages: coarse timing synchronization, joint timing synchronization and channel estimation, and fine time adjustment.

Chapter 4 proposes a joint timing synchronization and channel estimation scheme for communication systems with multiple transmit antennas based on a well-designed training sequence arrangement. In this chapter, the proposed approach can be applied to either multiple-input single-output (MISO) communication systems or MIMO communication systems.

Chapter 5 presents two VTR OFDM-based communication systems by utilizing network source coding schemes. First, two VTR-OFDM systems that exploit different network source coding strategies are proposed, and the system performance characteristics of these two proposed VTR OFDM-based communication systems are evaluated.

Finally, Chapter 6 summarizes of the contributions of the entire thesis and also

provides future research directions.

Chapter 2

Semiblind Frequency-Domain Timing Synchronization and Channel Estimation

2.1 Introduction

Various synchronization techniques for OFDM systems have been developed using well-designed preambles [42, 44, 47, 48, 49, 50, 51, 52, 53, 54]. Although accurate timing estimation can be achieved, the bandwidth efficiency is also inevitably reduced. In order to reduce the waste of bandwidth, non-data aided synchronization algorithms based on the cyclic prefix have been proposed [55, 56, 57, 58, 59]. However, in some multipath fading channels with non-line-of-sight (NLOS) propagation at low SNR, both data-aided

and non-data-aided synchronization methods frequently lead to the delayed timing in channels where the delayed path has larger gain than the first path. In this case, the resulting ICI and ISI would degrade the system performance. Also, the channel coding would not perform well because of the synchronization errors. Therefore, in order to solve this problem, a fine time adjustment is needed to modify the frequently delayed timing to the actual delayed timing in channels. In [55], the proposed timing estimator performs well only for the AWGN channels. While the system operates in the multipath fading channels, the proposed algorithm exhibits significantly large fluctuation in the estimated timing offset. In [56], the proposed joint symbol timing and frequency offset estimator which assumes channel time-variation statistics are known has poor timing synchronization performance in the multipath fading channel with an exponential distribution. In [57], the proposed joint symbol timing and frequency offset estimator based on the ML criterion achieves better timing synchronization performance in the multipath fading channels with line-of-sight (LOS) propagation when SNR exceeds 30dB. In [58], the modified blind timing synchronization method achieves an unbiased estimator over the frequency selective fading channels when SNR is greater than 20dB. In [59], based on the least-squares approach, the proposed joint carrier frequency offset (CFO) and symbol timing estimator exhibits a floor effect on timing synchronization performance in the multipath fading channel with an exponential decaying power profile. It is noted that ML is equivalent to least squares in the presence of Gaussian noise [60]. In [44], a

well-designed time-domain training sequence is utilized to perform joint timing synchronization and channel estimation. Although the proposed timing estimator has excellent performance at low SNR [44], the power consumption of the proposed preamble is still too large to be adopted in some low-power wireless applications.

For wireless implantable medical devices, low-power consumption is necessary in order to prolong the battery operating time. This chapter presents a semiblind timing synchronization and channel estimation algorithm based on unit vectors, and demonstrates that this algorithm is suitable for multipath fading channels with both LOS and NLOS propagation. Therefore, the proposed preamble is suitable for any low-power wireless implantable medical device. In addition, we utilize only one nonzero sample in the training sequence to perform timing synchronization. Compared with the existing methods [42, 47, 48, 49, 50, 51, 52, 53], the number of nonzero elements in the proposed training sequence is the lowest. In this chapter, we first obtain a coarse timing estimate using the cross-correlation function outputs in the frequency-domain. Then, a fine time adjustment algorithm based on these outputs is applied. Finally, the channel response in the frequency-domain is obtained. Simulation results are represented to verify the effectiveness of our proposed algorithm. This chapter is based on our publications in [42, 43]

This chapter is organized as follows. Section 2.2 describes the system and the problem. In Section 2.3, the proposed semiblind frequency-domain timing synchronization

and channel estimation algorithm is presented. Simulation results are provided in Section 2.4. Finally, Section 2.5 concludes this chapter.

2.2 Problem Statement

2.2.1 System Description

In this subsection, we consider a training-sequence-based SISO OFDM system as shown in Fig. 2.1. The training sequence is an unit vector in an N-dimensional Cartesian coordinate system, where N represents the number of subcarriers in the OFDM system. Let $\mathbf{p}^T = [0 \ \cdots \ 0 \ 1 \ 0 \ \cdots \ 0] = \{p(n), \ \forall n \in \Omega_1\}$ denote the the proposed training sequence, where $\Omega_1 = \{0, 1, \cdots, N-1\}$, $p(n) = \delta(n-c)$, $c \in \{0, 1, \cdots, N-1\}$, the length of $\mathbf{p}^T$ is N, and the power of $\mathbf{p}^T$ is equal to $1/N$. Consider the transmitted packet $\mathbf{s}^T = [\mathbf{p}^T \ \mathbf{x}^T] = \{s(n), \forall n \in \Omega_2\}$, where $\mathbf{x}^T$ consists of ℓ OFDM symbols, the length of $\mathbf{x}^T$ is $\ell \cdot (N + N_{CP})$, N_{CP} denotes the length of cyclic prefix, ℓ is a positive integer, and $\Omega_2 = \{0, 1, \cdots, \ell \cdot (N + N_{CP}) + N - 1\}$. Assume cyclic prefix in each OFDM symbol is longer than the maximum delay spread of the channel, and the path delays in the channels are sample-spaced. Therefore, the received signal at the receiver can be expressed as

$$r(n) = e^{\frac{j2\pi\epsilon n}{N}} \sum_{k=0}^{K-1} h(k)s(n-\tau-k) + w(n), \tag{2.1}$$

where ϵ is the CFO normalized to the OFDM subcarrier spacing, τ is the timing offset, $h(k)$ represents the kth tap CIR, K is the number of taps in the channel, and $w(n)$ is a

complex AWGN sample. After coarse frequency synchronization, the CFO-compensated received signal at the receiver is

$$\begin{aligned} \hat{r}(n) &= r(n) \cdot e^{\frac{-j2\pi(\epsilon+\Delta\epsilon)n}{N}} \\ &= e^{\frac{-j2\pi(\Delta\epsilon n)}{N}} \sum_{k=0}^{K-1} h(k)s(n-\tau-k) + \hat{w}(n), \end{aligned} \tag{2.2}$$

where $\Delta\epsilon$ denotes the residual CFO and $\hat{w}(n) = w(n)e^{\frac{-j2\pi(\epsilon+\Delta\epsilon)n}{N}}$.

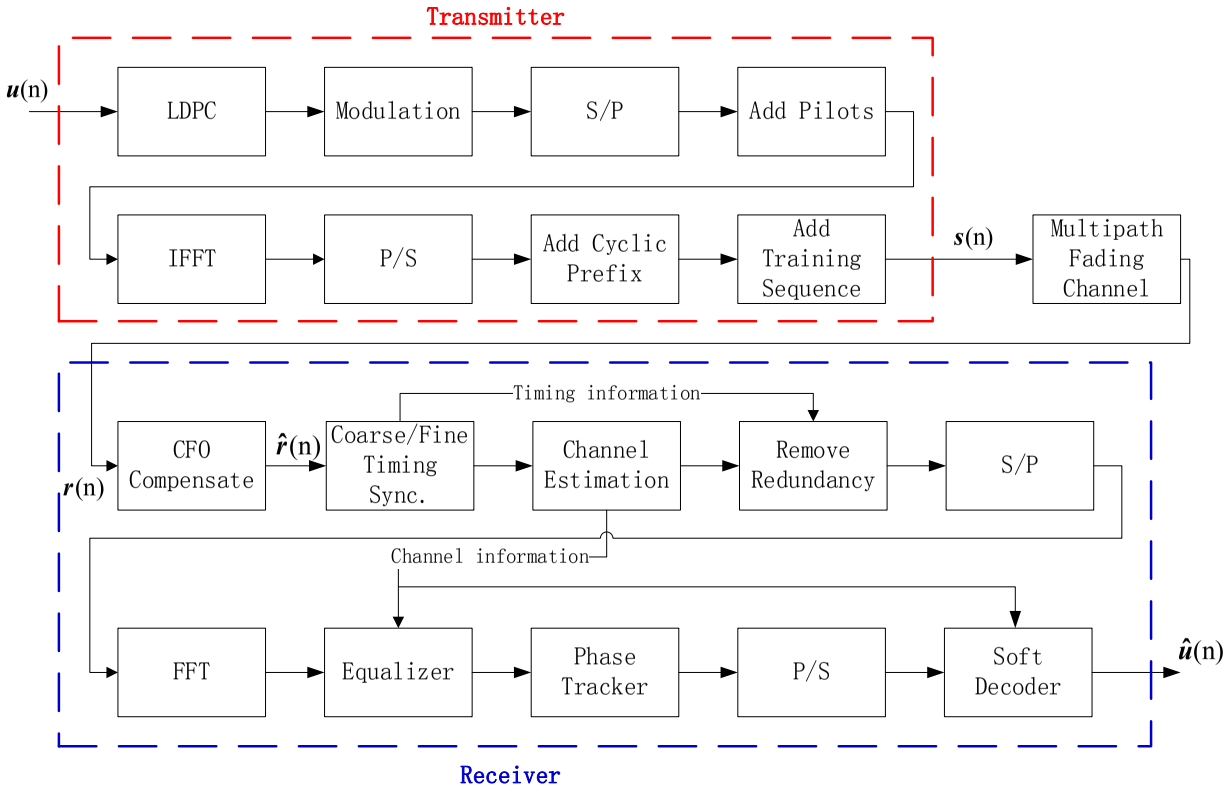

Figure 2.1: The training-sequence-based single-input single-output OFDM system architecture.

2.2.2 Timing Synchronization in The Time-Domain

For any training-sequence-based communication system, timing synchronization can be easily achieved based on a well-designed timing metric in the time-domain. However, in this chapter, the proposed training sequence is a delta function with unit amplitude. Thus, if we perform timing synchronization in the time-domain, the cross-correlation function outputs $M(d)$ can be expressed as follows:

$$\begin{aligned} \hat{\tau} &= \arg\max_{d\in\Omega_3}\{|M(d)|\} \\ M(d) &= \sum_{n=0}^{N-1}\frac{\hat{r}(n+d)\cdot p(n)}{N} = \frac{\hat{r}(c+d)}{N}, \end{aligned} \tag{2.3}$$

where $\hat{\tau}$ is the estimated timing offset, $|\hat{r}(n)|$ represents the absolute value of $\hat{r}(n)$, Ω_3 is the observation interval, $\Omega_3 = \{0, 1, \ldots, D-1\}$, and D is the length of observation interval. If there is no residual CFO in Equation (2.2), we rewrite $|M(d)|$ in Equation (2.3) as follows:

$$\begin{aligned} & N\cdot|M(d)| \in \\ & \{|\hat{w}(c)|, |\hat{w}(c+1)|, \cdots, |\hat{w}(c+\tau-1)|, \\ & |h(0)+\hat{w}(c+\tau)|, \cdots, |h(K-1)+\hat{w}(c+\tau+K-1)|, \\ & |\hat{w}(c+\tau+K)|, \cdots, |\hat{w}(\tau+N-1)|, \\ & |h(0)x(0)+\hat{w}(N+\tau)|, \\ & |\sum_{k=0}^{1}h(k)x(1-k)+\hat{w}(N+1+\tau)|, \cdots\}. \end{aligned} \tag{2.4}$$

From Equation (2.4), it is possible that all cross-correlation function outputs related to the channel, $|h(k)+\hat{w}(c+\tau+k)|$, are smaller than other elements in $N\cdot|M(d)|$ at low

SNR, where $k \in \{0, 1, \cdots, K-1\}$. Thus, we will have wrong timing estimates at low SNR as shown in Fig. 2.2. In Fig. 2.2, a delayed timing offset (τ) is 65, and c is 31. Then, a maximum cross-correlation function output near the 96th sample is expected. However, in Fig. 2.2, a wrong timing estimate is obtained when SNR is -5dB.

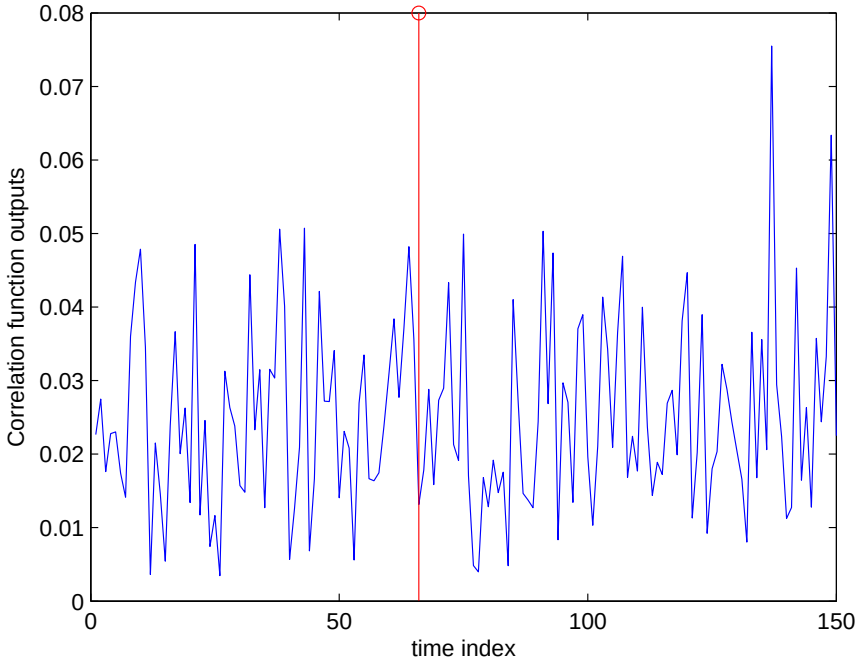

Figure 2.2: Cross-correlation function outputs based on Equation (2.3), where SNR = -5dB, timing offset (τ) is 65, $N = 64$, $N_{CP} = 16$, $\ell = 17$, $c = 31$, $K = 6$, and the red-line indicates the correct delayed timing in the channel.

2.3 The Proposed Approach

2.3.1 Coarse Timing Synchronization

In order to achieve better timing synchronization performance at low SNR, from Section 2.2.2, a synchronization method in the time-domain is not suitable for the proposed preamble. However, much more information in the frequency-domain can be utilized to achieve better timing synchronization performance. Consider two unit vectors, $p_1(n) = \delta(n - c_1)$ and $p_2(n) = \delta(n - c_2)$. The cross-correlation function outputs between these two unit vectors in the frequency-domain are

$$\frac{1}{N}\sum_{m=0}^{N-1}\{e^{\frac{-j2\pi mc_1}{N}} \times e^{\frac{j2\pi mc_2}{N}}\} = \begin{cases} 0, \ \forall c_1 \neq c_2 \\ \\ 1, \ c_1 = c_2, \end{cases} \tag{2.5}$$

where $\forall c_1, c_2 \in \{0, 1, \cdots, N-1\}$ and m represents the subcarrier index. Therefore, based on Equation (2.5), a frequency-domain timing synchronization scheme based on the cross-correlation function outputs is proposed. By employing the cross-correlation function in the frequency-domain, a timing metric for coarse timing synchronization is given by

$$\begin{aligned} \tau_c &= \arg\max_{d_1 \in \Omega_c}\{M_1(d_1)\} \\ M_1(d_1) &= |\Re\{U(d_1)\}| + |\Im\{U(d_1)\}| \\ U(d_1) &= \frac{1}{N}\sum_{m=0}^{N-1}\{R(d_1, m) \times b^*(m)\} \\ R(d_1, m) &= \sum_{n=0}^{N-1}\hat{r}(n + d_1) \cdot e^{\frac{-j2\pi mn}{N}}, \end{aligned} \tag{2.6}$$

where τ_c is the coarse timing estimate, $\Re\{u\}$ and $\Im\{u\}$ represent the real part and the imaginary part of u, respectively, $R(\cdot,\cdot)$ denotes the Fourier transform of the received signal $\hat{r}$, $b^*(m)$ is the complex conjugate of $b(m)$, $|b(m)|$ denotes the absolute value of $b(m)$, $b(m) = e^{\frac{-j2\pi mc}{N}}$, Ω_c is the observation interval, $\Omega_c = \{0, 1, \cdots, L-1\}$, d_1 is the time index, $d_1 \in \{0, 1, \cdots, L-1\}$, $R(d_1, m)$ represents the value of the mth subcarrier with respect to d_1, $U(d_1)$ is the cross-correlation function output in the frequency-domain, and L is the length of observation interval. In addition, if there is no CFO in Equation (2.1), $M_1(d_1)$ in Equation (2.6) can be further modified to

$$M_1(d_1) = |\Re\{U(d_1)\}|. \tag{2.7}$$

However, by using both real part and imaginary part of the cross-correlation function output, more information can be utilized to obtain a better coarse timing estimate.

Assume an unit vector $p_i(n) = \delta(n - c_i)$ is transmitted over a two-ray multipath fading channel ($\mathbf{h}_i$) without AWGN, a delayed timing offset is given by τ, and the power profile of the channel is equal to $\{0.3,\ 0.7\}$, where $c_i \in \{0, 1, \cdots, N-1\}$. Therefore, the received signal is

$$r_i(n) = \sum_{k=0}^{1} h_i(k)\delta(n - c_i - k - \tau). \tag{2.8}$$

Consider $\mathbf{h}_i^T = [0.3873 + 0.3873j\ \ 0.5916 + 0.5916j]$. Then, the received signal $r_i(n)$ is

$$r_i(n) = \begin{cases} 0.3873 + 0.3873j, & n = c_i + \tau \\ 0.5916 + 0.5916j, & n = c_i + \tau + 1 \\ 0, & else. \end{cases} \tag{2.9}$$

Based on Equation (2.6), the cross-correlation function output ($M_1(d_1)$) is

$$M_1(d_1) = \begin{cases} 0.7746, \ d_1 = \tau \\ 1.1836, \ d_1 = \tau + 1 \\ 0, \ else. \end{cases} \tag{2.10}$$

Thus, a coarse timing estimate (τ_c) is

$$\tau_c = \tau + 1. \tag{2.11}$$

From Equation (2.10), although $M_1(d_1)$ gives a maximum value when d_1 is at the delayed timing of the path with the largest gain in multipath fading channels, the actual delayed timing cannot be obtained.

In addition, for the general CIR $\mathbf{h}$ in Equation (2.1), the received training sequence is

$$\begin{aligned} \hat{\mathbf{r}} = [0 \ \cdots \ 0 \ & e^{\frac{-j2\pi\Delta\epsilon(\tau+c_i)}{N}} h(0)\delta(\tau + c_i) \\ & e^{\frac{-j2\pi\Delta\epsilon(\tau+c_i+1)}{N}} h(1)\delta(\tau + c_i + 1) \ \cdots \\ & e^{\frac{-j2\pi\Delta\epsilon(\tau+c_i+K-1)}{N}} h(K-1)\delta(\tau + c_i + K - 1) \ 0 \ \cdots \ 0]^T + \hat{\mathbf{w}}, \end{aligned} \tag{2.12}$$

where $E[\hat{\mathbf{w}}] = 0$ and $E[\cdot]$ is the expectation operation. Then, the corresponding timing

metric $M_1(d_1)$ is

$$M_1(d_1) = \begin{cases} |h(k)| \cdot \{|\cos(\frac{2\pi\Delta\epsilon(\tau+c_i+k)}{N} - \theta_k)| + \\ |\sin(\frac{2\pi\Delta\epsilon(\tau+c_i+k)}{N} - \theta_k)|\},\ d_1 \in \{\tau+k\} \\ 0,\ else \end{cases} \tag{2.13}$$

$$= \begin{cases} |h(k)| \cdot A_k,\ d_1 \in \{\tau+k\} \\ 0,\ else, \end{cases}$$

where $k \in \{0, \cdots, K-1\}$, $h(k) = |h(k)|e^{j\theta_k}$, $|h(k)| = \sqrt{(\Re\{h(k)\})^2 + (\Im\{h(k)\})^2}$, and $\theta_k = tan^{-1}\frac{\Im\{h(k)\}}{\Re\{h(k)\}}$. From Equation (2.13), we can easily obtain

$$\sqrt{2} \geq A_k \geq 1 \tag{2.14}$$

and

$$\sqrt{2} \cdot |h(k)| \geq M_1(\tau+k) \geq |h(k)|. \tag{2.15}$$

2.3.2 Fine time adjustment

Let us pay attention to Equation (2.10) and Equation (2.13). In Equation (2.10) and Equation (2.13), two cross-correlation function outputs related to the multipath fading channel have a strong connection, and the correct timing offset can be found using a simple threshold on cross-correlation outputs. Then, by utilizing the cross-correlation outputs at two adjacent timing indices, we can obtain the actual delayed timing in the channels. First, a SOV $\mathbf{v}$ based on the coarse timing estimate is utilized to perform fine

time adjustment, where

$$\begin{aligned}\mathbf{v}^T &= [\tau_c \ \tau_c - 1 \ \tau_c - 2 \ \cdots \ \tau_c - V + 1] \\ &= \{v(n), \ \forall n \in \Omega_v\},\end{aligned} \tag{2.16}$$

the length of the SOV is V, and $\Omega_v = \{0, 1, \cdots, V-1\}$. If $M_1(v(i+1)) > \beta \cdot M_1(v(i))$ and $M_1(v(i+2)) < \beta \cdot M_1(v(i+1))$, the final timing estimate ($\hat{\tau}$) is $v(i+1)$, where β is a threshold and $i \in \Omega_v$. The detailed procedure of fine time adjustment is described in **Algorithm** 1.

Algorithm 1 *Fine Time Adjustment*

Initial Inputs: $M_1(v(i))$, $\mathbf{v}$

```
for i = 0 to V − 1 do
    if M1(v(i + 1)) > β · M1(v(i)) then
        u = i + 1
    else
        break
    end if
end for
τ̂ = v(u)
```

In **Algorithm** 1, β is utilized to perform fine time adjustment. Based on Equation (2.13), τ_c is approximately equal to the timing index of the path with the largest gain in multipath fading channels. Therefore, the time difference between the timing index of the path with the largest gain and the timing index of the first delayed path in the channels is approximately equal to $N_I - 1$, where the actual number of iterations executed in **Algorithm** 1 is N_I and $N_I < V$.

Assume the second path has the largest power in the channel. If the correct delayed timing is obtained, $M_1(\tau) > \beta \cdot M_1(\tau + 1)$ and $M_1(\tau - 1) < \beta \cdot M_1(\tau)$ must be satisfied.

Based on these two conditions, we have

$$0 < \beta < \frac{M_1(\tau)}{M_1(\tau+1)} = \frac{|h(0)| \cdot A_0}{|h(1)| \cdot A_1} = \sqrt{\frac{|h(0)|^2}{|h(1)|^2}} \cdot \frac{A_0}{A_1}. \tag{2.17}$$

Because the bound of $\frac{A_0}{A_1}$ is

$$\frac{1}{\sqrt{2}} \leq \frac{A_0}{A_1} \leq \sqrt{2}, \tag{2.18}$$

we obtain the bound of the threshold β given by

$$0 < \beta < \sqrt{\frac{|h(0)|^2}{|h(1)|^2}} \cdot \frac{1}{\sqrt{2}}. \tag{2.19}$$

In general, assume the kth tap has the largest power in the channel. Then, the threshold β in the fine time adjustment can be chosen by satisfying:

$$0 < \beta < \sqrt{\frac{|h(k-1)|^2}{|h(k)|^2}} \cdot \frac{1}{\sqrt{2}}, \tag{2.20}$$

where $k > 0$. Moreover, if the first path is the path with the largest gain in the channel, the threshold can be easily set to

$$0 < \beta < \sqrt{\frac{|h(k')|^2}{|h(0)|^2}} \cdot \frac{1}{\sqrt{2}}, \tag{2.21}$$

where the k'th tap has the second-largest power in the channel.

2.3.3 Channel Estimation

After the final timing estimate ($\hat{\tau}$) is found, the channel response in the frequency-domain could be obtained in a simple way. Therefore, the estimated channel response in the frequency-domain is

$$\hat{H}(m) = \frac{\sum_{n=0}^{N-1} \hat{r}(n+\hat{\tau}) \cdot e^{\frac{-j2\pi mn}{N}}}{b(m)}, \tag{2.22}$$

where $\hat{H}(m)$ is the estimated channel response on the mth subcarrier.

2.4 Simulation Results

A packet-based LDPC coded SISO OFDM system was used for simulations, where each codeword is encoded with code (1600,800) [61] and each packet consists of a training sequence followed by 17 random OFDM data symbols. The structure of OFDM data symbols follows the IEEE 802.11a standard defined in [51], where $N = 64$ and $N_{CP} = 16$. The training sequence of each packet is an unit vector with unit amplitude in the time-domain, where $c = 31$ and the power of the training sequence is $1/64$. Quaternary phase-shift keying (QPSK) modulation was adopted in simulations. For each packet transmission, the residual CFO was modeled as a random variable that is uniformly distributed within ± 0.1 OFDM subcarrier spacing. In addition, the phase tracker based on the pilots in the frequency-domain is utilized to compensate the phase error [51].

In this chapter, we evaluate the proposed approach and other related schemes [49, 51, 55] under 6-path Rayleigh channels, where the power profiles of their first four taps are described in Table 2.1 and σ_i^2 represents the $(i+1)$th tap power in the channel. Compared with [49, 51, 55], we can easily demonstrate the performance of the proposed approach. A delayed timing offset (τ) is given by 65 samples. Channel Models I and II (CH I and CH II) represent multipath fading channels with NLOS propagation, and Channel Model III (CH III) is a typical multipath fading channel with LOS propagation. For CH I, the power of second tap dominates all channel taps. As for CH II, the third

tap has the strongest power in the channel, and it is the worst channel model to evaluate the timing synchronization performance in this chapter. Moreover, assume all channels are quasi-stationary during each packet transmission.

Table 2.1: The Power Profiles of Different Channel Models

	CH I (NLOS)	CH II (NLOS)	CH III (LOS)
σ_0^2	0.3432	0.1885	0.5211
σ_1^2	0.6211	0.3223	0.4338
σ_2^2	0.0329	0.48	0.0420
σ_3^2	0.0015	0.0079	0.0023

The main motivation of this chapter is to achieve perfect timing synchronization in very low SNR environments by using unit vectors in an N-dimensional Cartesian coordinate system. In **Algorithm** 1, although the number of iterations is defined by V, the number of iterations actually depends on the comparison between cross-correlation function outputs. In this chapter, the actual number of iterations executed in **Algorithm** 1 (N_I) is less than 3. In addition, in CH I and CH II, the thresholds β in the fine time adjustment should be less than 0.5256 and 0.5794, respectively. Therefore, based on the SNR, we employ different thresholds β defined in fine time adjustment to achieve better performance. For SNR $\leq$ 0dB, β is 0.5. As for SNR $>$ 0dB, β is 0.3. In [49], the time-domain training sequence is generated by a Golay complementary

sequence, i.e., ± 1, and the length of the time-domain training sequence is N. In addition, the actual threshold in [49] is $\eta|\hat{h}_{max}|$, where η is a threshold factor and $|\hat{h}_{max}|$ is the strongest channel tap gain estimate. The same criterion for β is applied to η. Moreover, in this chapter, pre-simulations and mathematical derivations are not required to choose the threshold in fine time adjustment [49, 50, 52]. Let $L = 200$ and $V = 50$. Therefore, the length of the interval for fine-timing estimation in [49] is also set to 50. For [55], we use four concatenated cyclic prefixes to perform timing synchronization. The corresponding results are reported in Fig. 2.3, Fig. 2.4, and Fig. 2.5. The perfect timing synchronization is defined as the successful acquisition of the position of the first tap in different channel models.

In Fig. 2.3, the simulation results show that our proposed approach has better timing synchronization performance at very low SNR. In CH I, the proposed approach achieves perfect timing synchronization when SNR exceeds 1dB. As for CH II, perfect timing synchronization is achievable using the proposed algorithm when SNR = 6dB. In CH III, the proposed approach achieves perfect timing synchronization when SNR exceeds -5dB. Moreover, for c=63, the perfect timing synchronization is achievable at low SNR by only appending one sample to the front of the transmitted packet. The synchronization methods used in IEEE 802.11 standards lead to the delayed path with the maximum gain in channels. Also, the standardized methods are only suitable for the channels with LOS propagation. In CH III, the first tap power is approximately equal to the second tap power. Thus, higher SNR is needed to achieve perfect timing synchronization for [51].

As for [49], the reason why the scheme has poor timing synchronization performance is that AWGN affects the entire fine time adjustment process at low SNR, especially in CH I and CH II. Therefore, low SNR and wide interval in fine time adjustment significantly degrade the performance in [49, 50, 52]. For [55], the proposed timing estimator is only suitable in an AWGN channel at high SNR; therefore, the timing estimator has poor performance in all channel models. Besides the probability of perfect timing synchronization, we also evaluate the bias and root mean squared error (RMSE) of each approach in Fig. 2.4 and Fig. 2.5, respectively. In Fig. 2.4 and Fig. 2.5, our proposed approach has better performance than other methods in [49, 51, 55]. In Fig. 2.4, our proposed approach performs approximately unbiased at any low SNR, and wide interval in fine time adjustment [49] leads the timing estimator to have negative biases. In Fig. 2.5, zero RMSE can be achieved using the proposed approach due to the ability to identify the first arrival path in all channel models.

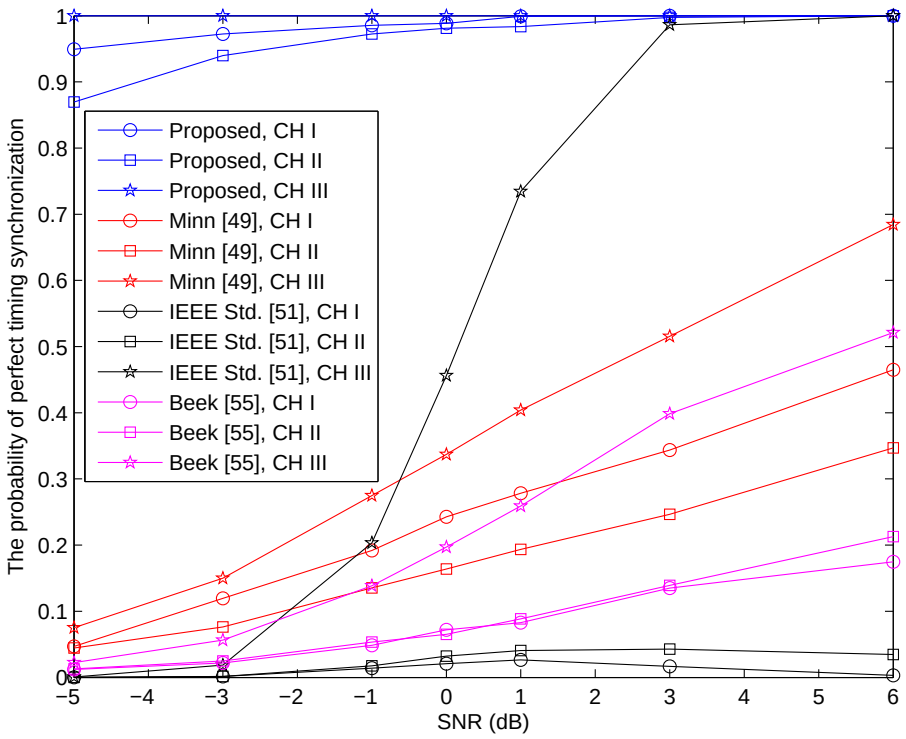

Figure 2.3: The probability of perfect timing synchronization, $prob(\tau = \hat{\tau})$, where $prob(\cdot)$ is the probability function and $\hat{\tau}$ is the estimated timing offset.

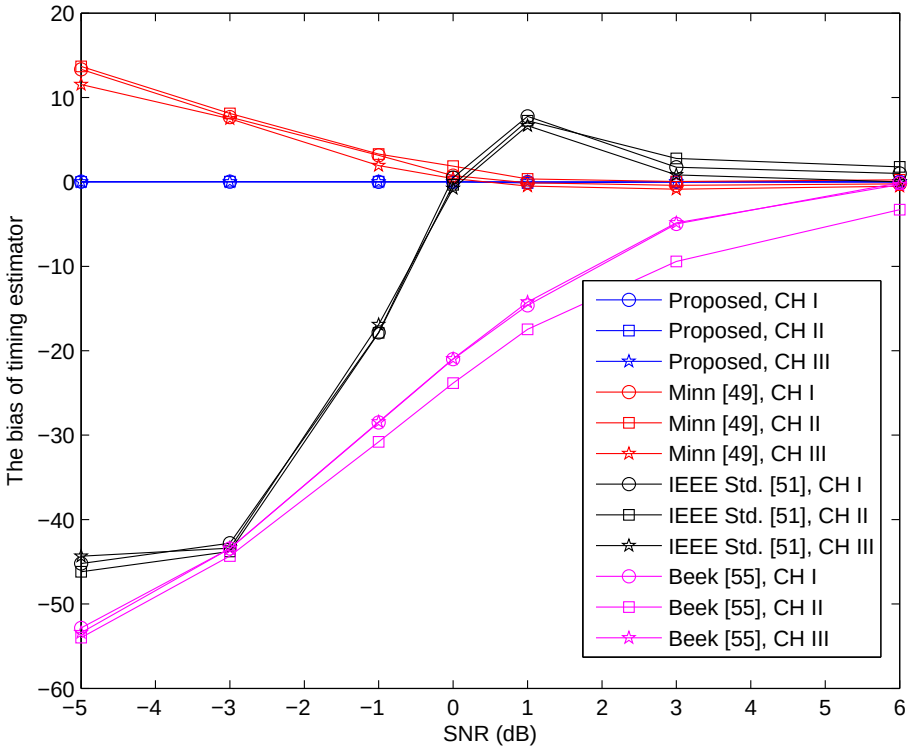

Figure 2.4: The bias of timing estimator, $E[\hat{\tau}-\tau]$, where $E[\cdot]$ is the expectation function.

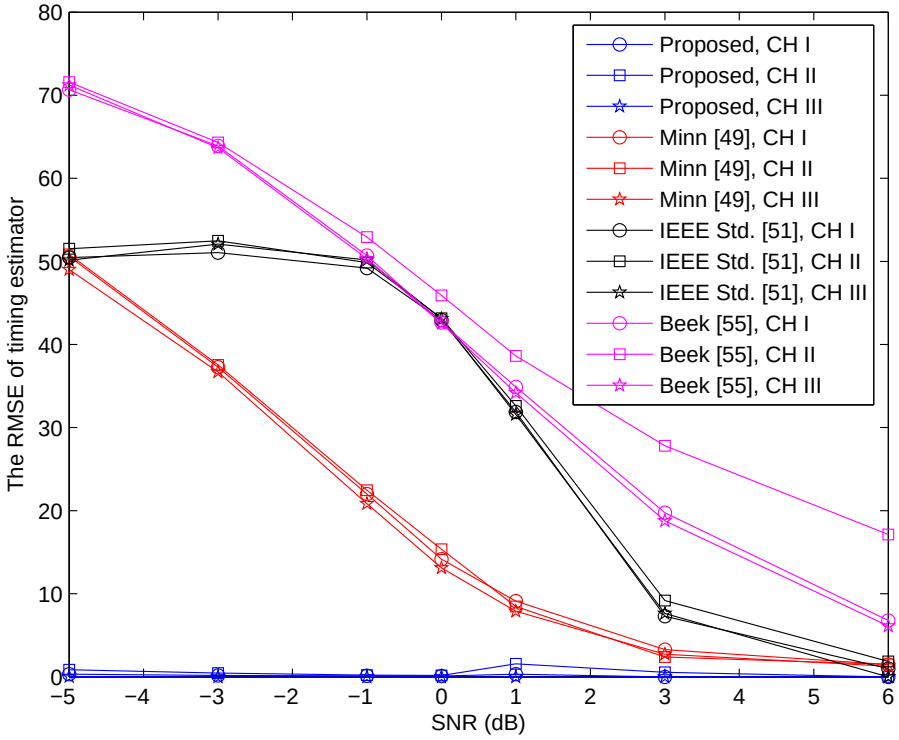

Figure 2.5: The root mean squared error of timing estimator, $\sqrt{E[|\hat{\tau} - \tau|^2]}$.

In Fig. 2.6, we compare the proposed approach with [49] in terms of BER. For CH III, a comparison BER of less than 10^{-4} can be achieved using our proposed approach when SNR exceeds 6dB, because there are no timing errors to process the received signals. As for CH I and CH II, low BER is still achievable when SNR exceeds 8dB. In addition, the BER performance of [49] decreases slowly and still does not reach 10^{-2} when SNR = 8dB in CH I and CH II.

2.5 Summary

In this chapter, we have presented a semiblind frequency-domain timing synchronization and channel estimation scheme for OFDM systems based on unit vectors. Simulation results show that there are no timing errors in our proposed timing estimator when SNR exceeds 6dB. In addition, for an LDPC coded SISO OFDM system, BER is less than 10^{-4} under the channel models with NLOS propagation when SNR exceeds 8dB.

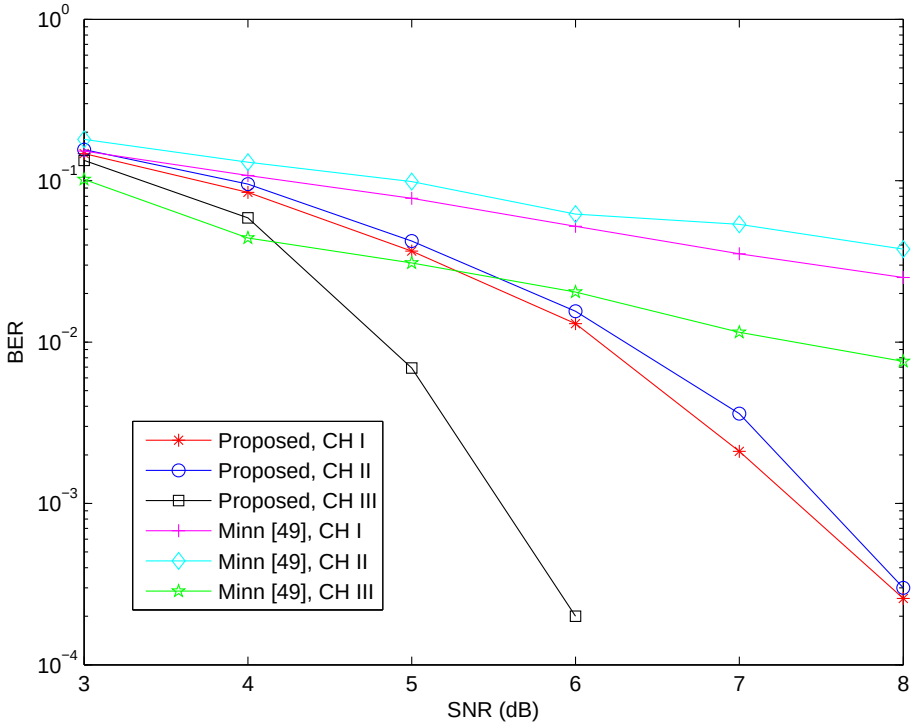

Figure 2.6: BER comparisons in all channel models.

Chapter 3

Optimized Joint Timing Synchronization and Channel Estimation

3.1 Introduction

Numerous synchronization techniques for OFDM systems have been developed using well-designed timing metrics based on repetitive signals [47, 48, 53, 55, 62, 63, 64, 65, 66]. However, in some multipath fading channels with NLOS propagation, these methods frequently lead to the delayed timing in channels where the delayed path has the larger gain than the first path. In this case, the resultant ISI would degrade the system performance, and the channel coding would not perform well because of the errors in

timing synchronization. In order to solve this problem, a fine time adjustment is needed to modify the frequently delayed timing to the actual delayed timing in channels. Most studies always perform timing synchronization and channel estimation in a separate way; however, errors in timing synchronization can affect the channel estimation. Recently, some joint synchronization and channel estimation designs for OFDM systems have been discussed [49, 50, 52, 67, 68, 69, 70, 71]. In [49], a repetitive training sequence with special sign patterns was proposed to have better coarse timing synchronization. After coarse timing synchronization, CIR estimates are obtained based on the training sequence using least squared method and then utilized in fine time adjustment to find the delay timing estimate of the first actual channel tap using a threshold factor. In [50], a more theoretical approach using ML principle was derived, where the same threshold factor was applied to perform fine time adjustment. In [52] and [67], a joint timing synchronization and channel estimation approach based on different training sequences was proposed. Then, the optimal and suboptimal threshold factors are derived by analyzing the probability density functions (pdfs) of the cross-correlation function outputs in Rayleigh and Ricean fading channels. In [68], a low complexity joint approach was proposed to estimate the timing and CIR using an orthogonal sequence and then applied a proper ratio to perform fine time adjustment. In [69], a joint approach was proposed using ML estimation and generalized Akaike information criterion to find the symbol timing offset and CIR. In [70], a joint approach was proposed using the regression method to estimate timing and CIR simultaneously. Then, the timing offset

is obtained by finding the first path with the maximum gain in CIR estimates. In [71], the proposed timing estimator is based on the channel interpolation results using pilots in the frequency domain. It is noted that the fine time adjustment approaches using threshold factors in [49, 50, 52, 67] are not optimized when SNR is very small. In [52] and [67], these derived optimal and suboptimal threshold factors could be determined only when SNR exceeds 0dB. In addition, a wide searching interval for fine time adjustment would also lead these approaches to have wrong estimates of delayed timing [49, 50, 52, 67]. As for [68] and [70], these two approaches are only suitable for the channel models with LOS propagation.

In this chapter, we develop a joint timing synchronization and channel estimation algorithm suitable for the multipath fading channels with LOS and NLOS propagation at any SNR that is either greater or smaller than 0dB. Moreover, the fine time adjustment can be performed in a wider range than that in [52, 67, 68], and the computational complexity of this chapter is significantly lower than that in [70]. Also, the proposed approach is suitable for any low power wireless communications device. In this chapter, we first obtain a coarse timing estimate using the cross-correlation function outputs based on the proposed training sequence, and then apply the ML principle to find the advanced timing, relative timing indices, and CIR estimates. The reason why we use the advanced timing instead of the coarse timing estimate to perform fine time adjustment is that we can have better timing synchronization performance at very low SNR. Finally, the designed metric based on the MMSE criterion is utilized to perform

fine time adjustment. Simulation results are given to verify the effectiveness of our proposed algorithm. This chapter is based on our publication in [44].

This chapter is organized as follows. Section 3.2 describes the system model. In Section 3.3, the proposed joint fine time synchronization and channel estimation scheme is presented. Simulation results are provided in Section 3.4. Finally, Section 3.5 concludes this chapter.

3.2 System Description

In this chapter, we consider a training-sequence-based SIMO OFDM system. The training sequence is composed of two identical pseudo-noise (PN) sequences and a guard interval. Let $\mathbf{c} = [c_0\ c_2\ \cdots\ c_{N_c-1}]^T$, $\mathbf{g} = [0_{N_g \times 1}]$, and $\mathbf{p}^T = [\mathbf{c}^T\ \mathbf{g}^T\ \mathbf{c}^T]$ denote the PN sequence, guard interval, and the proposed training sequence, respectively. Consider the transmitted packet $\mathbf{s}^T = [\mathbf{p}^T\ \mathbf{x}^T] = \{s(n), \forall n \in \Omega\}$, where $\mathbf{x}^T$ consists of m OFDM symbols, the length of $\mathbf{x}^T$ is $m \cdot (N + N_{CP})$, N represents the number of subcarriers in the OFDM system, N_{CP} denotes the length of cyclic prefix, m is a positive integer, and $\Omega = \{0, 1, \cdots, m \cdot (N + N_{CP}) + 2N_c + N_g - 1\}$. Assume cyclic prefix in each OFDM symbol and guard interval in $\mathbf{p}^T$ are longer than the maximum delay spread of the channel, and the path delays in the channels are sample-spaced. Therefore, the received signal at the ith receiver can be expressed as

$$r_i(n) = e^{\frac{j2\pi\epsilon n}{N}} \sum_{k=0}^{K-1} h_i(k)s(n - \tau_i - k) + w(n), \tag{3.1}$$

where ϵ is the CFO normalized to the OFDM subcarrier spacing, τ_i is the timing offset, $h_i(k)$ represents the kth tap CIR from the transmitter to the ith receiver, K is the number of taps in the channel, and $w(n)$ is a complex AWGN sample. After coarse frequency synchronization, the CFO-compensated received signal at the ith receiver is

$$\begin{aligned}\hat{r}_i(n) &= r_i(n) \cdot e^{\frac{-j2\pi(\epsilon+\Delta\epsilon)n}{N}} \\ &= e^{\frac{-j2\pi(\Delta\epsilon n)}{N}} \sum_{k=0}^{K-1} h_i(k)s(n-\tau_i-k) + \hat{w}(n),\end{aligned} \tag{3.2}$$

where $\Delta\epsilon$ denotes the residual CFO and $\hat{w}(n) = w(n)e^{\frac{-j2\pi(\epsilon+\Delta\epsilon)n}{N}}$.

3.3 The Proposed Approach

3.3.1 Coarse Timing Synchronization

It can be easily observed that the proposed training sequence is composed of two identical parts. Therefore, a coarse timing estimate at the ith receiver $\tau_{c,i}$ is obtained based on the cross-correlation function outputs as follows:

$$\begin{aligned}\tau_{c,i} &= \arg\max_{d\in\Omega_d}\{|M_i(d)|\} \\ M_i(d) &= \sum_{n=0}^{N_c-1} \frac{\hat{r}_i^*(n+d)\hat{r}_i(n+N_c+N_g+d)}{N_c},\end{aligned} \tag{3.3}$$

where $\hat{r}_i^*(n)$ denotes the complex conjugate of $\hat{r}_i(n)$, $|\hat{r}_i(n)|$ represents the absolute value of $\hat{r}_i(n)$, Ω_d is the observation interval, $\Omega_d = \{0, 1, \ldots, D-1\}$, and D is the length of observation interval. From Equation (3.1) and Equation (3.3), $M_i(d)$ will give a maximum value of almost one when d is at the delayed timing of the LOS path in multipath fading channels.

3.3.2 Maximum-likelihood based Channel Estimation

Assume there is no timing offset and CFO in Equation (3.1), the received training sequence at the ith receiver can be expressed as

$$\mathbf{r}_i = \mathbf{S}\mathbf{h}_i + \mathbf{w}, \tag{3.4}$$

where

$$\mathbf{r}_i = [r_i(0)\ r_i(1)\ \cdots\ r_i(N'-1)]^T, \tag{3.5}$$

$$\mathbf{S} = \begin{pmatrix} s(0) & 0 & \cdots & 0_{(K-1)\times 1} \\ s(1) & s(0) & \ddots & s(0) \\ \vdots & \vdots & \ddots & \vdots \\ s(N'-1) & s(N'-2) & \cdots & s(N'-K) \end{pmatrix}, \tag{3.6}$$

$$\mathbf{h}_i = [h_i(0)\ h_i(1)\ \cdots\ h_i(K-1)]^T, \tag{3.7}$$

$$\mathbf{w} = [w(0)\ w(1)\ \cdots\ w(N'-1)]^T, \tag{3.8}$$

$N' = 2N_c + N_g$, and $\mathbf{w} \sim N(0_{N'\times 1}, \sigma_w^2 \mathbf{I}_{N'\times N'})$. If there is a timing offset τ, the received training sequence is

$$\mathbf{r}_i(\tau) = [r_i(\tau)\ r_i(\tau+1)\ \cdots\ r_i(\tau+N'-1)]^T, \tag{3.9}$$

where Equation (3.5) is a special case of Equation (3.9) when $\tau = 0$. Then the likelihood function is given by

$$\Lambda(\mathbf{h}_i) = \frac{1}{(\pi\sigma_w^2)^{N'}} exp\{\frac{-1}{\sigma_w^2}\|\mathbf{r}_i(\tau) - \mathbf{S}\mathbf{h}_i\|^2\}, \tag{3.10}$$

and the ML estimate of $\mathbf{h}_i$ can be obtained by

$$\begin{aligned} \hat{\mathbf{h}}_{i,ML} &= \arg\max_{\mathbf{h}_i} \Lambda(\mathbf{h}_i) \\ &= (\mathbf{S}^H\mathbf{S})^{-}\mathbf{S}^H\mathbf{r}_i(\tau) \\ &= \mathbf{S}^{\dagger}\mathbf{r}_i(\tau), \end{aligned} \tag{3.11}$$

where $\mathbf{A}^H$ is the Hermitian of $\mathbf{A}$, $\mathbf{B}^{-}$ is the generalized inverse of $\mathbf{B}$, and $\mathbf{S}^{\dagger}$ is the Moore-Penrose pseudo-inverse of $\mathbf{S}$. For a fixed $\mathbf{c}$, we only need to compute $\mathbf{S}^{\dagger}$ once, and different CIR estimates can be obtained simply by multiplying the received training sequence at each receiver with $\mathbf{S}^{\dagger}$.

3.3.3 Joint Timing Synchronization and Channel Estimation

In this subsection, we utilize coarse timing estimate and CIR estimate based on the ML criterion to develop a joint timing synchronization and channel estimation algorithm such that the receiver can perform the proposed approach with lower computational complexity and power. After coarse timing synchronization, a SOV $\mathbf{v}_i$ at the ith receiver is applied to obtain an advanced timing, relative timing indices, and the corresponding

CIR estimates, where

$$\begin{aligned}\mathbf{v}_i^T &= [\tau_{c,i}+L \ \cdots \ \tau_{c,i}+1 \ \tau_{c,i} \ \tau_{c,i}-1 \ \cdots \ \tau_{c,i}-L] \\ &= \{v_i(l_1), \ \forall l_1 \in \Omega_{v_i}\},\end{aligned} \tag{3.12}$$

$\Omega_{v_i} = \{0, 1, \cdots, 2L\}$, the length of observation interval is $2L+1$, and L is a positive integer without any constraint. In Equation (3.12), $\mathbf{v}_i$ consists of $2L+1$ timing indices. Based on these timing indices in $\mathbf{v}_i$, the corresponding CIR estimates with K' taps are obtained by Equation (3.11), where

$$\tilde{\mathbf{h}}_{i,v_i(l_1)} = \tilde{\mathbf{S}}^{\dagger}\hat{\mathbf{r}}_i(v_i(l_1)), \tag{3.13}$$

$$\hat{\mathbf{r}}_i(v_i(l_1)) = [\hat{r}_i(v_i(l_1)) \ \hat{r}_i(v_i(l_1)+1) \ \cdots \ \hat{r}_i(v_i(l_1)+N'-1)]^T, \tag{3.14}$$

$$\tilde{\mathbf{S}} = \begin{pmatrix} s(0) & 0 & \cdots & 0_{(K'-1)\times 1} \\ s(1) & s(0) & \ddots & s(0) \\ \vdots & \vdots & \ddots & \vdots \\ s(N'-1) & s(N'-2) & \cdots & s(N'-K') \end{pmatrix}, \tag{3.15}$$

$\forall l_1 \in \Omega_{v_i}$, and $\tilde{\mathbf{h}}_{i,v_i(l_1)}$ is the CIR estimate corresponding to the time index $v_i(l_1)$. In order to avoid any loss of the channel information, K' should be at least equal to or larger than K. After we obtain $2L+1$ CIR estimates, the advanced timing at the ith receiver $\tau_{ad,i}$ is given by

$$\tau_{ad,i} = \arg \max_{v_i(l_1), \ l_1 \in \Omega_{v_i}} |\tilde{\mathbf{h}}_{i,v_i(l_1)}(0)|, \tag{3.16}$$

where $\tilde{\mathbf{h}}_{i,v_i(l_1)}(0)$ is the first tap in the CIR estimate. Then, relative timing indices $\mathbf{t}_i^T$ given by

$$\mathbf{t}_i^T = [\tau_{ad,i}\ \tau_{ad,i} - 1\ \cdots\ \tau_{c,i} - L] = \{t_i(l_2),\ l_2 \in \Omega_{t_i}\} \tag{3.17}$$

and the corresponding CIR estimates $\tilde{\mathbf{h}}_{i,t_i(l_2)}$ are fed forward to perform fine time adjustment, where $\Omega_{t_i} = \{0, 1, \cdots, \tau_{ad,i} - \tau_{c,i} + L\}$.

3.3.4 Fine Time Adjustment

In this subsection, we exploit the MMSE criterion to perform fine time adjustment in an iterative manner based on the information of relative timing indices and the corresponding CIR estimates. First, a threshold on the first tap power β, which should be smaller than the tap power of the first path in the channel, is chosen in order to eliminate the AWGN effect and to reduce the computational complexity. In other words, if $|\tilde{\mathbf{h}}_{i,\tau_{ad,i}-1}(0)|^2 < \beta$, $\tau_{ad,i}$ is the estimated timing offset; otherwise, the algorithm keeps running until $|\tilde{\mathbf{h}}_{i,t_i(f)}(0)|^2 < \beta$ for some f, where $f \in \Omega_{t_i}$. Then, let $\mathbf{q}_{t_i(l_2)}^T$ denote the convolution of the training sequence and the corresponding CIR estimate $\tilde{\mathbf{h}}_{i,t_i(l_2)}^T$, where

$$\mathbf{q}_{t_i(l_2)}^T = \begin{cases} \mathbf{p}^T * \tilde{\mathbf{h}}_{i,t_i(l_2)}^T(0 : l_2),\ \forall l_2 \leq K' - 1 \\ \mathbf{p}^T * \tilde{\mathbf{h}}_{i,t_i(l_2)}^T,\ \forall l_2 \geq K' \end{cases} \tag{3.18}$$

and $\tilde{\mathbf{h}}^T_{i,t_i(l_2)}(0:l_2)$ contains the information of $\tilde{\mathbf{h}}^T_{i,t_i(l_2)}$ from the first tap to the l_2th tap. Then, the mean squared error (MSE) of the timing index $t_i(l_2)$ is given by

$$\begin{aligned}\phi_i(t_i(l_2)) = \frac{1}{3}\{ &\sum_{n=0}^{2N_c+N_g-1} |\hat{\mathbf{r}}_i(t_i(l_2)+n) - \mathbf{q}_{t_i(l_2)}(n)|^2 \\ &+ \sum_{n=0}^{N_c+N_g-1} |\hat{\mathbf{r}}_i(t_i(l_2)+n) - \mathbf{q}_{t_i(l_2)}(n)|^2 \\ &+ \sum_{n=0}^{N_c-1} |\hat{\mathbf{r}}_i(t_i(l_2)+n) - \mathbf{q}_{t_i(l_2)}(n)|^2\}.\end{aligned} \tag{3.19}$$

From Equation (3.18), Equation (3.19), and reasonable CIR estimates, we have

$$\phi_i(\tau_i + \delta) > \phi_i(\tau_i), \tag{3.20}$$

where $\delta \neq 0$, δ is an integer, and $\tau_i + \delta \in \mathbf{t}_i^T$. Thus, the estimated timing offset can be obtained based on the MMSE criterion as shown in Equation (3.20). Assume a set $\Omega_U = \{0, 1, \cdots, u-1\}$ is composed of consecutive timing indices that satisfy the condition $|\tilde{\mathbf{h}}_{i,t_i(u')}(0)|^2 > \beta,\ \forall u' \in \Omega_U$. Then, the estimated timing offset $\hat{\tau}_i$ and the CIR estimate $\hat{\mathbf{h}}_i$ at the ith receiver based on the threshold β and Equation (3.19) can be expressed as

$$\begin{cases} \hat{\tau}_i = \arg\min_{t_i(u'),\ u' \in \Omega_U} \phi_i(t_i(u')) \\ \hat{\mathbf{h}}_i = \tilde{\mathbf{h}}_{i,\hat{\tau}_i}. \end{cases} \tag{3.21}$$

The detailed procedure of fine time adjustment is described in **Algorithm** 2, and the total number of iterations in **Algorithm** 2 depends on the location of the strongest path in the channel.

Algorithm 2 *Fine Time Adjustment*

Initial Inputs: $\mathbf{t}_i^T$, $\tilde{\mathbf{h}}_{i,\mathbf{t}_i^T}$

for $k = 0$ **to** $\tau_{ad,i} - \tau_{c,i} + L$ **do**
  if $|\tilde{\mathbf{h}}_{i,t_i(k)}(0)|^2 < \beta$ **then**
    u = k
    break
  else
    Calculate $\phi_i(t_i(k))$
  end if
end for
$\hat{\tau}_i = \arg\min_{t_i(u'),\ u' \in \{0,1,\cdots,u-1\}} \phi_i(t_i(u'))$
$\hat{\mathbf{h}}_i = \tilde{\mathbf{h}}_{i,\hat{\tau}_i}$

3.4 Simulation Results

A packet-based LDPC coded 1x2 SIMO-OFDM system with MRC was used for simulations, where each codeword is encoded with code rate (3200,1600) [61] and each packet consists of a training sequence followed by 34 random OFDM data symbols. Gold code is utilized to be the pseudo-noise sequence with the spreading factor equal to 1. The length of training sequence in each packet is 80 identical samples, where $N_c = 32$ and $N_g = 16$. The structure of OFDM data symbols follows the IEEE 802.11a standard defined in [51], where $N = 64$ and $N_{CP} = 16$. QPSK modulation was adopted in simulations. For each packet transmission, the residual CFO was modeled as a random variable that is uniformly distributed within ± 0.1 OFDM subcarrier spacing. In addition, the phase tracker based on the pilots in the frequency-domain [51] is utilized to compensate the phase error at each receiver.

We compare the proposed approach with two related schemes [49, 51] under 6-path

Rayleigh channels, where the power profiles of their first four taps are described in Table 3.1. Different fading channels (Ricean, Nakagami) would not affect the results, because the power profiles in different channel models have already been defined in Table 3.1. Channel Models I and II (CH I and CH II) represent multipath fading channels with NLOS propagation, and Channel Model III (CH III) is a typical multipath fading channel with LOS propagation. Moreover, assume all channels are quasi-stationary during each packet transmission.

Table 3.1: The Power Profiles of Different Channel Models

	CH I (NLOS)	CH II (NLOS)	CH III (LOS)
σ_0^2	0.1932	0.1885	0.7211
σ_1^2	0.7711	0.3223	0.2338
σ_2^2	0.0329	0.48	0.0420
σ_3^2	0.0015	0.0079	0.0023

The main motivation of this chapter is to achieve perfect timing synchronization in very low SNR environments. The parameters L and K' related to the observation interval in joint timing synchronization and channel estimation are set to be 50 and 6, respectively. Therefore, the number of possible relative timing indices for fine time adjustment in our proposed approach is greater than 50. In addition, the threshold β defined in fine time adjustment is selected to be 0.09. For fairness, the designed

maximum channel delay spread for fine time adjustment used in [49] is 50 samples. In addition, the coarse timing estimate in the proposed approach is provided to [49] when their estimate is smaller than 30. The corresponding results are reported in Table 3.2, Table 3.3, and Table 3.4. The perfect timing synchronization is defined as the successful acquisition of the position of the first tap in different channel models. The actual threshold used in [49] is $\eta|\hat{h}_{max}|$, where η is a threshold factor and $|\hat{h}_{max}|$ is the strongest channel tap gain estimate. Moreover, in this chapter, pre-simulations and mathematical derivations are not required to choose the threshold in fine time adjustment [49, 50, 52, 67]. In Table 3.2, the simulation results show that our proposed approach has excellent timing synchronization performance at very low SNR. In CH I and CH II, the proposed approach achieves perfect timing synchronization when SNR exceeds 1dB. Moreover, in CH III, the proposed approach achieves perfect timing synchronization when SNR exceeds -5dB. The synchronization methods used in IEEE 802.11 standards lead to find the delayed path with the maximum gain in channels and achieve perfect timing synchronization in CH III when SNR exceeds 1dB. As for [49], the reason why the scheme has poor timing synchronization performance is that AWGN affects the entire fine time adjustment process at low SNR, especially in CH I and CH II. Therefore, low SNR and wide interval in fine time adjustment significantly degrade the performance in [49, 50, 52, 67].

Besides the probability of perfect timing synchronization, we also evaluate the bias

and RMSE of the proposed timing estimator. The simulation results are listed in Table 3.3 and Table 3.4. In Table 3.3 and Table 3.4, our proposed approach has better performance than that in [49]. In Table 3.3, our proposed approach performs approximately unbiased at any low SNR, and wide interval in fine time adjustment [49] leads the timing estimator to have negative biases. In Table 3.4, zero RMSE can be achieved using the proposed approach when SNR exceeds 1dB due to the ability to identify the first arrival path in all channel models. Moreover, the performance of channel estimation in this chapter is similar to that in [49], because the CIR estimates are obtained based on the ML estimation. Also, there is no such "one-shot" scheme that has better performance in channel estimation when SNR is smaller than 1dB. Thus, in this chapter, we do not discuss the simulation results on the performance in channel estimation.

In Fig. 3.1, we compare the proposed approach with [49] in terms of BER. For CH I and CH III, a comparison of BER of less than 10^{-5} can be achieved using our proposed approach when SNR exceeds 0dB, because there are no timing errors to process the received signals. As for CH II, BER is still less than 10^{-5} when SNR exceeds 1dB. In addition, the BER performance of [49] decreases slowly and still does not reach to 10^{-3} in CH I and CH II when SNR = 2dB, because the timing estimator does not perform well. In summary, lower BER performance at low SNR is achievable only when a communication system has better timing synchronization performance.

Table 3.2: The Probability of Perfect Timing Synchronization

	SNR=-5dB	SNR=-3dB	SNR=-1dB	SNR=0dB	SNR=1dB	SNR=3dB	SNR=5dB
Proposed (CH I)	0.9760	0.9930	0.9990	0.9999	1	1	1
Proposed (CH II)	0.9707	0.9911	0.9979	0.9993	0.9999	1	1
Proposed (CH III)	0.9999	1	1	1	1	1	1
IEEE 802.11 Std. [51] (CH III)	0.0038	0.1801	0.8496	0.9803	0.9994	1	1
Minn [49] (CH I, $\eta = 0.2$)	0.3858	0.4078	0.4174	0.4214	0.4217	0.4319	0.4354
Minn [49] (CH II, $\eta = 0.2$)	0.3108	0.3179	0.3243	0.3248	0.3264	0.3257	0.3214
Minn [49] (CH III, $\eta = 0.2$)	0.7794	0.8824	0.9231	0.9362	0.9399	0.9568	0.9668

Table 3.3: The Bias of Timing Estimator

	SNR=-5dB	SNR=-3dB	SNR=-1dB	SNR=0dB	SNR=1dB	SNR=3dB	SNR=5dB
Proposed (CH I)	0.0234	0.0069	0.0014	0.0001	0	0	0
Proposed (CH II)	0.0296	0.097	0.0021	0.0003	0.0001	0	0
Proposed (CH III)	-1.5×10^{-4}	0	0	0	0	0	0
IEEE 802.11 Std. [51] (CH III)	-472.7819	-330.6224	-29.5763	-2.4043	-0.0188	0	0
Minn [49] (CH I, $\eta = 0.2$)	-0.8992	-0.6004	-0.5614	-0.5597	-0.5577	-0.5526	-0.5489
Minn [49] (CH II, $\eta = 0.2$)	-1.2654	-1.0575	-1.0149	-1.0356	-1.0479	-1.0695	-1.0716
Minn [49] (CH III, $\eta = 0.2$)	-0.6420	-0.1412	-0.0853	-0.0728	-0.0676	-0.0448	-0.0353

Table 3.4: The Root Mean Squared Error of Timing Estimator

	SNR=-5dB	SNR=-3dB	SNR=-1dB	SNR=0dB	SNR=1dB	SNR=3dB	SNR=5dB
Proposed (CH I)	0.2220	0.1196	0.0519	0.0283	0	0	0
Proposed (CH II)	0.2579	0.1471	0.0700	0.0418	0.0229	0	0
Proposed (CH III)	0.0171	0	0	0	0	0	0
Minn [49] (CH I, $\eta = 0.2$)	21.1694	4.1588	1.8916	1.5387	1.4194	1.3004	1.2274
Minn [49] (CH II, $\eta = 0.2$)	23.0266	6.1732	2.5213	2.3590	2.2172	2.1874	2.1510
Minn [49] (CH III, $\eta = 0.2$)	21.5924	4.6842	1.0666	0.7607	0.5063	0.3069	0.2110

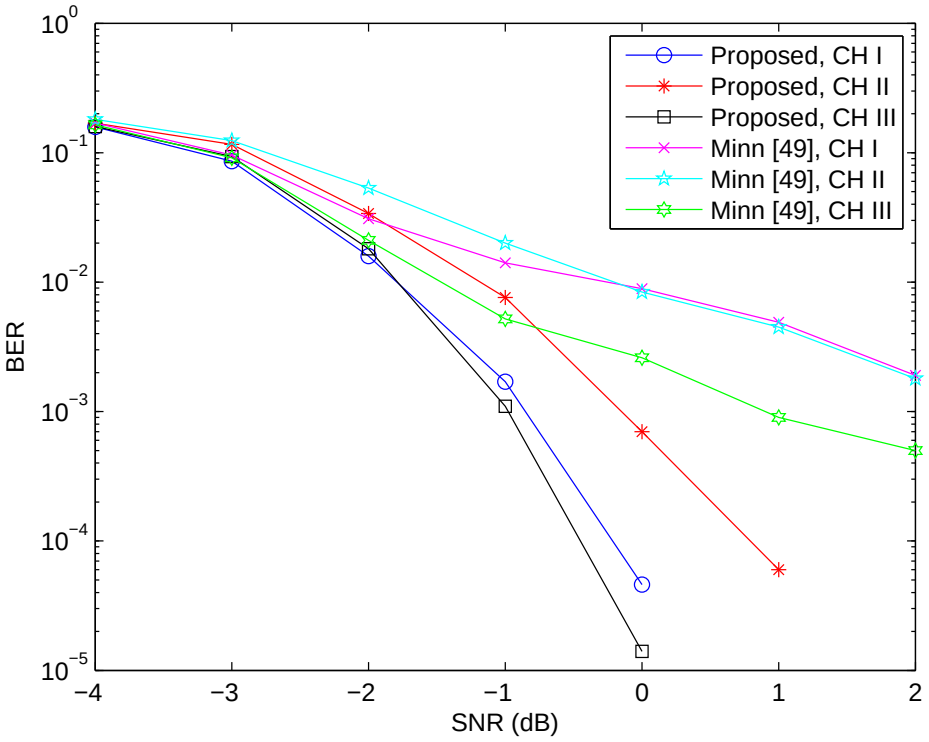

Figure 3.1: BER comparisons in all channel models.

3.5 Summary

In this chapter, we have presented a joint timing synchronization and channel estimation scheme for training-sequence-based OFDM systems. Simulation results show that there are no timing errors in our proposed timing estimator when SNR exceeds 1dB. Moreover, for an LDPC coded 1x2 SIMO-OFDM system using our proposed approach, BER is less than 10^{-5} when SNR exceeds 1dB.

Chapter 4

Optimized Joint Timing Synchronization and Channel Estimation with Multiple Transmit Antennas

4.1 Introduction

In communication systems, timing and channel estimates are two important parameters at the receiver in order to reconstruct the signal. To further enhance the system performance, spatial diversity techniques can be applied to communication systems. By employing the spatial diversity techniques, multiple transmit antenna arrays are known

to perform better than the conventional single transmit antenna, because the effects of multipath fading channels and interference can be more effectively exploited [72, 73]. MISO and MIMO use multiple transmit antenna arrays and offer significant increases in data throughput and link range without additional bandwidth or increased transmit power. Recently, OFDM has been of great interest for both wired and wireless applications due to its high spectrum efficiency and robustness against multipath fading channels [22], and the resultant MISO-OFDM and MIMO-OFDM systems have been recognized as promising solutions to support next generation broadband wireless communication systems [74]. However, compared with the single carrier systems, OFDM systems are much more sensitive to synchronization errors [75]. Several approaches have been proposed to address this problem [47, 48, 49, 50, 52, 55, 67, 68, 70]. In addition, the performance of multiple-input signal processing depends on the amount of channel information. Therefore, excellent synchronization and channel estimation are essential to fully exploit the advantages of MISO-OFDM and MIMO-OFDM systems.

In [76], a training sequence arrangement based on modulatable orthogonal sequences (MOS) for MIMO-OFDM systems was proposed to synchronize different transmit antennas. However, the mutual interference among training sequences transmitted by different transmit antennas becomes more severe when the number of transmit antennas increases, and the synchronization performance degrades correspondingly. In [77], a joint fine time synchronization and channel estimation scheme based on a non-overlapping training sequence arrangement was proposed. Although the proposed training sequence

arrangement is free from mutual interference, the time-division alignment of training sequence decreases the system efficiency. In [78], a joint fine time synchronization and channel estimation approach based on a unique MOS was proposed. The mutual interference among different training sequences is eliminated because of a careful training sequence arrangement. This joint approach relies on a threshold to identify the first significant tap using the estimated CIRs. However, the threshold has to be determined in a trial-and-error manner. In [79], a joint timing synchronization and channel estimation approach based on the same training sequence arrangement was proposed. First, the optimal and suboptimal threshold factors are derived by analyzing the pdfs of the cross-correlation function outputs in Rayleigh and Ricean fading channels. Then, a majority vote refinement approach based on the timing estimates was also proposed for fine time adjustment in MIMO systems. However, these derived optimal and suboptimal threshold factors could be determined only when SNR exceeds 0dB, and this joint approach is not suitable for MISO systems.

This chapter develops a joint timing synchronization and channel estimation algorithm suitable for downlink MISO and MIMO networks based on a time-domain training sequence arrangement in the short-range wireless transmission environment. In this chapter, we first obtain a coarse timing estimate using the cross-correlation function outputs based on the proposed training sequences at each receive antenna, and then apply the generalized ML algorithm to find the advanced timing, relative timing indices, and the corresponding CIR estimates. Finally, the designed metric based on the

MMSE criterion is utilized to perform fine time adjustment. Simulation results verify the effectiveness of our proposed algorithm. This chapter is based on our publication in [45]. This chapter addresses synchronization and channel estimation aspects of a multiple transmit antenna system whereas [44] only considered those of a single transmit antenna system.

This chapter is organized as follows. Section 4.2 describes the system model. In Section 4.3, a joint fine time synchronization and channel estimation scheme for communication systems with multiple transmit antennas is presented. Simulation results are provided in Section 4.4. Finally, Section 4.5 concludes this chapter.

4.2 System Description

In this chapter, we consider a centralized multiple-input OFDM-based communication system, which means the transmit antennas are co-located on a single device. Moreover, receive antennas are not required to be co-located on a single device. Consider a multiple-input communication system that is formed by N_T transmit antennas and N_R receive antennas, where $N_T > 1$ and $N_R \geq 1$. The training sequence arrangement used to assist joint timing synchronization and channel estimation is shown in Fig. 4.1, where the training sequence assigned to each transmit antenna is composed of two identical PN sequences and a guard interval. The reason why we utilize the PN sequences in the proposed training sequence arrangement is that sequences are easily generated to specify different transmit antennas.

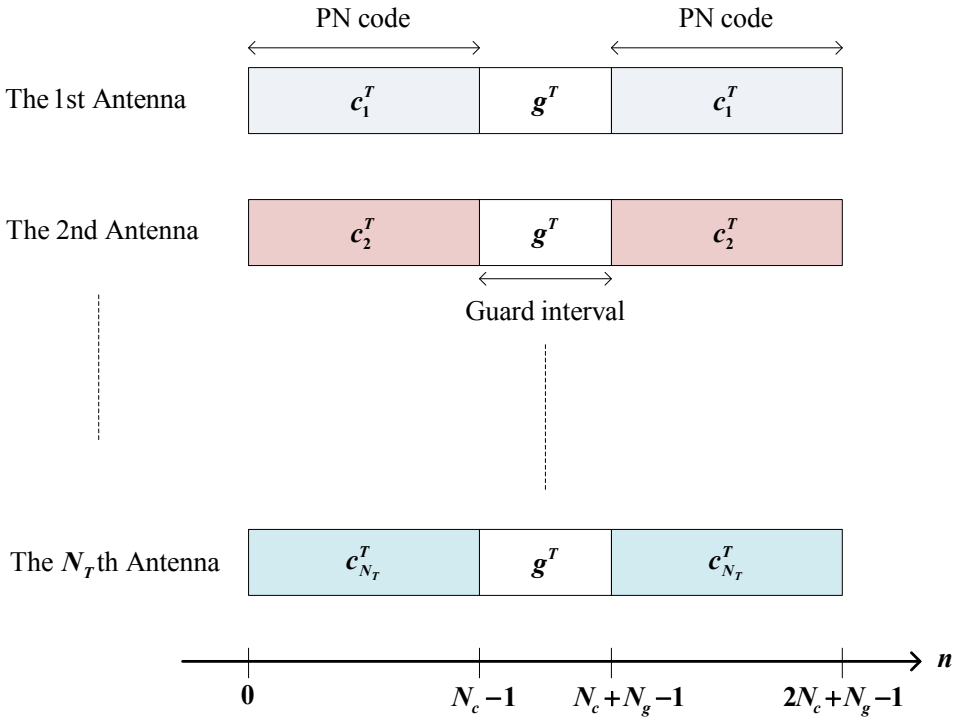

Figure 4.1: The proposed training sequence arrangement for multiple-input systems.

Let $\mathbf{p}_{\alpha_1}^T = p_{\alpha_1}(n)$ and $\mathbf{p}_{\alpha_2}^T = p_{\alpha_2}(n)$ denote training sequences assigned to the α_1th transmit antenna and the α_2th transmit antenna, respectively, where $\mathbf{p}_{\alpha_1}^T = [\mathbf{c}_{\alpha_1}^T\ \mathbf{g}^T\ \mathbf{c}_{\alpha_1}^T]$, $\mathbf{p}_{\alpha_2}^T = [\mathbf{c}_{\alpha_2}^T\ \mathbf{g}^T\ \mathbf{c}_{\alpha_2}^T]$, $n \in \{0, 1, \ldots, 2N_c + N_g - 1\}$, $\mathbf{c}_{\alpha_1}^T$ and $\mathbf{c}_{\alpha_2}^T$ are the corresponding PN sequences, $\mathbf{g}^T$ is the guard interval, N_c is the length of $\mathbf{c}_{\alpha_1}^T$ and $\mathbf{c}_{\alpha_2}^T$, N_g is the length of $\mathbf{g}^T$, and $N_g \geq 0$. In order to eliminate the mutual interference from different transmit antennas, the cross-correlation values between different assigned PN sequences are zero, i.e.,

$$\mathbf{c}_{\alpha_1}^T \cdot \mathbf{c}_{\alpha_2} = 0,\ \forall \alpha_1 \neq \alpha_2,\ \alpha_1, \alpha_2 \in \{1, 2, \ldots, N_T\}. \tag{4.1}$$

Consider the transmitted packet at the ith transmit antenna $\mathbf{s}_i^T = [\mathbf{p}_i^T\ \mathbf{x}_i^T] = \{s_i(n), \forall n \in \Omega\}$, where $\mathbf{x}_i^T$ consists of m OFDM symbols, the length of $\mathbf{x}_i^T$ is $m \cdot (N + N_{CP})$, N represents the number of subcarriers in the OFDM system, N_{CP} denotes the length of cyclic prefix, m is a positive integer, and $\Omega = \{0, 1, \cdots, m \cdot (N + N_{CP}) + 2N_c + N_g - 1\}$. Assume cyclic prefix in each OFDM symbol and guard interval in $\mathbf{p}_i^T$ are longer than the maximum delay spread of the channel, and the path delays in the channels are sample-spaced. Therefore, the received signal at the bth receiver can be expressed as

$$r_b(n) = e^{\frac{j2\pi\epsilon_b n}{N}} \sum_{i=1}^{N_T} \sum_{k=0}^{K-1} h_{ib}(k) s_i(n - \tau_b - k) + w(n), \tag{4.2}$$

where $b \in \{1, \ldots, N_R\}$, ϵ_b is the CFO normalized to the OFDM subcarrier spacing, τ_b is the timing offset from all transmit antennas to the bth receive antenna, $h_{ib}(k)$ represents the kth tap CIR from the ith transmitter to the bth receiver, K is the number of taps in the channel, and $w(n)$ is a complex AWGN sample. Based on the proposed training

arrangement, if $N_g \geq K$, the training sequences are free of ISI caused by multipath fading channels. In addition, during each packet transmission, all channels are assumed to be slow time-varying channels, and the upper bounds for $2N_c + N_g$ and N_g are

$$T_s \cdot \{2N_c + N_g + m \cdot (N + N_{CP})\} \ll T_{coh} \tag{4.3}$$

$$2N_c + N_g << \frac{T_{coh}}{T_s} - m \cdot (N + N_{CP}) \tag{4.4}$$

$$N_g << \frac{T_{coh}}{T_s} - m \cdot (N + N_{CP}) - 2N_c, \tag{4.5}$$

where T_s and T_{coh} represent the sample duration and the coherent time in channels, respectively. From Equation (4.5), the length of guard interval is bounded by

$$K \leq N_g << \frac{T_{coh}}{T_s} - m \cdot (N + N_{CP}) - 2N_c. \tag{4.6}$$

Therefore, the optimal bound for the length of training sequences, $\{\mathbf{p}_i^T, \forall i\}$, is

$$2N_c + K \leq 2N_c + N_g << \frac{T_{coh}}{T_s} - m \cdot (N + N_{CP}). \tag{4.7}$$

4.3 The Proposed Approach

The state diagram of the proposed approach is shown in Fig. 4.2. In Fig. 4.2, the proposed approach consists of three blocks. In this section, we will thoroughly explain the mechanism in each block.

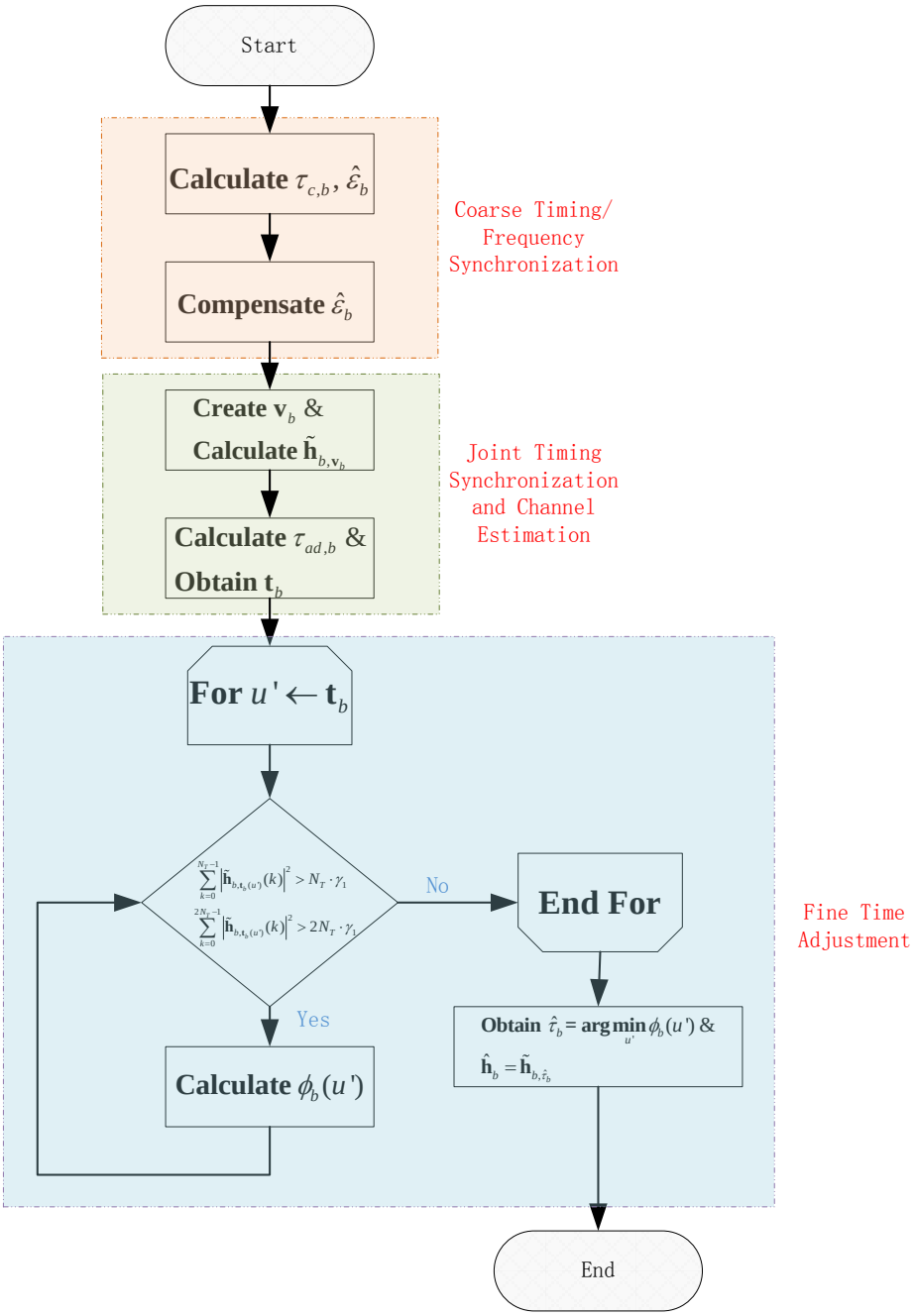

Figure 4.2: The state diagram of the proposed approach.

4.3.1 Coarse Timing and Frequency Synchronization

It can be easily observed that the proposed training sequence is composed of two identical parts. Therefore, a coarse timing estimate at the bth receiver $\tau_{c,b}$ is obtained based on the cross-correlation function outputs as follows:

$$\begin{aligned} \tau_{c,b} &= \arg\max_{d\in\Omega_d}\{|M_b(d)|\} \\ M_b(d) &= \sum_{n=0}^{N_c-1} \frac{r_b^*(n+d)r_b(n+N_c+N_g+d)}{N_c}, \end{aligned} \tag{4.8}$$

where $r_b^*(n)$ denotes the complex conjugate of $r_b(n)$, $|r_b(n)|$ represents the absolute value of $r_b(n)$, Ω_d is the observation interval, $\Omega_d = \{0, 1, \ldots, D-1\}$, and D is the length of observation interval. From Equation (4.2) and Equation (4.8), $M_b(d)$ will give a maximum value of almost one when d is at the delayed timing of the LOS path in multipath fading channels. Then the estimated CFO $\hat{\epsilon}_b$ is

$$\hat{\epsilon}_b = \frac{N}{2\pi(N_c+N_g)} \tan^{-1}\left(\frac{\Im\{M_b(\tau_{c,b})\}}{\Re\{M_b(\tau_{c,b})\}}\right), \tag{4.9}$$

where $\Re\{x\}$ and $\Im\{x\}$ describe the real and the imaginary parts of x, respectively. After coarse frequency synchronization, the CFO-compensated received signal at the bth receiver is

$$\begin{aligned} &\hat{r}_b(n) \\ &= r_b(n)\cdot e^{\frac{-j2\pi(\epsilon_b+\Delta\epsilon_b)n}{N}} \\ &= e^{\frac{-j2\pi(\Delta\epsilon_b n)}{N}} \sum_{i=1}^{N_T}\sum_{k=0}^{K-1} h_{ib}(k)s_i(n-\tau_b-k) + \hat{w}(n), \end{aligned} \tag{4.10}$$

where $\Delta\epsilon_b = \hat{\epsilon}_b - \epsilon_b$ denotes the residual CFO and $\hat{w}(n) = w(n)e^{\frac{-j2\pi(\epsilon_b+\Delta\epsilon_b)n}{N}}$.

4.3.2 Generalized Maximum-likelihood based Channel Estimation

Assume there is no timing offset and CFO in Equation (4.2), the received training sequence at the bth receiver can be expressed as

$$\mathbf{r}_b = \mathbf{S}\mathbf{h}_b + \mathbf{w}, \tag{4.11}$$

where

$$\mathbf{r}_b = [r_b(0)\ r_b(1)\ \cdots\ r_b(N'-1)]^T, \tag{4.12}$$

$$\mathbf{S} = (\mathbf{S}_0\ \mathbf{S}_1\ \cdots\ \mathbf{S}_{K-1}), \tag{4.13}$$

$$\mathbf{S}_0 = \begin{pmatrix} p_1(0) & \cdots & p_{N_T}(0) \\ p_1(1) & \cdots & p_{N_T}(1) \\ \vdots & \vdots & \vdots \\ p_1(N'-1) & \cdots & p_{N_T}(N'-1) \end{pmatrix}, \tag{4.14}$$

$$\mathbf{S}_0 = \begin{pmatrix} 0 & \cdots & 0 \\ p_1(0) & \cdots & p_{N_T}(0) \\ \vdots & \vdots & \vdots \\ p_{N_T}(N'-2) & \cdots & p_{N_T}(N'-2) \end{pmatrix}, \tag{4.15}$$

$$\mathbf{S}_{K-1} = \begin{pmatrix} 0_{(K-1)\times 1} & \cdots & 0_{(K-1)\times 1} \\ p_1(0) & \cdots & p_{N_T}(0) \\ \vdots & \vdots & \vdots \\ p_1(N'-K) & \cdots & p_{N_T}(N'-K) \end{pmatrix}, \tag{4.16}$$

$$\mathbf{h}_b = [h_{1b}(0) \ \cdots \ h_{N_T b}(0) \ h_{1b}(1) \ \cdots \ h_{N_T b}(1) \ \cdots \ h_{1b}(K-1) \ \cdots \ h_{N_T b}(K-1)]^T, \tag{4.17}$$

$$\mathbf{w} = [w(0) \ w(1) \ \cdots \ w(N'-1)]^T, \tag{4.18}$$

$N' = 2N_c + N_g$, $\mathbf{w} \sim N(0_{N'\times 1}, \sigma_w^2 \mathbf{I}_{N'\times N'})$, $\mathbf{I}_{N'\times N'}$ is a $N' \times N'$ identity matrix, $\{w(n), \ \forall n\}$ is independent identically distributed, and $h_{ib}(k)$ is the kth tap CIR from the ith transmit antenna to the bth receive antenna. In Equation (4.17), $\mathbf{h}_b$ contains different CIRs from all transmit antennas. In general, the received training sequence is

$$\mathbf{r}_b(\tau) = [r_b(\tau) \ r_b(\tau+1) \ \cdots \ r_b(\tau+N'-1)]^T, \tag{4.19}$$

where Equation (4.12) is a special case of Equation (4.19) when $\tau = 0$ and $\epsilon_b = 0$. Then, the likelihood function is given by

$$\Lambda(\mathbf{h}_b) = \frac{1}{(\pi\sigma_w^2)^{N'}} exp\{\frac{-1}{\sigma_w^2} \|\mathbf{r}_b(\tau) - \mathbf{\Gamma}(\epsilon_b)\mathbf{S}\mathbf{h}_b\|^2\}, \tag{4.20}$$

and the ML estimate of $\mathbf{h}_b$ can be obtained by

$$\begin{aligned}\hat{\mathbf{h}}_{b,ML} &= \arg\max_{\mathbf{h}_b} \Lambda(\mathbf{h}_b) \\ &= (\mathbf{S}^H\mathbf{S})^{-}\mathbf{S}^H\mathbf{\Gamma}^H(\epsilon_b)\mathbf{r}_b(\tau) \\ &= \mathbf{S}^\dagger\mathbf{\Gamma}^H(\epsilon_b)\mathbf{r}_b(\tau),\end{aligned} \tag{4.21}$$

where $\mathbf{A}^H$ is the Hermitian of $\mathbf{A}$, $\mathbf{B}^-$ is the generalized inverse of $\mathbf{B}$, $\mathbf{S}^\dagger$ is the Moore-Penrose pseudo-inverse of $\mathbf{S}$,

$$\mathbf{\Gamma}(\epsilon_b) = diag(e^{\frac{j2\pi\epsilon_b\tau}{N}}, e^{\frac{j2\pi\epsilon_b(\tau+1)}{N}}, \cdots, e^{\frac{j2\pi\epsilon_b(\tau+N'-1)}{N}}), \tag{4.22}$$

and $diag(\cdot)$ represents a diagonal matrix. For fixed PN sequences $\mathbf{c}_i$, $\forall i \in \{1, \ldots, N_T\}$, we only need to compute $\mathbf{S}^\dagger$ once, and different CIR estimates can be obtained simply by multiplying the received training sequence at each receiver with $\mathbf{S}^\dagger$.

4.3.3 Joint Timing Synchronization and Channel Estimation

In this subsection, we utilize coarse timing estimate and CIR estimate based on the generalized ML criterion to develop a joint timing synchronization and channel estimation algorithm. After coarse timing synchronization, a SOV $\mathbf{v}_b$ at the bth receiver is applied to obtain an advanced timing, relative timing indices, and the corresponding CIR estimates, where

$$\begin{aligned}\mathbf{v}_b^T &= [\tau_{c,b} + L \ \cdots \ \tau_{c,b} + 1 \ \tau_{c,b} \ \tau_{c,b} - 1 \ \cdots \ \tau_{c,b} - L] \\ &= \{v_b(l_1), \ \forall l_1 \in \Omega_{v_b}\},\end{aligned} \tag{4.23}$$

$\Omega_{v_b} = \{0, 1, \cdots, 2L\}$, the length of observation interval is $2L + 1$, and L is a positive integer without any constraint. In Equation (4.23), $\mathbf{v}_b$ consists of $2L+1$ timing indices. Based on these timing indices in $\mathbf{v}_b$, the corresponding CIR estimates with K' taps are obtained by Equation (4.21), where

$$\tilde{\mathbf{h}}_{b,v_b(l_1)} = \tilde{\mathbf{S}}^{\dagger}\hat{\mathbf{r}}_b(v_b(l_1)), \tag{4.24}$$

$$\begin{aligned}\tilde{\mathbf{h}}_{b,v_b(l_1)} = [&\tilde{h}_{1b,v_b(l_1)}(0) \ \cdots \ \tilde{h}_{N_T b,v_b(l_1)}(0) \ \tilde{h}_{1b,v_b(l_1)}(1) \ \cdots \ \tilde{h}_{N_T b,v_b(l_1)}(1) \ \cdots \\ &\tilde{h}_{1b,v_b(l_1)}(K'-1) \ \cdots \ \tilde{h}_{N_T b,v_b(l_1)}(K'-1)]^T,\end{aligned} \tag{4.25}$$

$$\tilde{\mathbf{S}} = \left(\tilde{\mathbf{S}}_0 \ \tilde{\mathbf{S}}_1 \ \cdots \ \tilde{\mathbf{S}}_{K'-1}\right), \tag{4.26}$$

$$\tilde{\mathbf{S}}_0 = \begin{pmatrix} p_1(0) & \cdots & p_{N_T}(0) \\ p_1(1) & \cdots & p_{N_T}(1) \\ \vdots & \vdots & \vdots \\ p_1(N'-1) & \cdots & p_{N_T}(N'-1) \end{pmatrix}, \tag{4.27}$$

$$\tilde{\mathbf{S}}_1 = \begin{pmatrix} 0 & \cdots & 0 \\ p_1(0) & \cdots & p_{N_T}(0) \\ \vdots & \vdots & \vdots \\ p_{N_T}(N'-2) & \cdots & p_{N_T}(N'-2) \end{pmatrix}, \tag{4.28}$$

$$\tilde{\mathbf{S}}_{K'-1} = \begin{pmatrix} 0_{(K'-1)\times 1} & \cdots & 0_{(K'-1)\times 1} \\ p_1(0) & \cdots & p_{N_T}(0) \\ \vdots & \vdots & \vdots \\ p_1(N'-K') & \cdots & p_{N_T}(N'-K') \end{pmatrix}, \tag{4.29}$$

$$\begin{aligned} &\hat{\mathbf{r}}_b(v_b(l_1)) = \\ &[\hat{r}_b(v_b(l_1))\ \hat{r}_b(v_b(l_1)+1)\ \cdots\ \hat{r}_b(v_b(l_1)+N'-1)]^T, \end{aligned} \tag{4.30}$$

$\forall l_1 \in \Omega_{v_b}$, $\tilde{\mathbf{h}}_{b,v_b(l_1)}$ is the CIR estimate corresponding to the time index $v_b(l_1)$, and $\tilde{h}_{ib,v_b(l_1)}(k)$ is the estimated $(k+1)$th tap CIR from the ith transmit antenna to the bth receive antenna corresponding to the time index $v_b(l_1)$. In order to avoid any loss of the channel information, K' should be at least equal to or greater than K.

If $N_g \geq K$, $\tilde{\mathbf{h}}_{b,v_b(l_1)}$ can be obtained in an efficient way by averaging two channel estimates, $\bar{\mathbf{h}}_{A,v_b(l_1)}$ and $\bar{\mathbf{h}}_{B,v_b(l_1)}$, where

$$\begin{aligned} \bar{\mathbf{h}}_{A,v_b(l_1)} &= \bar{\mathbf{S}}^{\dagger}\bar{\mathbf{r}}_b(v_b(l_1)), \\ \bar{\mathbf{h}}_{B,v_b(l_1)} &= \bar{\mathbf{S}}^{\dagger}\bar{\mathbf{r}}_b(v_b(l_1)+N_c+N_g), \\ \tilde{\mathbf{h}}_{b,v_b(l_1)} &= \frac{\bar{\mathbf{h}}_{A,v_b(l_1)} + \bar{\mathbf{h}}_{B,v_b(l_1)}}{2}, \end{aligned} \tag{4.31}$$

$$\begin{aligned} &\bar{\mathbf{r}}_b(v_b(l_1)) = \\ &[\hat{r}_b(v_b(l_1))\ \hat{r}_b(v_b(l_1)+1)\ \cdots\ \hat{r}_b(v_b(l_1)+N_c-1)]^T, \end{aligned} \tag{4.32}$$

$$\bar{\mathbf{r}}_b(v_b(l_1)+N_c+N_g) = \\ [\hat{r}_b(v_b(l_1)+N_c+N_g)\ \hat{r}_b(v_b(l_1)+N_c+N_g+1)\ \cdots\ \hat{r}_b(v_b(l_1)+N'-1)]^T, \tag{4.33}$$

and

$$\bar{\mathbf{S}} = \left(\bar{\mathbf{S}}_0\ \bar{\mathbf{S}}_1\ \cdots\ \bar{\mathbf{S}}_{K'-1}\right). \tag{4.34}$$

$$\bar{\mathbf{S}}_0 = \begin{pmatrix} p_1(0) & \cdots & p_{N_T}(0) \\ p_1(1) & \cdots & p_{N_T}(1) \\ \vdots & \vdots & \vdots \\ p_1(N_c-1) & \cdots & p_{N_T}(N_c-1) \end{pmatrix}. \tag{4.35}$$

$$\bar{\mathbf{S}}_1 = \begin{pmatrix} 0 & \cdots & 0 \\ p_1(0) & \cdots & p_{N_T}(0) \\ \vdots & \vdots & \vdots \\ p_{N_T}(N_c-2) & \cdots & p_{N_T}(N_c-2) \end{pmatrix}. \tag{4.36}$$

$$\bar{\mathbf{S}}_{K'-1} = \begin{pmatrix} 0_{(K'-1)\times 1} & \cdots & 0_{(K'-1)\times 1} \\ p_1(0) & \cdots & p_{N_T}(0) \\ \vdots & \vdots & \vdots \\ p_1(N_c-K') & \cdots & p_{N_T}(N_c-K') \end{pmatrix}. \tag{4.37}$$

After we obtain $2L+1$ CIR estimates, the advanced timing at the bth receiver $\tau_{ad,b}$ is given by

$$\tau_{ad,b} = \arg \max_{v_b(l_1),\ l_1\in\Omega_{v_b}} \sum_{k=0}^{2N_T-1} |\tilde{\mathbf{h}}_{b,v_b(l_1)}(k)|, \tag{4.38}$$

where $\tilde{\mathbf{h}}_{b,v_b(l_1)}(0)$ is the first tap in Equation (4.25). Then, relative timing indices in the modified SOV $\mathbf{t}_b^T$ and the corresponding CIR estimates $\tilde{\mathbf{h}}_{b,t_b(l_2)}$ are fed forward to perform fine time adjustment, where

$$\mathbf{t}_b^T = [\tau_{ad,b}\ \tau_{ad,b} - 1\ \cdots\ \tau_{c,b} - L] = \{t_b(l_2),\ l_2 \in \Omega_{t_b}\}, \tag{4.39}$$

and $\Omega_{t_b} = \{0, 1, \cdots, \tau_{ad,b} - \tau_{c,b} + L\}$.

4.3.4 Fine Time Adjustment

In this subsection, we exploit the MMSE criterion to perform fine time adjustment in an iterative manner based on the information of relative timing indices and the corresponding CIR estimates. First, two thresholds on the sum of the first N_T tap powers $N_T \cdot \gamma_1$ and the sum of the first $2N_T$ tap powers $2N_T \cdot \gamma_1$ are chosen in order to eliminate the AWGN effect and to reduce the computational complexity, where γ_1 should be less than the tap power of the first path in the channel model. In other words, if $\sum_{k=0}^{N_T-1} |\tilde{\mathbf{h}}_{b,\tau_{ad,b}-1}(k)|^2 < N_T \cdot \gamma_1$ or $\sum_{k=0}^{2N_T-1} |\tilde{\mathbf{h}}_{b,\tau_{ad,b}-1}(k)|^2 < 2N_T \cdot \gamma_1$, $\tau_{ad,b}$ is the estimated timing offset; otherwise, the algorithm keeps running until $\sum_{k=0}^{N_T-1} |\tilde{\mathbf{h}}_{b,t_b(f)}(k)|^2 < N_T \cdot \gamma_1$ or $\sum_{k=0}^{2N_T-1} |\tilde{\mathbf{h}}_{b,t_b(f)}(k)|^2 < 2N_T \cdot \gamma_1$ for some f, where $f \in \Omega_{t_b}$.

Let $\mathbf{q}_{t_b(l_2)}^T$ denote the convolution of the training sequence and the corresponding CIR estimate $\tilde{\mathbf{h}}_{b,t_b(l_2)}^T$, where

$$\mathbf{q}_{t_b(l_2)}^T = \sum_{i=1}^{N_T} \mathbf{p}_i^T * \tilde{\mathbf{h}}_{ib,t_b(l_2)}^T, \tag{4.40}$$

$$\tilde{\mathbf{h}}^{T}_{ib,t_b(l_2)} = [\tilde{h}_{ib,t_b(l_2)}(0)\ \tilde{h}_{ib,t_b(l_2)}(1)\ \cdots\ \tilde{h}_{ib,t_b(l_2)}(K'-1)], \tag{4.41}$$

and $\tilde{\mathbf{h}}^{T}_{ib,t_b(l_2)}$ is the CIR estimate from the ith transmit antenna to the bth receive antenna. Then, the MSE of the timing index $t_b(l_2)$ is given by

$$\phi_b(t_b(l_2)) = \sum_{n=0}^{2N_c+N_g+K'-1} |\hat{\mathbf{r}}_b(t_b(l_2)+n) - \mathbf{q}_{t_b(l_2)}(n)|^2. \tag{4.42}$$

Thus, the estimated timing offset can be obtained by solving

$$\begin{aligned} &\min\ \phi_b(t_b(l_2)) \\ &s.t.\ \sum_{k=0}^{N_T-1} |\tilde{\mathbf{h}}_{b,t_b(u')}(k)|^2 > N_T \cdot \gamma_1, \\ &\quad \sum_{k=0}^{2N_T-1} |\tilde{\mathbf{h}}_{b,t_b(u')}(k)|^2 > 2N_T \cdot \gamma_1. \end{aligned} \tag{4.43}$$

From Equation (4.40), Equation (4.42), and reasonable CIR estimates, we have

$$\phi_b(\tau_b + \delta) > \phi_b(\tau_b), \tag{4.44}$$

where $\delta \neq 0$, δ is an integer, and $\tau_b + \delta \in \mathbf{t}_b^T$. Consider a set $\Omega_U = \{0, 1, \cdots, u-1\}$ composed of consecutive timing indices that satisfy the following conditions:

$$\begin{cases} \sum_{k=0}^{N_T-1} |\tilde{\mathbf{h}}_{b,t_b(u')}(k)|^2 > N_T \cdot \gamma_1, \\ \sum_{k=0}^{2N_T-1} |\tilde{\mathbf{h}}_{b,t_b(u')}(k)|^2 > 2N_T \cdot \gamma_1, \\ \forall u' \in \Omega_U. \end{cases} \tag{4.45}$$

Then, the estimated timing offset $\hat{\tau}_b$ and the CIR estimate $\hat{\mathbf{h}}_b$ at the bth receiver based

on the thresholds and Equation (4.42) can be expressed as

$$\begin{cases} \hat{\tau}_b = \arg\min_{t_b(u'),\ u' \in \Omega_U} \phi_b(t_b(u')) \\ \hat{\mathbf{h}}_b = \tilde{\mathbf{h}}_{b,\hat{\tau}_b}. \end{cases} \tag{4.46}$$

The detailed procedure of fine time adjustment is described in **Algorithm** 3.

Algorithm 3 *Fine Time Adjustment*

Initial Inputs: $\mathbf{t}_b^T$, $\tilde{\mathbf{h}}_{b,\mathbf{t}_b^T}$

for $m = 0$ **to** $\tau_{ad,b} - \tau_{c,b} + L$ **do**
  if $\sum_{k=0}^{N_T-1} |\tilde{\mathbf{h}}_{b,t_b(m)}(k)|^2 > N_T \cdot \gamma_1$ and $\sum_{k=0}^{2N_T-1} |\tilde{\mathbf{h}}_{b,t_b(m)}(k)|^2 > 2N_T \cdot \gamma_1$ **then**
    Calculate $\phi_b(t_b(m))$
  else
    u = m
    break
  end if
end for
$\hat{\tau}_b = \arg\min_{t_b(u'),\ u' \in \{0,1,\cdots,u-1\}} \phi_b(t_b(u'))$
$\hat{\mathbf{h}}_b = \tilde{\mathbf{h}}_{b,\hat{\tau}_b}$

4.4 Simulation Results

Packet-based $N_T \times N_R$ MIMO-OFDM systems were used for simulations, where each packet consists of a training sequence followed by 34 random OFDM data symbols. In this chapter, we mainly consider 2×2 and 3×3 MIMO-OFDM systems, where $N_T \times N_R = 2 \times 2$ and $N_T \times N_R = 3 \times 3$. Gold code is selected to be the pseudo-noise sequences used in the proposed training sequence arrangement with the spreading factor equal to 1. The training sequence of each packet is 80 identical samples at

each transmitter, where $N_c = 32$ and $N_g = 16$. The structure of OFDM data symbols follows the IEEE 802.11a standard defined in [51], where $N = 64$ and $N_{CP} = 16$. QPSK modulation was adopted in simulations.

The power profiles of different channel models used in simulation are summarized in Table 4.1, where σ_i^2 represents the $(i+1)$th tap power in the corresponding channel. Different fading channels (Rayleigh, Ricean, and Nakagami) would not affect the results, because tap powers in the channel models have been defined in Table 4.1. Channel Models I and II (CH I and CH II) represent multipath fading channels with NLOS propagation, and Channel Model III (CH III) is a typical multipath fading channel with LOS propagation. For CH I, the power of second tap dominates all channel taps. As for CH II, the third tap has the strongest power in the channel, and it is the worst channel model to evaluate the timing synchronization performance in this chapter. Moreover, all channels are assumed to be quasi-stationary during each packet transmission. In this chapter, all transmit-receive links follow the same channel model.

Table 4.1: The Power Profiles of Different Channel Models

	CH I (NLOS)	CH II (NLOS)	CH III (LOS)
σ_0^2	0.1232	0.1285	0.7211
σ_1^2	0.7711	0.2223	0.2338
σ_2^2	0.1029	0.6000	0.0420
σ_3^2	0.0015	0.0478	0.0022
σ_4^2	0.0001	0.0010	0.0006
σ_5^2	0.0002	0.0001	0.0001

The main motivation of this chapter is to achieve perfect timing synchronization in very low SNR environments. The parameters L and K' related to the observation interval in joint timing synchronization and channel estimation are set to be 50 and 6, respectively. Therefore, the number of possible relative timing indices for fine time adjustment in our proposed approach is approximately equal to 50. For comparison, the designed maximum channel delay spread for fine time adjustment used in [78] is set to be 20 samples. In addition, the coarse timing estimate in the proposed approach is provided to [78] before the joint timing synchronization and channel estimation scheme is performed.

Fig. 4.3 shows the averaged bias of coarse timing estimate ($E[\hat{\tau}_c - \tau]$) based on our proposed algorithm at each receive antenna. In Fig. 4.3, the averaged biases of

coarse timing estimates in CH I and CH II are greater than 1, and the averaged biases of coarse timing estimate in CH III are approximately equal to 0. Simulation results show that the proposed algorithm provides good initial values for further process of timing synchronization. In addition, constant CFOs (ϵ_b) equal to 0.5 are introduced to demonstrate the performance of CFO estimator. The MSEs of estimated CFOs ($|\hat{\epsilon}_b - \epsilon_b|^2$) in all channel models are listed in Table 4.2. Simulation results in Table 4.2 indicate that the residual CFO ($\Delta\epsilon_b = \hat{\epsilon}_b - \epsilon_b$) can be modeled as a random variable that is uniformly distributed within $[-0.04,\ 0.04]$. Fig. 4.3 and Table 4.2 demonstrate that our proposed algorithm has excellent coarse timing and frequency synchronization performance.

Table 4.2: The Mean Squared Error of Coarse Frequency Offset Estimator at Each Receive Antenna

	SNR=-5dB	SNR=-3dB	SNR=-1dB	SNR=0dB	SNR=1dB
Proposed (2×2 MIMO)	0.0011	0.0006	0.0004	0.0003	0.0002
Proposed (3×3 MIMO)	0.0012	0.0007	0.0004	0.0003	0.0003

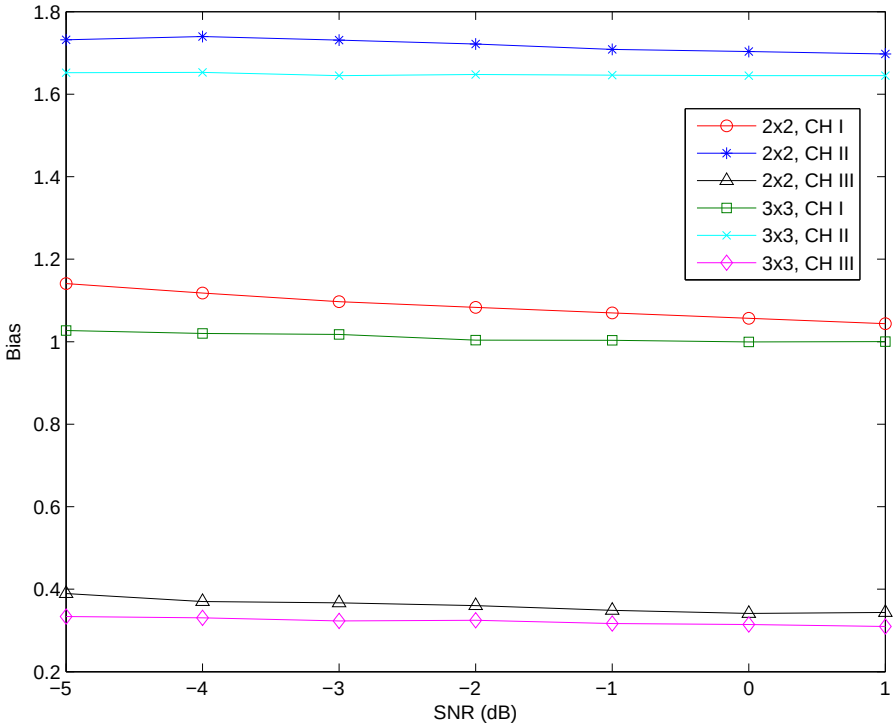

Figure 4.3: The averaged bias of coarse timing estimates, $E[\hat{\tau}_c - \tau]$.

After we discuss the coarse timing and frequency synchronization performance, the timing synchronization performance is evaluated with a residual CFO $\Delta\epsilon_b = 0.1$. We demonstrate the timing synchronization performance using the probability of perfect timing synchronization, the bias of timing estimator, and the RMSE of timing estimator. The corresponding results are reported in Fig. 4.4, Fig. 4.5, and Fig. 4.6. The perfect timing synchronization is defined as the successful acquisition of the position of the first tap in different channel models. The actual threshold used in [78] is $\alpha|\hat{h}_{max}|$, where α is a threshold factor and $|\hat{h}_{max}|$ is the strongest channel tap gain estimate. In this chapter, pre-simulations and mathematical derivations are not required to choose thresholds in fine time adjustment [49, 50, 52, 67]. Moreover, the timing synchronization performance is calculated based on the estimated timing offset at each receive antenna. In Fig. 4.4, the simulation results show that our proposed approach has better timing synchronization performance at very low SNR. In CH I, CH II, and CH III, the proposed approach achieves 99% in probability of perfect timing synchronization when SNR exceeds -3dB. As for [78], different choices in threshold factor α may cause poor timing synchronization performance. In Fig. 4.4, the maximum probability of perfect timing synchronization in [78] is less than 0.624 in CH III, where $\alpha = 0.5$. However, in this case, the probabilities of perfect timing synchronization are less than 0.25 in CH I and CH II. In addition, if we choose $\alpha = 0.25$, the probabilities of perfect timing synchronization are approximately equal to 0.5 in all channel models. Reason why the scheme [78] has

poor timing synchronization performance is that AWGN affects the entire fine time adjustment process at low SNR, especially in CH I and CH II. In addition, pre-simulations for searching a proper α are also required. Therefore, low SNR and wide interval in fine time adjustment significantly degrade the performance in [49, 50, 52, 67]. In Fig. 4.5 and Fig. 4.6, our proposed approach has better timing synchronization performance than the joint scheme [78]. In Fig. 4.5, our proposed approach performs approximately unbiased at any low SNR, and wide interval in fine time adjustment [78] leads the timing estimator to have nonzero biases. In Fig. 4.6, zero RMSE can be achieved using the proposed approach when SNR exceeds 1dB due to the ability to identify the first arrival path in all channel models; however, the joint scheme [78] still has large RMSE.

Moreover, the channel estimation performance is shown in Fig. 4.7 and Fig. 4.8. The channel estimation performance is evaluated after the estimated timing offset is obtained. In Fig. 4.7 and Fig. 4.8, the proposed approach has more consistent and better channel estimation performance in 2×2 and 3×3 MIMO systems, and the joint scheme [78] has poor channel estimation performance because of incorrect estimated timing offsets. In addition, the performance of the proposed approach is close to the Cramér-Rao bound (CRB) [80].

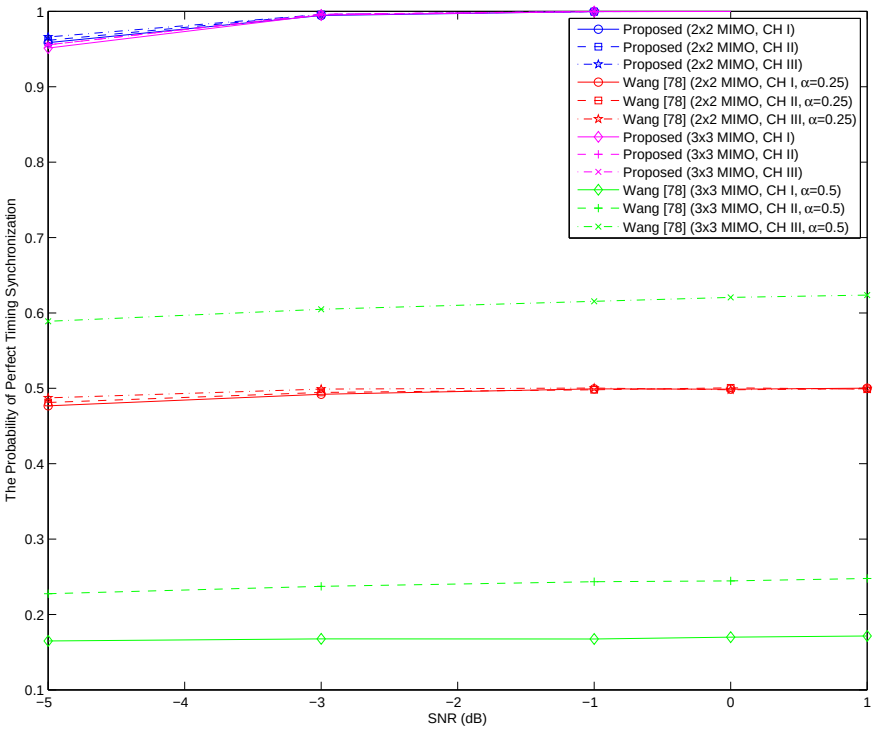

Figure 4.4: The probability of perfect timing synchronization, $prob(\tau = \hat{\tau})$.

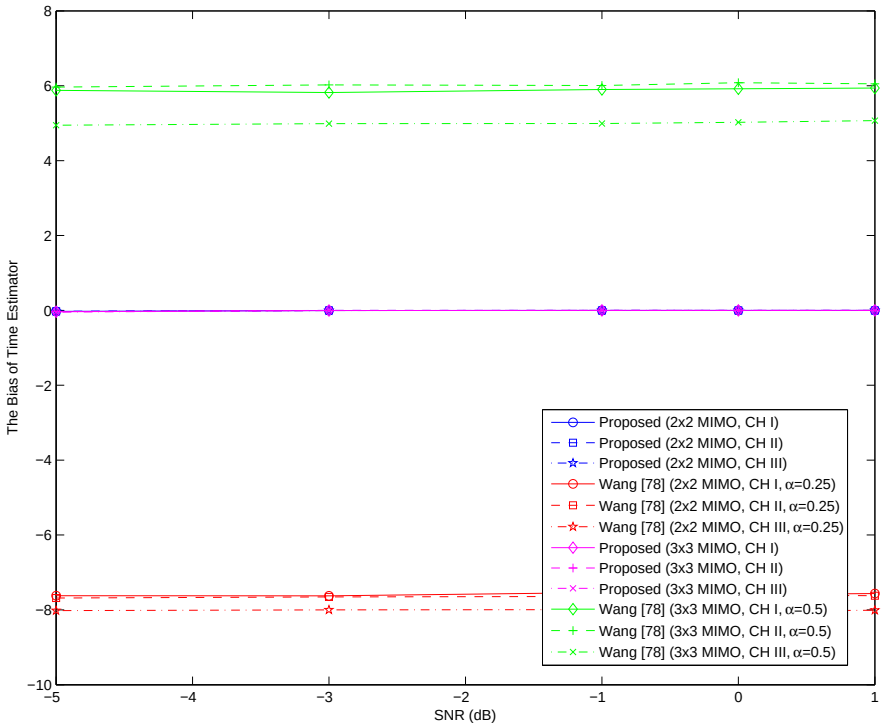

Figure 4.5: The bias of timing estimator, $E[\hat{\tau} - \tau]$.

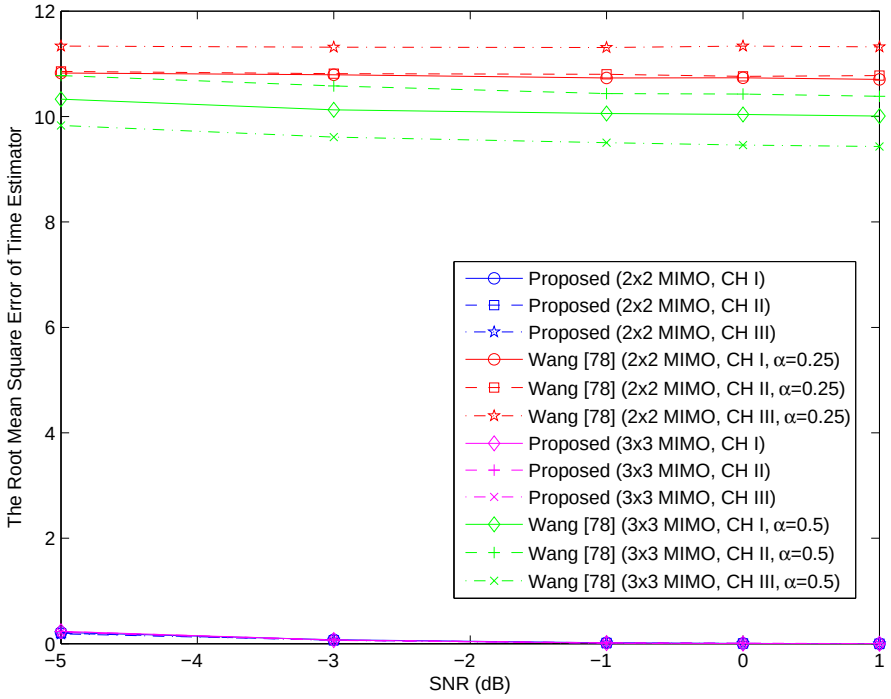

Figure 4.6: The root mean squared error of timing estimator, $\sqrt{E[|\hat{\tau} - \tau|^2]}$.

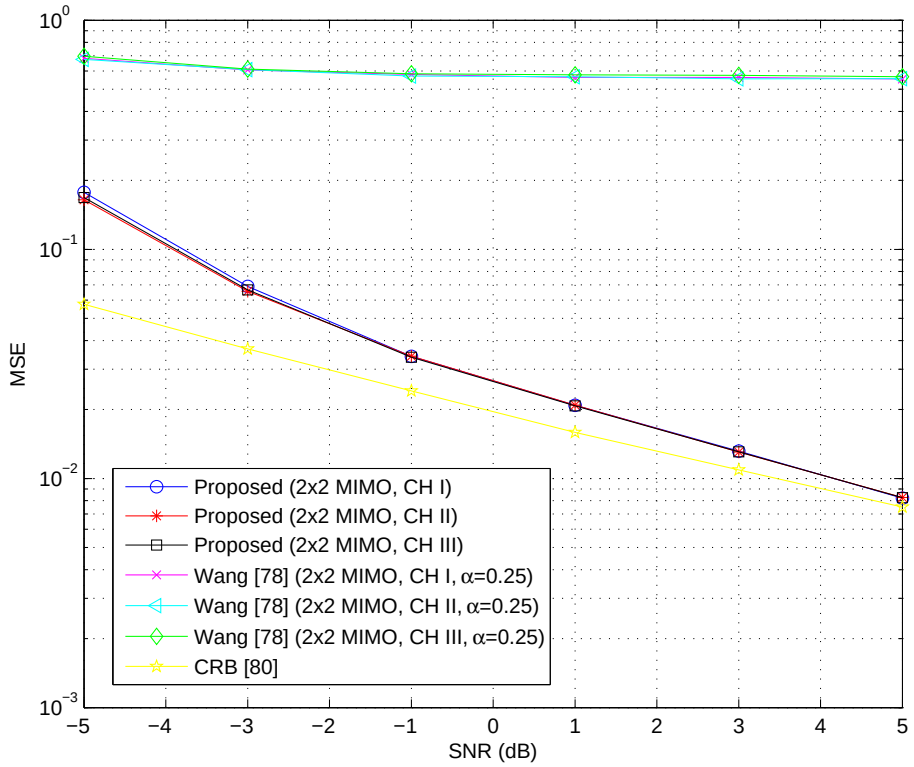

Figure 4.7: The MSE of CIR estimates for a 2x2 MIMO system.

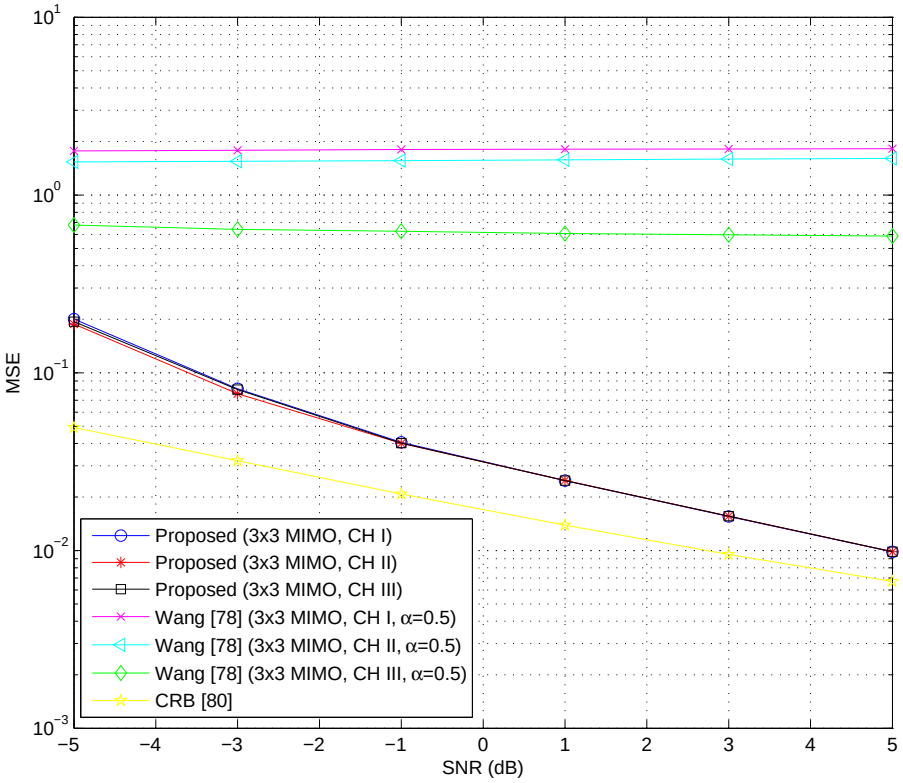

Figure 4.8: The MSE of CIR estimates for a 3x3 MIMO system.

4.5 Summary

In this chapter, we have presented a joint timing synchronization and channel estimation scheme for centralized multiple-input communication systems based on a well-designed training sequence arrangement. Simulation results show that there are no timing errors in our proposed timing estimator when SNR exceeds 0dB. In addition, the proposed approach has excellent channel estimation performance, because the proposed timing estimator has better timing synchronization performance.

Chapter 5

Variable Transmission Rate Communication Systems via Network Source Coding

5.1 Introduction

To the best of the author's knowledge, the following properties have not been demonstrated yet [34, 35, 36, 37, 38, 39, 40, 81]: 1.) the VTR OFDM-based communication systems using network source coding, and 2.) the performance improvement after applying the network source coding to OFDM systems. In this chapter, two VTR-OFDM communication systems are proposed to evaluate the performance of network source coding schemes. First, a VTR-SISO-OFDM system is presented, and the proposed 3-stage

encoder in this system generates different transmission rates. Functions implemented in this 3-stage encoder determine the codebook sizes and the achievable transmission rates. The performance of the VTR-SISO-OFDM system based on the proposed 3-stage encoder/decoder is evaluated. Then, a VTR-MB-OFDM system is proposed. The proposed VTR-MB-OFDM system transmits two correlated sources using the multiterminal source coding scheme [34, 82, 83, 84]. The transmission rates are adjusted based on four switch configurations at the transmitter, and 16 switch configurations control the information interchanges during the entire data transmission. The performance of the proposed VTR-MB-OFDM system for these 16 switch configurations is also evaluated. We then analyze the variable transmission bit rate for these two proposed VTR-OFDM communication systems. The advantages of the proposed systems include availability of different transmission rates, abilities of different users to share the network resource, and robustness in wireless communication environments. This chapter is based on our publication in [46].

The rest of the chapter is organized as follows. In Section 5.2, a VTR-SISO-OFDM communication system is proposed. A VTR-MB-OFDM system based on the multiterminal source coding scheme is introduced in Section 5.3. Performance analysis and simulation results are presented in Section 5.4. Finally, the chapter is concluded in Section 5.5.

5.2 The VTR-SISO-OFDM System

We propose a VTR-SISO-OFDM system with three different transmission rates in this section. The main goal of the proposed VTR-SISO-OFDM system is to design a VTR communication system and to recover the source data with the help of the side information. A 3-stage encoder is proposed in Section 5.2.1. In Section 5.2.2, the feasibilities of functions used in the encoder and the variable transmission rates of the proposed VTR-SISO-OFDM system are discussed. Finally, the corresponding decoder is described in Section 5.2.3.

5.2.1 The Proposed 3-stage Encoder in the VTR-SISO-OFDM System

Fig. 5.1(a) shows the 3-stage encoder in the proposed VTR-SISO-OFDM system. Let $\mathbf{a}^T$, $\mathbf{b}^T$, $\mathbf{c}^T$, and $\mathbf{d}^T$ be discrete random variables, where $\mathbf{a}^T$ is the source data, $\mathbf{b}^T$, $\mathbf{c}^T$, and $\mathbf{d}^T$ represent the side information, and $\mathbf{a}^T$, $\mathbf{b}^T$, $\mathbf{c}^T$, and $\mathbf{d}^T$ are independent. Consider the source data $\{a_i\}$ which is independently selected from the set $\{1, 2, \ldots, A\}$, where $\mathbf{a}^T = [a_1, a_2, \ldots, a_L] = \{a_i\}$, $i \in \{1, 2, \ldots, L\}$, i is the sample index, L represents the total number of transmitted symbols, the probability of $\mathbf{a}^T$ is

$$p(\mathbf{a}^T) = \prod_{i=1}^{L} p(a_i), \tag{5.1}$$

and the cardinality of $\mathbf{a}^T$ is A^L. Moreover, the length of the side information ($\mathbf{b}^T$, $\mathbf{c}^T$, and $\mathbf{d}^T$) is also L, where $\mathbf{b}^T = [b_1, b_2, \ldots, b_L] = \{b_i\}$, $\mathbf{c}^T = [c_1, c_2, \ldots, c_L] = \{c_i\}$,

$\mathbf{d}^T = [d_1, d_2, \ldots, d_L] = \{d_i\}$, the probabilities of $\mathbf{b}^T, \mathbf{c}^T$, and $\mathbf{d}^T$ are given by:

$$\begin{aligned} p(\mathbf{b}^T) &= \prod_{i=1}^{L} p(b_i) \\ p(\mathbf{c}^T) &= \prod_{i=1}^{L} p(c_i) \\ p(\mathbf{d}^T) &= \prod_{i=1}^{L} p(d_i), \end{aligned} \tag{5.2}$$

and $\{b_i\}$, $\{c_i\}$, and $\{d_i\}$ are randomly chosen from the sets $\{1, 2, \ldots, B\}$, $\{1, 2, \ldots, C\}$, and $\{1, 2, \ldots, D\}$, respectively. In Fig. 5.1(a), the output symbols $\mathbf{w}^T = \{w_i\}$, $\mathbf{k}^T = \{k_i\}$, and $\mathbf{e}^T = \{e_i\}$ are

$$\begin{aligned} w_i &= f(a_i, b_i) \in \{min(f(i_1, j_1)), \ldots, max(f(i_1, j_1))\} = \mathbf{m} \\ k_i &= g(w_i, c_i) \in \{min(g(m_{i_2}, j_2)), \ldots, max(g(m_{i_2}, j_2))\} = \mathbf{y} \\ e_i &= h(k_i, d_i) \in \{min(h(y_{i_3}, j_3)), \ldots, max(h(y_{i_3}, j_3))\} = \mathbf{o}, \end{aligned} \tag{5.3}$$

where $f(\cdot)$, $g(\cdot)$, and $h(\cdot)$ are injective or surjective functions, $i_1 \in \{1, 2, \ldots, A\}$, $j_1 \in \{1, 2, \ldots, B\}$, $i_2 \in \{1, 2, \ldots, W\}$, $j_2 \in \{1, 2, \ldots, C\}$, $i_3 \in \{1, 2, \ldots, K\}$, $j_3 \in \{1, 2, \ldots, D\}$, $\mathbf{m}$, $\mathbf{y}$, and $\mathbf{o}$ are ordered sets that contain distinct elements, and W, K, and E are the number of elements in $\mathbf{m}$, $\mathbf{y}$, and $\mathbf{o}$, respectively.

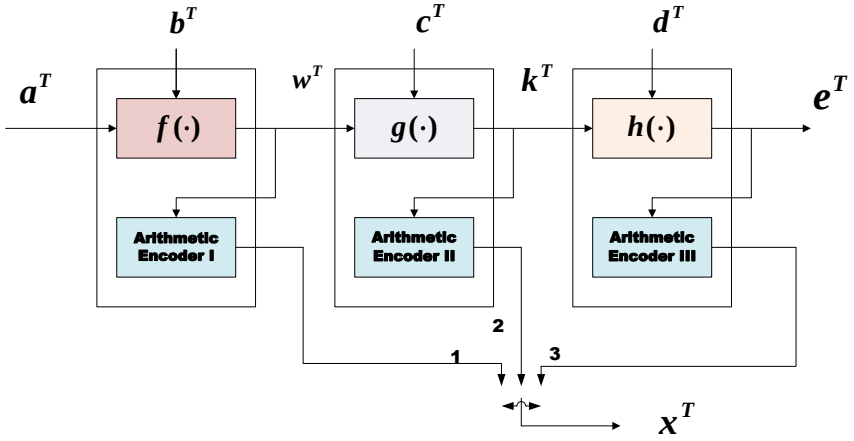

(a) The proposed 3-stage encoder.

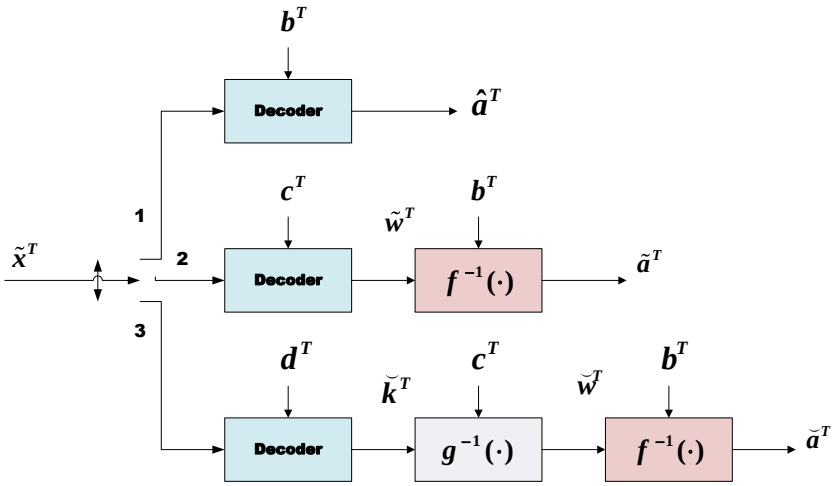

(b) The proposed 3-stage decoder.

Figure 5.1: The 3-stage encoder/decoder in the proposed VTR-SISO-OFDM system.

If $f(\cdot)$, $g(\cdot)$, and $h(\cdot)$ are injective functions, the probabilities of w_i, k_i, and e_i are given by:

$$\begin{aligned} p(w_i) &= p(f(a_i, b_i)) = p(a_i, b_i) \\ p(k_i) &= p(g(w_i, c_i)) = p(a_i, b_i, c_i) \\ p(e_i) &= p(h(k_i, d_i)) = p(a_i, b_i, c_i, d_i), \end{aligned} \tag{5.4}$$

and the corresponding entropies are

$$\begin{aligned} H(w_i) &= \sum_{i_1=1}^{A} \sum_{j_1=1}^{B} -p(f(i_1, j_1)) \cdot \log_2(p(f(i_1, j_1))) \\ H(k_i) &= \sum_{i_2=1}^{W} \sum_{j_2=1}^{C} -p(g(m_{i_2}, j_2)) \cdot \log_2(p(g(m_{i_2}, j_2))) \\ H(e_i) &= \sum_{i_3=1}^{K} \sum_{j_3=1}^{D} -p(h(y_{i_3}, j_3)) \cdot \log_2(p(h(y_{i_3}, j_3))), \end{aligned} \tag{5.5}$$

where $p(f(i_1, j_1))$ is the probability of the outcome $f(i_1, j_1)$, $p(a_i, b_i)$ is the joint probability of (a_i, b_i), m_{i_2} means the i_2th element in $\mathbf{m}$, and y_{i_3} means the i_3th element in $\mathbf{y}$. In addition, if $f(\cdot)$, $g(\cdot)$, and $h(\cdot)$ are surjective functions, the probabilities of w_i, k_i, and e_i are given by:

$$\begin{aligned} p(w_i = i_2) &= \sum_{i_1=1}^{A} p(i_1) \cdot \{ \sum_{j_1=1}^{B} p(j_1 | f(i_1, j_1) = i_2) \} \\ p(k_i = i_3) &= \sum_{i_2=1}^{W} p(i_2) \cdot \{ \sum_{j_2=1}^{C} p(j_2 | g(i_2, j_2) = i_3) \} \\ p(e_i = i_4) &= \sum_{i_3=1}^{K} p(i_3) \cdot \{ \sum_{j_3=1}^{D} p(j_3 | h(i_3, j_3) = i_4) \}, \end{aligned} \tag{5.6}$$

and the corresponding entropies are

$$H(w_i) =$$
$$\sum_{i_2=1}^{W} -[\sum_{i_1=1}^{A} p(i_1) \cdot \{\sum_{j_1=1}^{B} p(j_1|f(i_1,j_1)=i_2)\}] \cdot \log_2(\sum_{i_1=1}^{A} p(i_1) \cdot \{\sum_{j_1=1}^{B} p(j_1|f(i_1,j_1)=i_2)\})$$

$$H(k_i) =$$
$$\sum_{i_3=1}^{K} -[\sum_{i_2=1}^{W} p(i_2) \cdot \{\sum_{j_2=1}^{C} p(j_2|g(i_2,j_2)=i_3)\}] \cdot \log_2(\sum_{i_2=1}^{W} p(i_2) \cdot \{\sum_{j_2=1}^{C} p(j_2|g(i_2,j_2)=i_3)\})$$

$$H(e_i) =$$
$$\sum_{i_4=1}^{E} -[\sum_{i_3=1}^{K} p(i_3) \cdot \{\sum_{j_3=1}^{D} p(j_3|h(i_3,j_3)=i_4)\}] \cdot \log_2(\sum_{i_3=1}^{K} p(i_3) \cdot \{\sum_{j_3=1}^{D} p(j_3|h(i_3,j_3)=i_4)\}), \tag{5.7}$$

where $i_4 \in \{1, 2, \ldots, E\}$ and $p(j_1|f(i_1,j_1)=i_2)$ is the conditional probability.

From Equation (5.4), if $f(\cdot)$, $g(\cdot)$, and $h(\cdot)$ are injective functions, we do not need any extra information to reconstruct a_i, w_i, and k_i. However, from Equation (5.6), if $f(\cdot)$, $g(\cdot)$, and $h(\cdot)$ are surjective functions, the extra information is needed to create an one-to-one relationship between each input pair and the output symbol. Therefore, the actual input symbols a_i, w_i, and k_i could be retrieved based on the extra information. For example, consider a surjective function $f(\cdot)$, where

$$f(a_i, b_i) = |a_i - b_i|. \tag{5.8}$$

Assume $A > 4$, $B > 4$, $L = 3$, $\mathbf{a}^T = [1, 3, 2]$, and $\mathbf{b}^T = [2, 2, 3]$. Then, we have

$$\begin{aligned} & f(a_1 = 1, b_1 = 2) = f(a_2 = 3, b_2 = 2) = f(a_3 = 2, b_3 = 3) = 1 \\ & f(1, 2) = f(2, 3) = |-1| = 1 \\ & f(3, 2) = |1| = 1 \\ & \mathbf{w}^T = [1, 1, 1]. \end{aligned} \tag{5.9}$$

Without any extra information,

$$\begin{aligned} a_1 &= f^{-1}(w_1, b_1) = f^{-1}(1, 2) = \delta_1 \\ a_2 &= f^{-1}(w_2, b_2) = f^{-1}(1, 2) = \delta_1 \\ a_3 &= f^{-1}(w_3, b_3) = f^{-1}(1, 3) = \delta_2, \end{aligned} \tag{5.10}$$

where δ_1 could be 1 or 3 and δ_2 could be 2 or 4. Thus, $\mathbf{a}^T$ is given by:

$$\begin{aligned} \mathbf{a}^T \in \{&[1, 1, 2],\ [1, 1, 4],\ [1, 3, 2],\ [1, 3, 4], \\ &[3, 1, 2],\ [3, 1, 4],\ [3, 3, 2],\ [3, 3, 4]\}. \end{aligned} \tag{5.11}$$

From Equation (5.9), in order to obtain the correct input symbol a_i, the extra information could be chosen by satisfying:

$$\Phi_1 = \{i | (a_i - b_i) < 0,\ \forall i\}, \tag{5.12}$$

where Φ_1 is a set and Φ_1 contains sample index i that satisfies $(a_i - b_i) < 0$. Based on Equation (5.12), we have

$$\Phi_1 = \{1, 3\}. \tag{5.13}$$

Therefore, with the help of the extra information, the input symbol is reconstructed by

$$\begin{aligned} a_i &= f^{-1}(w_i, b_i, \Phi_1) \\ a_i &= b_i - w_i,\ i \in \Phi_1 \\ a_i &= b_i + w_i,\ i \notin \Phi_1. \end{aligned} \tag{5.14}$$

Based on Equation (5.14), we have

$$\begin{aligned} a_1 &= f^{-1}(1, 2, i \in \Phi_1) = 1 \\ a_2 &= f^{-1}(1, 2, i \notin \Phi_1) = 3 \\ a_3 &= f^{-1}(1, 3, i \in \Phi_1) = 2 \\ \mathbf{a}^T &= [1, 3, 2]. \end{aligned} \tag{5.15}$$

Moreover, if $g(\cdot)$ and $h(\cdot)$ are surjective functions, Φ_2 and Φ_3 are the corresponding extra information to obtain $w_i = g^{-1}(k_i, c_i, \Phi_2)$ and $k_i = h^{-1}(e_i, d_i, \Phi_3)$.

After $\mathbf{w}^T$, $\mathbf{k}^T$, and $\mathbf{e}^T$ are generated, we apply the arithmetic coding scheme to encode each symbol in these data streams. First, assume $f(\cdot)$, $g(\cdot)$, and $h(\cdot)$ are injective functions. Codebooks for different arithmetic encoders are $\mathbf{Q}_t$, where $t \in \{1, 2, 3\}$. In Equation (5.16), $\mathbf{Q}_t$ contains the information of all possible input source data, the side information, probabilities of each possible outcome, and the corresponding binary

codeword as follows:

$$\begin{aligned}
&\mathbf{Q}_1(l_1,:) = [(i_1,j_1),\ f(i_1,j_1),\ p(f(i_1,j_1)),\ \mathbf{x}^T_{f(i_1,j_1)}] \\
&\mathbf{Q}_2(l_2,:) = [(m_{i_2},j_2),\ g(m_{i_2},j_2),\ p(g(m_{i_2},j_2)),\ \mathbf{x}^T_{g(m_{i_2},j_2)}] \\
&\mathbf{Q}_3(l_3,:) = [(y_{i_3},j_3),\ h(y_{i_3},j_3),\ p(h(y_{i_3},j_3)),\ \mathbf{x}^T_{h(y_{i_3},j_3)}] \\
&l_1 = (i_1-1)\times B + j_1 \\
&l_2 = (i_2-1)\times C + j_2 \\
&l_3 = (i_3-1)\times D + j_3,
\end{aligned} \tag{5.16}$$

where l_1, l_2, and l_3 are the row indices, $\mathbf{Q}_1(l_1,:)$ means the l_1th row in $\mathbf{Q}_1$, $\mathbf{x}^T_{f(i_1,j_1)}$ is the codeword corresponding to the outcome $f(i_1,j_1)$, and the numbers of possible outcomes in $\mathbf{Q}_1$, $\mathbf{Q}_2$, and $\mathbf{Q}_3$ are $A\times B$, $W\times C$, and $K\times D$, respectively. In addition, how to generate the encoded bit stream $\mathbf{x}^T$ depends on the selected switch, where

$$\mathbf{x}^T \in \{\mathbf{x}^T_{f(\mathbf{a}^T,\ \mathbf{b}^T)},\ \mathbf{x}^T_{g(\mathbf{w}^T,\mathbf{c}^T)},\ \mathbf{x}^T_{h(\mathbf{k}^T,\mathbf{d}^T)}\}, \tag{5.17}$$

$f(\mathbf{a}^T,\mathbf{b}^T) = \{f(a_i,b_i),\ \forall i\}$, $g(\mathbf{w}^T,\mathbf{c}^T) = \{g(w_i,c_i),\ \forall i\}$, and $h(\mathbf{k}^T,\mathbf{d}^T) = \{h(k_i,d_i),\ \forall i\}$. From Equation (5.16), if we introduce more and more stages in the encoder, the Hamming distances between any two adjacent codewords at the output of higher stages become smaller and smaller. The encoding rates (R_{enc,S_t}) of the 3-stage encoder are

$$\begin{aligned}
R_{enc,S_1} &= \sum_{i_1=1}^{A}\sum_{j_1=1}^{B}[1+\lceil -\log_2 p(i_1,j_1)\rceil]\cdot p(i_1,j_1) \\
R_{enc,S_2} &= \sum_{i_2=1}^{W}\sum_{j_2=1}^{C}[1+\lceil -\log_2 p(m_{i_2},j_2)\rceil]\cdot p(m_{i_2},j_2) \\
R_{enc,S_3} &= \sum_{i_3=1}^{K}\sum_{j_3=1}^{D}[1+\lceil -\log_2 p(y_{i_3},j_3)\rceil]\cdot p(y_{i_3},j_3).
\end{aligned} \tag{5.18}$$

Moreover, the 3-stage encoder provides three different lengths of $\mathbf{x}^T$, because the numbers of possible outcomes in $\mathbf{w}^T$, $\mathbf{k}^T$, and $\mathbf{e}^T$ are different. These three different lengths of $\mathbf{x}^T$ are

$$\begin{aligned} Len_{S_1} &= \sum_{i=1}^{L} Len(x^T_{f(a_i,b_i)}) \\ &= \sum_{i=1}^{L} [1 + \lceil -\log_2 p(a_i, b_i) \rceil] \\ Len_{S_2} &= \sum_{i=1}^{L} Len(x^T_{g(w_i,c_i)}) \\ &= \sum_{i=1}^{L} [1 + \lceil -\log_2 p(a_i, b_i, c_i) \rceil] \\ Len_{S_3} &= \sum_{i=1}^{L} Len(x^T_{h(k_i,d_i)}) \\ &= \sum_{i=1}^{L} [1 + \lceil -\log_2 p(a_i, b_i, c_i, d_i) \rceil]. \end{aligned} \tag{5.19}$$

If $f(\cdot)$, $g(\cdot)$, and $h(\cdot)$ are surjective functions, the codebooks $\mathbf{Q}_t$, the encoding rates (R_{enc,S_t}), and three lengths of $\mathbf{x}^T$ are different from Equation (5.16), Equation (5.18), and Equation (5.19). Therefore, we utilize the probabilities $p(w_i = i_2)$, $p(k_i = i_3)$, and $p(e_i = i_4)$ in Equation (5.6) to derive the corresponding codebooks, encoding rates, and different lengths of the encoded bit streams for surjective functions. First, the

codebooks $\mathbf{Q}_t$ are

$$\begin{aligned}
&\mathbf{Q}_1(l_1,:) = [(i_1,j_1),\ f(i_1,j_1),\ p(w_i = i_2),\ \mathbf{x}_{w_i}^T] \\
&\mathbf{Q}_2(l_2,:) = [(m_{i_2},j_2),\ g(m_{i_2},j_2),\ p(k_i = i_3),\ \mathbf{x}_{k_i}^T] \\
&\mathbf{Q}_3(l_3,:) = [(y_{i_3},j_3),\ h(y_{i_3},j_3),\ p(e_i = i_4),\ \mathbf{x}_{e_i}^T] \\
&l_1 = (i_1 - 1) \times B + j_1 \\
&l_2 = (i_2 - 1) \times C + j_2 \\
&l_3 = (i_3 - 1) \times D + j_3.
\end{aligned} \tag{5.20}$$

Then, the encoding rates (R_{enc,S_t}) are given by:

$$\begin{aligned}
R_{enc,S_1} &= \sum_{i_2=1}^{W} [1 + \lceil -\log_2 p(w_i = i_2) \rceil] \cdot p(w_i = i_2) \\
R_{enc,S_2} &= \sum_{i_3=1}^{K} [1 + \lceil -\log_2 p(k_i = i_3) \rceil] \cdot p(k_i = i_3) \\
R_{enc,S_3} &= \sum_{i_4=1}^{E} [1 + \lceil -\log_2 p(e_i = i_4) \rceil] \cdot p(e_i = i_4).
\end{aligned} \tag{5.21}$$

Finally, three different lengths of $\mathbf{x}^T$ are

$$\begin{aligned} Len_{S_1} &= \sum_{i=1}^{L} Len(x^T_{f(a_i,b_i)}) \\ &= \sum_{i=1}^{L} [1 + \lceil -\log_2 p(w_i = i_2) \rceil] \\ Len_{S_2} &= \sum_{i=1}^{L} Len(x^T_{g(w_i,c_i)}) \\ &= \sum_{i=1}^{L} [1 + \lceil -\log_2 p(k_i = i_3) \rceil] \\ Len_{S_3} &= \sum_{i=1}^{L} Len(x^T_{h(k_i,d_i)}) \\ &= \sum_{i=1}^{L} [1 + \lceil -\log_2 p(e_i = i_4) \rceil]. \end{aligned} \tag{5.22}$$

From Equation (5.19) and Equation (5.22), the proposed 3-stage encoder generates three different transmission rates by selecting different output signals through varying the switch S_t.

In communication systems, two different ways utilized to transmit the data are continuous data transmission and packet data transmission. For the continuous data transmission such as voice, the transmission rate is controlled by the transport layer. In this case, the receiver knows the transmission rate during the entire data flow. As for the packet data transmission, each packet consists of the header and the data, and the information of the switch configuration can be hidden in the header of each packet. Therefore, in order to adjust the transmission rate without notifying the receiver, the transmitter first encodes the switch configuration and then includes the encoded bits in the header. The length of the header depends on the coding rate of the error correcting

codes. In this chapter, we consider the continuous data transmission.

After the entire encoding process, we pad the input data, $\mathbf{x}^T$, with a certain number of zeros (N_z) to maintain the total number of bits equal to $M \times N_T$, where $N_z = M \times N_T - Len_{S_t}$, M is the number of bits to represent a symbol, and N_T is the number of total subcarriers. Then, the modified bit stream, $[\mathbf{x}^T \ 0_{1\times N_z}]$, is transmitted using a SISO-OFDM system.

5.2.2 The Feasibilities of Functions and Variable Transmission Rate Analysis

Choosing the proper mapping functions in the encoder provides two advantages: 1.) the improvement of the system performance and 2.) the adjustability of the transmission rate. In order to reduce the size of codebook and to reconstruct the source data perfectly at the receiver, it is necessary to choose the mapping functions that generate smaller cardinalities in the encoder. Also, the help of the extra information provides us much more feasible ways to choose the mapping functions without any constraint.

The variable transmission bit rates (R_{b,S_t}) of the proposed VTR-SISO-OFDM system are

$$\begin{aligned} R_{b,S_t} &= f_s \times M \times \frac{N_u}{N_T + N_{CP}} \\ N_u &= \lceil \frac{Len_{S_t}}{M} \rceil, \end{aligned} \tag{5.23}$$

where f_s is the sampling rate, N_u is the number of used subcarriers, N_{CP} is the length of cyclic prefix, and $\lceil \cdot \rceil$ is the ceiling function. The rate factor, $\frac{N_u}{N_T}$, is derived from $\frac{R_{b,S_t}}{R_{b,raw}}$,

where $R_{b,raw}$ is the raw transmission rate, $R_{b,raw} = f_s \times M \times \frac{N_T}{N_T+N_{CP}}$, and $\frac{N_u}{N_T} < 1$. From Equation (5.23), the transmission rate can be adjusted by varying the number of used subcarriers, N_u. Moreover, the probability of each possible outcome affects the number of used subcarriers. Thus, the smaller the probability of each possible outcome, the higher the transmission rate. In Fig. 5.1(a), if the maximal transmission rate is achieved from the output bit stream through the switch S_3, the probability of each possible outcome is $p(i_1, j_1, j_2, j_3)$, where $f(\cdot)$, $g(\cdot)$, and $h(\cdot)$ are injective functions. Furthermore, the operation bandwidth of the proposed VTR-SISO-OFDM system depends on the switch S_t, and the variable operation bandwidths (BW_{S_t}) for the proposed VTR-SISO-OFDM system are

$$\begin{aligned} BW_{S_t} &= N_u \times \Delta f \\ &= \lceil \frac{Len_{S_t}}{M} \rceil \times \frac{BW}{N_T}, \end{aligned} \tag{5.24}$$

where Δf is the subcarrier spacing, $\Delta f = \frac{BW}{N_T}$, and BW is the original operation bandwidth.

5.2.3 The Proposed 3-stage Decoder in the VTR-SISO-OFDM System

At the receiver, the received bit stream is reconstructed by the demodulation process in the SISO-OFDM system. Once the estimated bit stream $\tilde{\mathbf{x}}^T$ is obtained at the receiver, the proposed decoder proceeds to process the data.

Fig. 5.1(b) shows the proposed 3-stage decoder in the VTR-SISO-OFDM system. First, the receiver utilizes the switch configuration assigned by the transport layer to

determine the decoding route. For example, if $S_3 = 1$, the decoder closes the switch S_3, and proceeds to decode $\tilde{\mathbf{x}}^T$. The side information $\mathbf{d}^T$ helps the arithmetic decoder 3 to perform the first stage decoding process. In the first stage, the arithmetic decoder 3 decodes $\tilde{\mathbf{x}}^T$ based on the minimum Hamming distance rule with the aid of $\mathbf{Q}_3$ and $\mathbf{d}^T$. Then, $\check{\mathbf{w}}^T$ is generated through performing $g^{-1}(\cdot)$ on $\check{\mathbf{k}}^T$, $\mathbf{c}^T$, and Φ_2. Finally, we obtain the estimated source data $\check{\mathbf{a}}^T$ after performing the inverse functions $f^{-1}(\cdot)$ on the estimated sequence $\check{\mathbf{w}}^T$, the side information $\mathbf{b}^T$, and the extra information Φ_1 as shown in Equation (5.25).

$$\begin{aligned} \check{\mathbf{a}}^T &= f^{-1}(\check{\mathbf{w}}^T, \mathbf{b}^T, \Phi_1) \\ &= f^{-1}(g^{-1}(\check{\mathbf{k}}^T, \mathbf{c}^T, \Phi_2), \mathbf{b}^T, \Phi_1), \end{aligned} \tag{5.25}$$

where $f^{-1}(\check{\mathbf{w}}^T, \mathbf{b}^T, \Phi_1) = \{f^{-1}(\check{w}_i, b_i, \Phi_1), \forall i\}$ and $g^{-1}(\check{\mathbf{k}}^T, \mathbf{c}^T, \Phi_2) = \{g^{-1}(\check{k}_i, c_i, \Phi_2), \forall i\}$. The entire decoding procedure is listed in **Algorithm** 4. In **Algorithm** 4, $Dist\{\cdot\}$ is the Hamming distance and $\mathbf{s}(i:j)$ means from the ith sample to the jth sample in $\mathbf{s}$.

5.3 The VTR-MB-OFDM System

In this section, a VTR-MB-OFDM system is proposed using the multiterminal source coding scheme.

Algorithm 4 *The decoding algorithm for the 3-stage decoder*

Initial Inputs: S_t, $\tilde{\mathbf{x}}^T$, $\mathbf{Q}_{S_t}$, Φ_1, Φ_2

for $i = 1$ **to** L **do**
  if S_1 is closed **then**
    $\hat{a}_i = \arg\min_{i_1} Dist\{\tilde{\mathbf{x}}^T(1 : length(\mathbf{x}^T_{f(i_1,b_i)})) - \mathbf{x}^T_{f(i_1,b_i)}\}$
    $\tilde{\mathbf{x}}^T = \tilde{\mathbf{x}}^T(length(\mathbf{x}^T_{f(\hat{a}_i,b_i)}) + 1 : length(\tilde{\mathbf{x}}^T))$
  else if S_2 is closed **then**
    $\tilde{w}_i = \arg\min_{m_{i_2}} Dist\{\tilde{\mathbf{x}}^T(1 : length(\mathbf{x}^T_{g(m_{i_2},c_i)})) - \mathbf{x}^T_{g(m_{i_2},c_i)}\}$
    $\tilde{a}_i = f^{-1}(\tilde{w}_i, b_i, \Phi_1)$
    $\tilde{\mathbf{x}}^T = \tilde{\mathbf{x}}^T(length(\mathbf{x}^T_{g(\tilde{w}_i,c_i)}) + 1 : length(\tilde{\mathbf{x}}^T))$
  else
    $\check{k}_i = \arg\min_{y_{i_3}} Dist\{\tilde{\mathbf{x}}^T(1 : length(\mathbf{x}^T_{h(y_{i_3},d_i)})) - \mathbf{x}^T_{h(y_{i_3},d_i)}\}$
    $\check{w}_i = g^{-1}(\check{k}_i, c_i, \Phi_2)$
    $\check{a}_i = f^{-1}(\check{w}_i, b_i, \Phi_1)$
    $\tilde{\mathbf{x}}^T = \tilde{\mathbf{x}}^T(length(\mathbf{x}^T_{h(\check{k}_i,d_i)}) + 1 : length(\tilde{\mathbf{x}}^T))$
  end if
end for

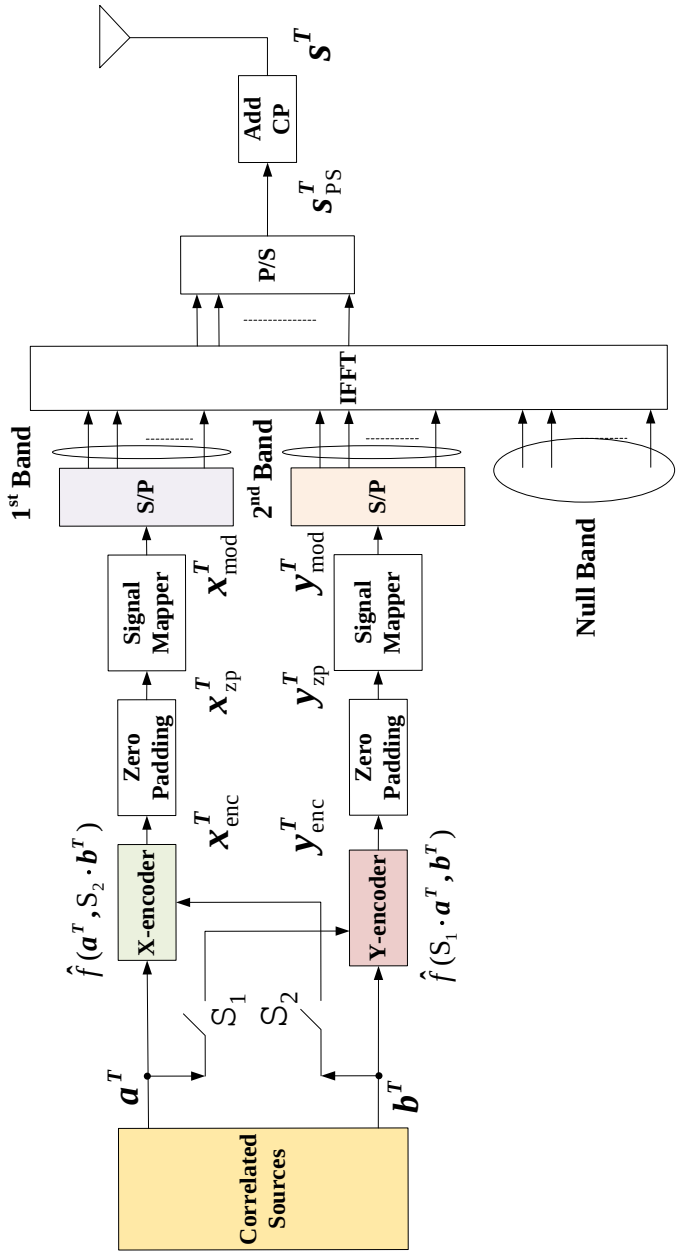

Figure 5.2: The transmitter in the proposed VTR-MB-OFDM system.

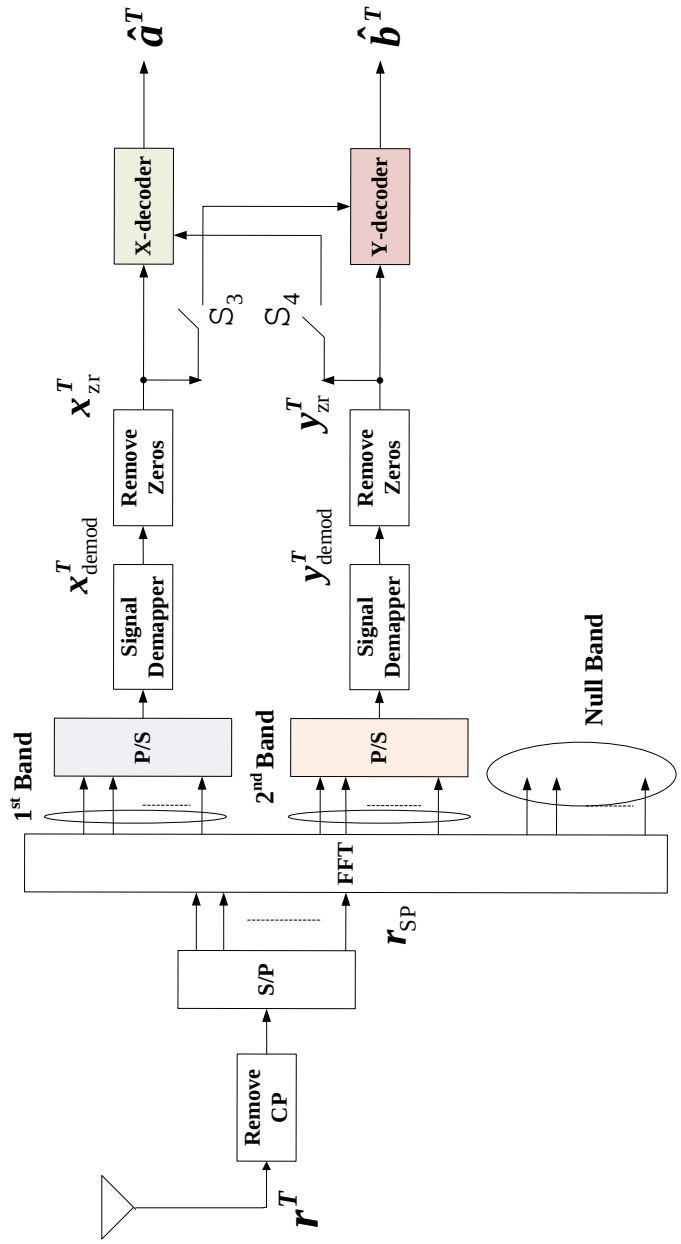

Figure 5.3: The receiver in the proposed VTR-MB-OFDM system.

5.3.1 The Proposed VTR-MB-OFDM System and Transmission Rate Analysis

The proposed VTR-MB-OFDM system is shown in Fig. 5.2 and Fig. 5.3. In Fig. 5.2, correlated information sequences $\mathbf{a}^T$ and $\mathbf{b}^T$ are generated by repeated independent drawings of a pair of discrete random variables, where $\mathbf{a}^T = [a_1, a_2, \ldots, a_L] = \{a_i\}$, $\mathbf{b}^T = [b_1, b_2, \ldots, b_L] = \{b_i\}$, $a_i \in \{1, 2, \ldots, A\}$, $b_i \in \{1, 2, \ldots, B\}$, $i \in \{1, 2, \ldots, L\}$, and L is the total number of drawings. In the proposed VTR-MB-OFDM system, $\hat{f}(\cdot)$ is an injective function. Thus, the entropies of $\hat{f}(a_i, S_2 \cdot b_i)$ and $\hat{f}(S_1 \cdot a_i, b_i)$ are

$$\begin{aligned} & H(\hat{f}(a_i, S_2 \cdot b_i)) \\ & = \begin{cases} \sum_{i_1=1}^{A} -p(i_1) \cdot \log_2(p(i_1)), \ if \ S_2 = 0, \\ \sum_{i_1=1}^{A} \sum_{j_1=1}^{B} -p(i_1, j_1) \cdot \log_2(p(i_1, j_1)), \ if \ S_2 = 1, \end{cases} \\ & H(\hat{f}(S_1 \cdot a_i, b_i)) \\ & = \begin{cases} \sum_{j_1=1}^{B} -p(j_1) \cdot \log_2(p(j_1)), \ if \ S_1 = 0, \\ \sum_{i_1=1}^{A} \sum_{j_1=1}^{B} -p(i_1, j_1) \cdot \log_2(p(i_1, j_1)), \ if \ S_1 = 1. \end{cases} \end{aligned} \tag{5.26}$$

X-encoder encodes $\hat{f}(\mathbf{a}^T, S_2 \cdot \mathbf{b}^T)$ to $\mathbf{x}_{enc}^T$ using the arithmetic coding scheme, where the function $\hat{f}(\cdot)$ maps each pair $(a_i, S_2 \cdot b_i)$ in $(\mathbf{a}^T, S_2 \cdot \mathbf{b}^T)$ to an unique value and the length of $\mathbf{x}_{enc}^T$ depends on S_2. Codebooks, $\mathbf{Q}_x$ and $\mathbf{Q}_y$, used to generate $\mathbf{x}_{enc}^T$ and $\mathbf{y}_{enc}^T$

are

$$\begin{aligned}
&\mathbf{Q}_x(\gamma_1,:) = [(\alpha_1,\beta_1),\ \hat{f}(\alpha_1,\beta_1),\ p(\hat{f}(\alpha_1,\beta_1)),\ \mathbf{x}^T_{\hat{f}(\alpha_1,\beta_1)}] \\
&\mathbf{Q}_y(\gamma_2,:) = [(\alpha_2,\beta_2),\ \hat{f}(\alpha_2,\beta_2),\ p(\hat{f}(\alpha_2,\beta_2)),\ \mathbf{y}^T_{\hat{f}(\alpha_2,\beta_2)}] \\
&\gamma_1 = \beta_1 \times A + \alpha_1 \\
&\gamma_2 = \alpha_2 \times B + \beta_2,
\end{aligned} \tag{5.27}$$

where γ_1 and γ_2 are the row indices, $\alpha_1 \in \{1,2,\ldots,A\}$, $\beta_1 \in \{0,1,\ldots,B\}$, $\alpha_2 \in \{0,1,\ldots,A\}$, $\beta_2 \in \{1,2,\ldots,B\}$, $\mathbf{x}^T_{\hat{f}(\alpha_1,\beta_1)}$ and $\mathbf{y}^T_{\hat{f}(\alpha_2,\beta_2)}$ are the codewords corresponding to the possible outcomes $\hat{f}(\alpha_1,\beta_1)$ and $\hat{f}(\alpha_2,\beta_2)$, $\mathbf{x}^T_{enc} = \mathbf{x}^T_{\hat{f}(\mathbf{a}^T,S_2\cdot\mathbf{b}^T)}$, and $\mathbf{y}^T_{enc} = \mathbf{y}^T_{\hat{f}(S_1\cdot\mathbf{a}^T,\mathbf{b}^T)}$. In order to satisfy the criterion of digital modulation, a zero vector is padded to the back of $\mathbf{x}^T_{enc}$ such that

$$\mathbf{x}^T_{zp} = \begin{cases} \mathbf{x}^T_{enc},\ if\ mod(X,M) = 0 \\ [\mathbf{x}^T_{enc}\ 0_{1\times(M-mod(X,M))}],\ if\ mod(X,M) \neq 0, \end{cases} \tag{5.28}$$

where X is the length of $\mathbf{x}^T_{enc}$, M is the number of bits to represent a symbol, $mod([M - mod(X,M)],M)$ is the length of the zero padding vector, the length of $\mathbf{x}^T_{zp}$ is $X + mod([M - mod(X,M)],M)$, X is

$$X = \begin{cases} \sum_{i=1}^{L}[1 + \lceil -\log_2 p(a_i)\rceil],\ if\ S_2 = 0 \\ \sum_{i=1}^{L}[1 + \lceil -\log_2 p(a_i,b_i)\rceil],\ if\ S_2 = 1, \end{cases} \tag{5.29}$$

and the encoding rate ($R_{enc,x[S_2]}$) of X-encoder is

$$\begin{aligned} R_{enc,x[0]} &= \sum_{i_1=1}^{A} [1 + \lceil -\log_2 p(i_1) \rceil] \cdot p(i_1) \\ R_{enc,x[1]} &= \sum_{i_1=1}^{A} \sum_{j_1=1}^{B} [1 + \lceil -\log_2 p(i_1, j_1) \rceil] \cdot p(i_1, j_1). \end{aligned} \tag{5.30}$$

After $\mathbf{x}_{zp}^T$ is modulated, we obtain $\mathbf{x}_{mod}^T$, and the bandwidth of the 1^{st} band occupied by $\mathbf{x}_{mod}^T$ is

$$BW_{1^{st}} = \lceil \frac{X}{M} \rceil \times \Delta f. \tag{5.31}$$

Y-encoder performs the same procedures to obtain $\mathbf{y}_{enc}^T$ by replacing $\hat{f}(\mathbf{a}^T, S_2 \cdot \mathbf{b}^T)$ to $\hat{f}(S_1 \cdot \mathbf{a}^T, \mathbf{b}^T)$. Then, we pad a zero vector with length $mod([M - mod(Y, M)], M)$ to the back of $\mathbf{y}_{enc}^T$ in order to generate $\mathbf{y}_{zp}^T$. The length of $\mathbf{y}_{zp}^T$ is $Y + mod([M - mod(Y, M)], M)$. In addition, the length of $\mathbf{y}_{enc}^T$, Y, is

$$Y = \begin{cases} \sum_{i=1}^{L} [1 + \lceil -\log_2 p(b_i) \rceil], \ if \ S_1 = 0 \\ \sum_{i=1}^{L} [1 + \lceil -\log_2 p(a_i, b_i) \rceil], \ if \ S_1 = 1, \end{cases} \tag{5.32}$$

and the encoding rate ($R_{enc,y[S_1]}$) of Y-encoder is

$$\begin{aligned} R_{enc,y[0]} &= \sum_{j_1=1}^{B} [1 + \lceil -\log_2 p(j_1) \rceil] \cdot p(j_1) \\ R_{enc,y[1]} &= \sum_{i_1=1}^{A} \sum_{j_1=1}^{B} [1 + \lceil -\log_2 p(i_1, j_1) \rceil] \cdot p(i_1, j_1). \end{aligned} \tag{5.33}$$

Thus, the bandwidth of the 2^{nd} band is

$$BW_{2^{nd}} = \lceil \frac{Y}{M} \rceil \times \Delta f. \tag{5.34}$$

From Equation (5.30) and Equation (5.33), when S_1 and S_2 are equal to one, the lengths of two encoded bit streams, X and Y, are identical; moreover, the allocated bandwidths of these two subbands, $BW_{1^{st}}$ and $BW_{2^{nd}}$, are also the same.

Two serial-to-parallel (S/P) convertors are applied to $\mathbf{x}_{mod}^T$ and $\mathbf{y}_{mod}^T$ before the N_T-point inverse fast Fourier transform (IFFT) operation. Then, in order to perform a N_T-point IFFT operation, we insert a null band occupying N_{null} subcarriers, where $N_{null} = N_T - \lceil \frac{X}{M} \rceil - \lceil \frac{Y}{M} \rceil$. After the N_T-point IFFT operation, $\mathbf{s}_{PS}^T$ is obtained using a parallel-to-serial (P/S) convertor. A cyclic prefix with length N_{CP} is inserted to the front of $\mathbf{s}_{PS}^T$ in order to reduce the ISI. Finally, $\mathbf{s}^T$ is transmitted using the radio frequency (RF) components, where

$$\mathbf{s}^T = \begin{cases} \mathbf{s}_{PS}^T(i + N_T - N_{CP}),\ i = 0, 1, \ldots, N_{CP} - 1 \\ \\ \mathbf{s}_{PS}^T(i),\ i = N_{CP}, N_{CP} + 1, \ldots, N_{CP} + N_T - 1. \end{cases} \tag{5.35}$$

The transmission bit rate of the proposed VTR-MB-OFDM system is related to the

switches S_1 and S_2. Therefore, four different transmission bit rates ($R_{b,[S_1\ S_2]}$) are

$$\begin{aligned}
R_{b,[0\ 0]} =&\{\lceil\frac{\sum_{i=1}^{L}[1+\lceil-\log_2 p(a_i)\rceil]}{M}\rceil+\\
&\lceil\frac{\sum_{i=1}^{L}[1+\lceil-\log_2 p(b_i)\rceil]}{M}\rceil\}\times\frac{M\cdot f_s}{N_T+N_{CP}},\\
R_{b,[0\ 1]} =&\{\lceil\frac{\sum_{i=1}^{L}[1+\lceil-\log_2 p(a_i)\rceil]}{M}\rceil+\\
&\lceil\frac{\sum_{i=1}^{L}[1+\lceil-\log_2 p(a_i,b_i)\rceil]}{M}\rceil\}\times\frac{M\cdot f_s}{N_T+N_{CP}},\\
R_{b,[1\ 0]} =&\{\lceil\frac{\sum_{i=1}^{L}[1+\lceil-\log_2 p(a_i,b_i)\rceil]}{M}\rceil+\\
&\lceil\frac{\sum_{i=1}^{L}[1+\lceil-\log_2 p(b_i)\rceil]}{M}\rceil\}\times\frac{M\cdot f_s}{N_T+N_{CP}},\\
R_{b,[1\ 1]} =&\{\lceil\frac{\sum_{i=1}^{L}[1+\lceil-\log_2 p(a_i,b_i)\rceil]}{M}\rceil+\\
&\lceil\frac{\sum_{i=1}^{L}[1+\lceil-\log_2 p(a_i,b_i)\rceil]}{M}\rceil\}\times\frac{M\cdot f_s}{N_T+N_{CP}}.
\end{aligned}\tag{5.36}$$

Assume the data is transmitted over an AWGN channel. At the receiver as shown in Fig. 5.3, the received signal $\mathbf{r}^T$ is

$$\mathbf{r}^T=\mathbf{s}^T+\mathbf{n}^T,\tag{5.37}$$

where $\mathbf{n}^T$ is the AWGN noise. First, the receiver performs the cyclic prefix removal on $\mathbf{r}^T$, the S/P operation, and the N_T-point FFT operation on $\mathbf{r}_{SP}$. After the FFT operation, symbols allocated in the specific subbands are extracted, and then demodulated by the corresponding signal demapper. $\mathbf{x}_{demod}^T$ is generated using the information from the first $\lceil\frac{X}{M}\rceil$ subcarriers, and $\mathbf{y}_{demod}^T$ is also generated using the information from the $(\lceil\frac{X}{M}\rceil+1)$th subcarrier to the $(\lceil\frac{X}{M}\rceil+\lceil\frac{Y}{M}\rceil)$th subcarrier. Then, $\mathbf{x}_{zr}^T$ is obtained by removing $mod(M-mod(X,M),M)$ samples at the back of $\mathbf{x}_{demod}^T$, and $\mathbf{y}_{zr}^T$ is also

obtained by removing $mod(M - mod(Y, M), M)$ samples at the back of $\mathbf{y}^T_{demod}$. Let us use $\mathbf{x}^T_{zr}$ to explain the decoding process, and $\mathbf{y}^T_{zr}$ is decoded using the same procedure. X-decoder decodes $\mathbf{x}^T_{zr}$ by minimizing the Hamming distances between codewords in the codebook $\mathbf{Q}_x$ and the partial bit stream in $\mathbf{x}^T_{zr}$ with or without the help of the side information through the switch S_3, and then the estimated source data $\hat{\mathbf{a}}^T$ is obtained. In **Algorithm** 5, we describe the overall decoding process used in X-decoder and Y-decoder.

Algorithm 5 *The decoding algorithm for multiterminal source decoder of the proposed VTR-MB-OFDM system*

Initial Inputs: $\mathbf{x}^T_{zr}$, $\mathbf{y}^T_{zr}$

for $i = 1$ **to** L **do**
  If $S_\tau = 1$, decode the corresponding inputs with the side information; otherwise, decode the corresponding inputs without the side information, where $\tau \in \{3, 4\}$.
  if $S_4 = 0$ **then**
    $j_1 = 0$
    $(\hat{a}_i, 0) = \arg\min_{(i_1,j_1)} Dist\{\mathbf{x}^T_{zr}(1 : length(\mathbf{x}^T_{\hat{f}(i_1,j_1)})) - \mathbf{x}^T_{\hat{f}(i_1,j_1)}\}$
  else
    $j_1 \in \{0, 1, \ldots, B\}$
    $(\hat{a}_i, j_1) = \arg\min_{(i_1,j_1)} Dist\{\mathbf{x}^T_{zr}(1 : length(\mathbf{x}^T_{\hat{f}(i_1,j_1)})) - \mathbf{x}^T_{\hat{f}(i_1,j_1)}\}$
  end if
  if $S_3 = 0$ **then**
    $i_2 = 0$
    $(0, \hat{b}_i) = \arg\min_{(i_2,j_2)} Dist\{\mathbf{y}^T_{zr}(1 : length(\mathbf{y}^T_{\hat{f}(i_2,j_2)})) - \mathbf{y}^T_{\hat{f}(i_2,j_2)}\}$
  else
    $i_2 \in \{0, 1, \ldots, A\}$
    $(i_2, \hat{b}_i) = \arg\min_{(i_2,j_2)} Dist\{\mathbf{y}^T_{zr}(1 : length(\mathbf{y}^T_{\hat{f}(i_2,j_2)})) - \mathbf{y}^T_{\hat{f}(i_2,j_2)}\}$
  end if
  $\mathbf{x}^T_{zr} = \mathbf{x}^T_{zr}(length(\mathbf{x}^T_{\hat{f}(\tilde{a}_i,j_1)}) + 1 : length(\mathbf{x}^T_{zr}))$
  $\mathbf{y}^T_{zr} = \mathbf{y}^T_{zr}(length(\mathbf{y}^T_{\hat{f}(i_2,\tilde{b}_i)}) + 1 : length(\mathbf{y}^T_{zr}))$
end for

5.4 Performance Analysis and Simulation Results

We evaluate the performance of two proposed VTR-OFDM systems: the VTR-SISO-OFDM system and the VTR-MB-OFDM system. Section 5.4.1 presents the performance of the proposed VTR-SISO-OFDM system, and then the performance of the proposed VTR-MB-OFDM system is demonstrated in Section 5.4.2.

5.4.1 Performance Evaluation of The VTR-SISO-OFDM System

Assume 10000 packets are transmitted using the VTR-SISO-OFDM system and each packet contains 2000 encoded messages. Consider the source data and the side information that follow the same probability distribution $p(z)$,

$$p(z = \lambda) = \frac{Z - \lambda + 1}{\sum_{\lambda=1}^{Z}(Z - \lambda + 1)}, \tag{5.38}$$

where z is a random variable, $z \in \{1, 2, \ldots, Z\}$, and $\sum_{\lambda=1}^{Z}(Z-\lambda+1)$ is the total number of possible outcomes.

The source data $\mathbf{a}^T = \{a_i\}$ is fed to the 3-stage encoder in order to evaluate the system performance under three different transmission rates, where $L = 2000$. Assume $A = 100$, and the maximum values in the side information are given by $B = 75$, $C = 50$, and $D = 25$ or $D = 5$. The pdf of source data, $p(a_i)$, is

$$p(a_i = i_1) = \frac{A - i_1 + 1}{N_a}, \tag{5.39}$$

where $N_a = \sum_{i_1=1}^{100}(100 - i_1 + 1) = 5050$. Then, the pdfs of the side information are

$$\begin{aligned} p(b_i = j_1) &= \frac{B - j_1 + 1}{N_b} \\ p(c_i = j_2) &= \frac{C - j_2 + 1}{N_c} \\ p(d_i = j_3) &= \frac{D - j_3 + 1}{N_d}, \end{aligned} \tag{5.40}$$

where $N_b = \sum_{j_1=1}^{75}(75 - j_1 + 1) = 2850$, $N_c = \sum_{j_2=1}^{50}(50 - j_2 + 1) = 1275$, and $N_d = \sum_{j_3=1}^{D}(D - j_3 + 1) = 325$ or 15.

The mapping functions in the proposed 3-stage encoder, $f(\alpha, \beta)$, $g(\alpha, \beta)$, and $h(\alpha, \beta)$, are

$$\begin{aligned} f(\alpha, \beta) &= mod(\alpha + \beta, \gamma) \\ g(\alpha, \beta) &= |\alpha - \beta| \\ h(\alpha, \beta) &= p(\alpha, \beta), \end{aligned} \tag{5.41}$$

where γ is the maximum prime number in $A + B$ and $p(\alpha, \beta)$ is the joint probability function on (α, β). From Equation (5.41), $f(\cdot)$ and $g(\cdot)$ are surjective functions, and $h(\cdot)$ represents an injective function. After applying the mapping functions to the input symbols and the side information at each stage, the corresponding output symbols, $\mathbf{w}^T$, $\mathbf{k}^T$, and $\mathbf{e}^T$, are

$$\begin{aligned} w_i &= mod(a_i + b_i, 173) \\ k_i &= |w_i - c_i| \\ e_i &= p(k_i, d_i), \end{aligned} \tag{5.42}$$

where $\gamma = 173$. Moreover, the cardinalities of $\mathbf{w}^T$, $\mathbf{k}^T$, and $\mathbf{e}^T$ are $W = 173$, $K = 172$,

and $E = 172 \times 25$ or $E = 172 \times 5$ depending on the value D. Thus, the transmission rate of the output signal at the 2^{nd} stage is the smallest, because K is less than W and E. In addition, Φ_1 and Φ_2 are chosen by satisfying:

$$\begin{aligned} \Phi_1 &= \{i|(a_i + b_i) = 175\} \\ \Phi_2 &= \{i|(w_i - c_i) < 0\}. \end{aligned} \tag{5.43}$$

Once the output symbols $\mathbf{w}^T$, $\mathbf{k}^T$, and $\mathbf{e}^T$ are generated, we apply the arithmetic code to encode each symbol to the specific codeword using the corresponding codebook at each stage. Cardinalities of different codebooks Q_t used to encode symbols at each stage are $A \times B$, $W \times C$, and E. Two bits for rate adjustment are added to the front of the output in order to construct the input bit stream. Then, we use a SISO-OFDM system with 16 quadrature amplitude modulation (QAM) signal mapper/demapper, 8192-point IFFT/FFT (N_T=8192), and N_{CP}=256 to transmit the data over an AWGN channel. Assume the operating bandwidth of the communication system is 20 MHz, and each sample is generated by a sampling frequency 5 MHz. The raw transmission bit rate of this SISO-OFDM system is 19.4 Mbps. In addition, the subcarrier spacing, Δf, is about 2.441 KHz.

Table 5.1: System Parameters of The Proposed VTR-SISO-OFDM System

	S_1	S_2	S_3	
			$D = 25$	$D = 5$
Entropy	7.4346	7.3323	11.7240	9.4815
Encoding rate (bits/sample), R_{enc,S_t}	9	8.8570	13.2461	11.0735
Averaged number of used subcarrier, $\lceil \frac{L \cdot R_{enc,S_t}}{M} \rceil$	4501	4429	6624	5537
Approximately allocated bandwidth (MHz.), $\lceil \frac{L \cdot R_{enc,S_t}}{M} \rceil \times \Delta f$	11	10.8	16.2	13.5
Transmission bit rate (Mbps), $R_{b,S_t} = \lceil \frac{L \cdot R_{enc,S_t}}{M} \rceil \times \frac{f_s \cdot M}{N_T + N_{CP}}$	10.7	10.5	15.7	13.1

Some system parameters of the proposed VTR-SISO-OFDM system are listed in Table 5.1, where S_1, S_2, and S_3 indicate which route we choose. In Table 5.1, we evaluate the entropies, encoding rates, used subcarriers, occupied bandwidth, and transmission rates. First, we notice that the encoding rates are greater than the entropies at each stage. It is important that the transmission of the proposed VTR-SISO-OFDM system is admissible under this condition. Furthermore, at the first two stages of the encoder, all system parameters are almost the same, because the cardinality of $\mathbf{w}^T$ is approximately equal to the cardinality of $\mathbf{k}^T$. At the third stage, Table 5.1 also shows that we can obtain higher encoding rates and higher entropies simply by increasing D; however, we can also expect that the Hamming distances between any two adjacent codewords become smaller and smaller with increasing D. In addition, we estimate the used subcarriers, the occupied bandwidths, and the transmission rates at each stage using $L \cdot R_{enc,S_t}$ instead of Len_{S_t}, because the entire packet transmission is a stochastic process which means Len_{S_t} is not a constant, and R_{enc,S_t} provides the average codeword length of possible output data samples. Furthermore, the rate factors, $\lceil \frac{L \cdot R_{enc,S_t}}{M} \rceil \times \frac{1}{N_T}$, at different stages are approximately equal to 0.55, 0.675, and 0.8.

We demonstrate the performance of the proposed VTR-SISO-OFDM system in Fig. 5.4. In Fig. 5.4, the SERs of the proposed VTR-SISO-OFDM system at different stages, S_1, S_2, and S_3, are compared with a traditional uncoded OFDM system (TRAD). If we transmit the data stream using the route S_1, SER is less than 10^{-6} when SNR is greater than 19dB. Although we can transmit data stream with higher

rate using the route S_3, SER is greater than 10^{-3} when SNR = 19dB. Reasons why we have higher SER using the route S_3 are the smaller Hamming distances between any two adjacent codewords and the error propagation during the entire decoding process. By decreasing D, we obtain better performance with lower transmission rate as shown in Table 5.1 and Fig. 5.4.

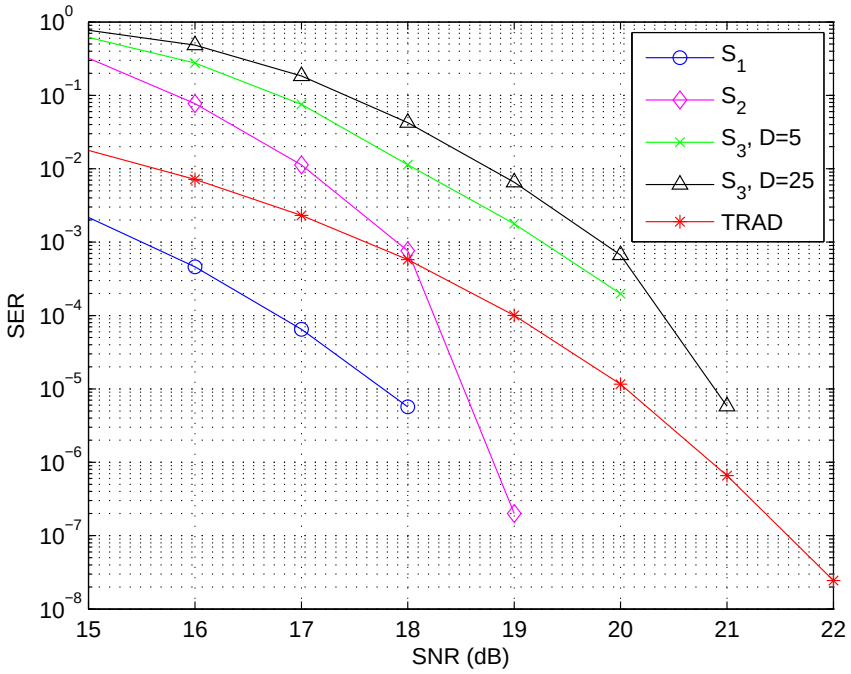

Figure 5.4: The performance of the proposed VTR-SISO-OFDM system at each stage with different D.

5.4.2 Performance Evaluation of The VTR-MB-OFDM System

Assume 10000 packets are transmitted using the proposed VTR-MB-OFDM system and each packet contains 2000 correlated information sequences, $\mathbf{a}^T$ and $\mathbf{b}^T$. After the correlated sequences are generated, we apply the multiterminal source coding to encode $\mathbf{a}^T$ and $\mathbf{b}^T$ with or without the side information from each other, and then these 2000 correlated sequences are transmitted using two different subbands in an MB-OFDM system. Each subband is occupied by 1000 encoded messages. In addition, the bandwidths and the transmission rates of these two subbands are not necessarily the same.

Let A and B be equal to N, and then correlated information sequences $\mathbf{a}^T$ and $\mathbf{b}^T$ are generated by 1000 independent drawings from $\begin{pmatrix} \mathbf{h} & \mathbf{l} \end{pmatrix}$, where $\mathbf{h}^T$ and $\mathbf{l}^T$ are

$$\begin{aligned} \mathbf{h}^T &= [\underbrace{1,\ldots,1}_{N},\underbrace{2,\ldots,2}_{N-1},\ldots,\underbrace{N-1,N-1}_{2},\underbrace{N}_{1}] \\ \mathbf{l}^T &= [\underbrace{N}_{1},\underbrace{N-1,N-1}_{2},\ldots,\underbrace{2,\ldots,2}_{N-1},\underbrace{1,\ldots,1}_{N}], \end{aligned} \tag{5.44}$$

N is a constant, $\underbrace{1,\ldots,1}_{N}$ means the number of 1s is N, L=1000, and the cross-correlation matrix of $\mathbf{h}^T$ and $\mathbf{l}^T$ when N=50 is

$$\mathbf{R} = \begin{pmatrix} 1 & -0.9302 \\ -0.9302 & 1 \end{pmatrix}. \tag{5.45}$$

From the cross-correlation coefficient $\mathbf{R}_{12}$ or $\mathbf{R}_{21}$, $\mathbf{h}^T$ is highly correlated with $\mathbf{l}^T$. Each input pair (a_i, b_i) is obtained by independent drawing from the row of $\begin{pmatrix} \mathbf{h} & \mathbf{l} \end{pmatrix}$. The

pdfs of $p(a_i)$ and $p(b_i)$ are

$$\begin{aligned} p(a_i = h_i) &= \frac{N - h_i + 1}{N \cdot (N+1)/2} \\ p(b_i = l_i) &= \frac{N - l_i + 1}{N \cdot (N+1)/2}. \end{aligned} \tag{5.46}$$

Moreover, the joint probability of $p(a_i, b_i)$ is

$$p(a_i = h_i, b_i = l_i) = \frac{OCCUR(h_i, l_i)}{N \cdot (N+1)/2}, \tag{5.47}$$

where $OCCUR(x)$ is the occurrence of x.

We evaluate the performance of the proposed VTR-MB-OFDM system using two different mapping functions, and these two mapping functions are

$$\begin{aligned} \hat{f}_1(\alpha, \beta) &= p(\alpha, \beta) \\ \hat{f}_2(\alpha, \beta) &= mod(\alpha + \beta, \gamma), \end{aligned} \tag{5.48}$$

where γ is the maximum prime number in $2 \cdot N$ and $p(\alpha, \beta)$ is the joint probability function on (α, β). Thus, $\hat{f}_1(\cdot)$ and $\hat{f}_2(\cdot)$ are injective functions. For the mapping function $\hat{f}_1(\cdot)$, we choose N to be 10, because we can achieve better performance using smaller N from the simulation results in Section 5.4.1. Then, A and B are equal to 10, and the number of distinct possible outcomes (h_i, l_i) is 17. After applying the mapping function $\hat{f}_1(\cdot)$ to the input pair (a_i, b_i) with different information interchanges, the outputs are $p(a_i, S_2 \cdot b_i)$ or $p(S_1 \cdot a_i, b_i)$. As for the mapping function $\hat{f}_2(\cdot)$, N is equal to 50, γ is 97, and the outputs of the input pair $(a_i, S_2 \cdot b_i)$ or $(S_1 \cdot a_i, b_i)$ are $mod(a_i + S_2 \cdot b_i, 97)$ or $mod(S_1 \cdot a_i + b_i, 97)$. Therefore, the maximum output of the $\hat{f}_2(a_i, b_i)$ is 51. In addition, the cardinalities of $\hat{f}_1(a_i, b_i)$ and $\hat{f}_2(a_i, b_i)$ are greater than

the cardinalities of $\mathbf{a}^T$ and $\mathbf{b}^T$. Thus, for these two mapping functions $\hat{f}_1(\cdot)$ and $\hat{f}_2(\cdot)$, the system operates in a higher transmission rate in order to fully utilize the available subcarriers.

Once the output symbols $\hat{f}(\mathbf{a}^T, S_2 \cdot \mathbf{b}^T)$ and $\hat{f}(S_1 \cdot \mathbf{a}^T, \mathbf{b}^T)$, are generated, we apply the arithmetic code to encode each symbol to the specific codeword using the corresponding codebook, Q_x and Q_y, at each encoder. Cardinalities of these two codebooks used to encode symbols at each encoder are varying with respect to the mapping functions and N. For the mapping function $\hat{f}_1(\cdot)$, the cardinality of each codebook is 27; however, the cardinality of codebooks for the mapping function $\hat{f}_2(\cdot)$ with larger N is 51. Then, we use an MB-OFDM system with 16-QAM signal mapper/demapper, 4096-point IFFT/FFT (N_T=4096), and N_{CP}=256 to transmit the input bit stream over an AWGN channel. Assume the operating bandwidth of the communication system is 20 MHz, and each sample is generated by a sampling frequency 5 MHz. The raw transmission bit rate of this MB-OFDM system is 18.8 Mbps. In addition, the subcarrier spacing, Δf, is about 4.882 KHz.

Table 5.2: System Parameters of The Proposed VTR-MB-OFDM System

	$prob,\ \hat{f}_1(\cdot),\ N = 10$		
	$x[0]$	$y[0]$	$x[1]\ \ (y[1])$
Entropy	3.1036	3.1036	3.8950
Encoding rate (bits/sample), $R_{enc} = R_{enc,x[S_2]}$ or $R_{enc,y[0]}$	4.5091	4.5091	5.3636
Averaged number of used subcarrier, $\lceil \frac{L \cdot R_{enc}}{M} \rceil$	1128	1128	1341
Approximately allocated bandwidth (MHz), $\lceil \frac{L \cdot R_{enc}}{M} \rceil \times \Delta f$	5.5	5.5	6.5
Transmission bit rate (Mbps), $R_b = \lceil \frac{L \cdot R_{enc}}{M} \rceil \times \frac{f_s \cdot M}{N_T + N_{CP}}$	5.18	5.18	6.16

	$modular,\ \hat{f}_2(\cdot),\ N = 50$		
	$x[0]$	$y[0]$	$x[1]\ \ (y[1])$
Entropy	5.3790	5.3790	6.3344
Encoding rate (bits/sample), $R_{enc} = R_{enc,x[S_2]}$ or $R_{enc,y[0]}$	7.8200	7.8200	7.8200
Averaged number of used subcarrier, $\lceil \frac{L \cdot R_{enc}}{M} \rceil$	1955	1955	1955
Approximately allocated bandwidth (MHz), $\lceil \frac{L \cdot R_{enc}}{M} \rceil \times \Delta f$	9.5	9.5	9.5
Transmission bit rate (Mbps), $R_b = \lceil \frac{L \cdot R_{enc}}{M} \rceil \times \frac{f_s \cdot M}{N_T + N_{CP}}$	8.98	8.98	8.98

Some system parameters of the proposed VTR-MB-OFDM system are listed in Table 5.2, where $x[0]$ means $S_2 = 0$ and $\hat{f}(\mathbf{a}^T, 0)$ are encoded, $y[0]$ means $S_1 = 0$ and $\hat{f}(0, \mathbf{b}^T)$ are encoded, $x[1]$ means $S_2 = 1$ and $\hat{f}(\mathbf{a}^T, \mathbf{b}^T)$ are encoded, and the system parameters of $x[1]$ are equal to the system parameters of $y[1]$. In Table 5.2, the encoding rates are greater than the entropies. It is important that the transmission of the proposed VTR-MB-OFDM system is also admissible. In addition, for both mapping functions, the number of used subcarriers, the occupied bandwidths, and the transmission rates are estimated using $L \cdot R_{enc}$ instead of X and Y, because the entire packet transmission is a stochastic process which means X and Y are not constants, and R_{enc} provides the averaged codeword length of possible output data samples. Furthermore, two important issues need to be addressed in Table 5.2. First, if the mapping function at both encoders is $\hat{f}_1(\cdot)$, the system parameters of $x[0]$ are equal to the system parameters of $y[0]$. This is because $\{a_i\}$ and $\{b_i\}$ have the same pdf. Second, the system parameters of $x[0]$, $y[0]$, and $x[1]$ are the same using the mapping function $\hat{f}_2(\cdot)$, because $\hat{f}_2(\cdot)$ maps the input pair $(a_i, S_2 \cdot b_i)$ or $(S_1 \cdot a_i, b_i)$ to a single value at both encoders. For the mapping function $\hat{f}_1(\cdot)$, 4 different switch configurations in $[S_1\ S_2]$ generate different transmission rates to transmit correlated sequences $\{a_i\}$ and $\{b_i\}$. Moreover, the rate factors of the proposed VTR-MB-OFDM system are approximately equal to 0.55, 0.6, 0.66, and 0.96.

The performance of the proposed VTR-MB-OFDM system over a noiseless channel is shown in Fig. 5.5. We evaluate the effects of 16 different switch configurations

$[S_1\ S_2\ S_3\ S_4]$ to the system performance using two different mapping functions, $\hat{f}_1(\cdot)$ and $\hat{f}_2(\cdot)$, at both encoders in Fig. 5.5(a) and Fig. 5.5(b). If the mapping function $\hat{f}_1(\cdot)$ is chosen, the SER reaches to 0.5 or 1 when

$$\begin{cases} [S_1\ S_2] \neq [0\ 0] \\ [S_3\ S_4] \neq [1\ 1] \\ [S_3\ S_4] \neq [S_1\ S_2]. \end{cases} \tag{5.49}$$

Moreover, if the mapping function $\hat{f}_2(\cdot)$ is chosen, the SER reaches to 0.5 or 1 when

$$[S_1\ S_2] = [1\ 1] \tag{5.50}$$

or

$$\begin{cases} [S_1\ S_2] \neq [0\ 0] \\ [S_3\ S_4] \neq [1\ 1] \\ [S_3\ S_4] \neq [S_1\ S_2]. \end{cases} \tag{5.51}$$

For $[S_1\ S_2] = [0\ 0]$, the input pairs are mapped independently; therefore, decoders can decode the estimated bit stream correctly with or without the side information. In the case of $[S_3\ S_4] \neq [S_1\ S_2]$ for both mapping functions, decoders decode the estimated bit stream in a way different from the way that encoders generate these encoded bit stream. In addition, for the mapping function $\hat{f}_2(\cdot)$, the reason why we have the highest SER when $[S_1\ S_2] = [1\ 1]$ is that the decoder can not map a single value back to the original input pair $\{\hat{a}_i, \hat{b}_i\}$ with or without the help of the side information.

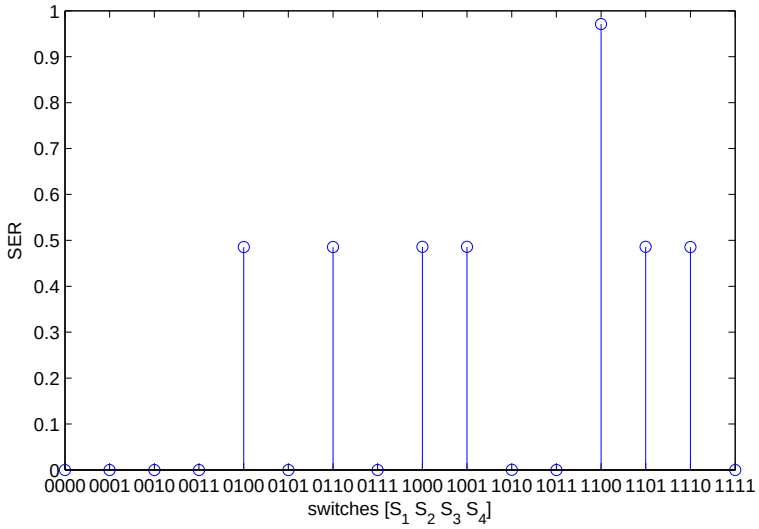

(a) $\hat{f}_1(\cdot)$

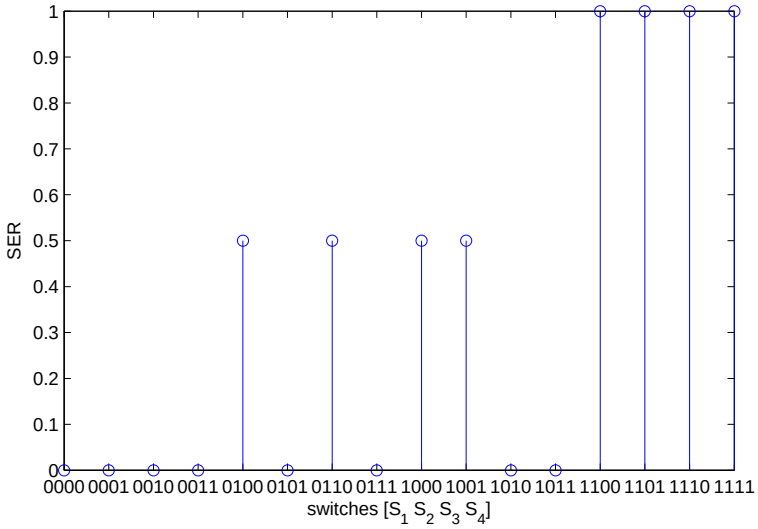

(b) $\hat{f}_2(\cdot)$

Figure 5.5: The performance of the proposed VTR-MB-OFDM system in a noiseless channel using two different mapping functions.

We demonstrate the performance of the proposed VTR-MB-OFDM system over an AWGN channel using two different mapping functions in Fig. 5.6 and Fig. 5.7. The system performance using the mapping function $\hat{f}_1(\cdot)$ is demonstrated in Fig. 5.6(a) to Fig. 5.6(d), and then the system performance using the mapping function $\hat{f}_2(\cdot)$ is also demonstrated in Fig. 5.7(a) to Fig. 5.7(d). From Fig. 5.6 and Fig. 5.7, the system performance over the noiseless channel is the same as the system performance over the noisy channel when SNR is greater than 19dB. Compared with a traditional uncoded OFDM system, the proposed VTR-MB-OFDM system has at least 1 to 4 dB gain in SNR to achieve the same SER. In addition, SER is less than 10^{-6} for some switch configurations when SNR is greater than 19dB.

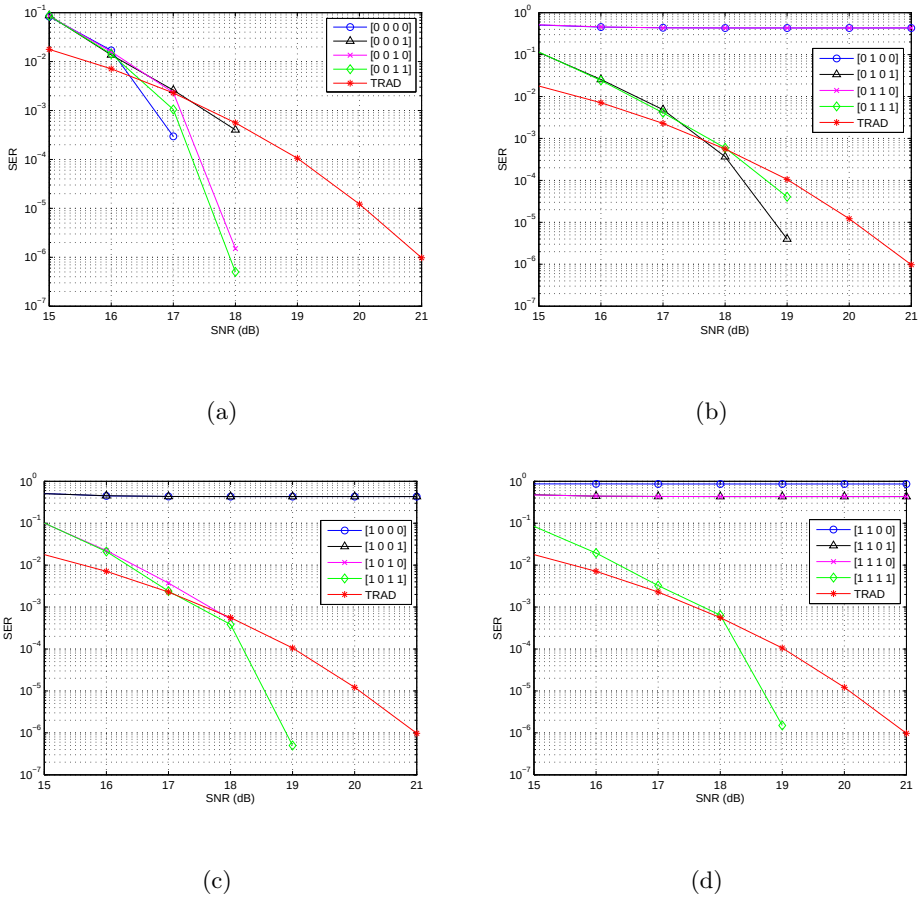

Figure 5.6: The performance of the proposed VTR-MB-OFDM system in an AWGN channel using the mapping function $\hat{f}_1(\cdot)$.

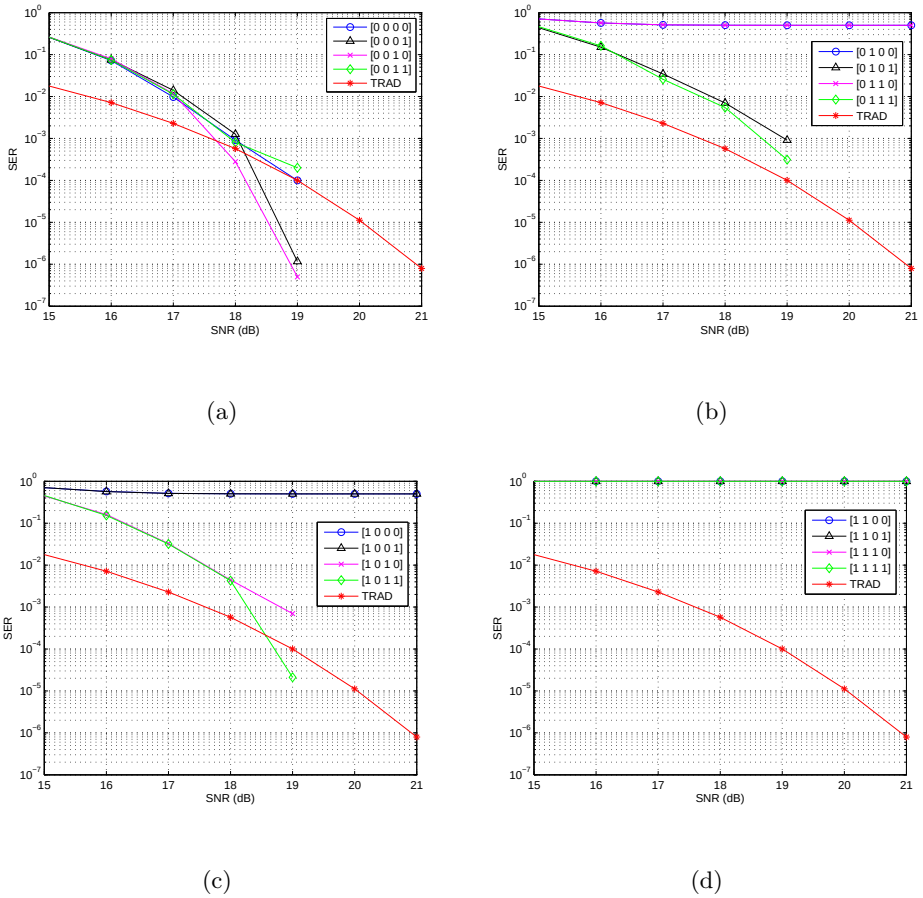

Figure 5.7: The performance of the proposed VTR-MB-OFDM system in an AWGN channel using the mapping function $\hat{f}_2(\cdot)$.

5.5 Summary

In this chapter, two VTR OFDM systems using network coding schemes are presented, and the performance characteristics of these two proposed systems are evaluated. Compared with a traditional uncoded OFDM system, the simulation results show that the proposed VTR-SISO-OFDM system has at least 1 to 3 dB gain in SNR to achieve the same SER, and the proposed VTR-MB-OFDM system has at least 1 to 4 dB gain in SNR to achieve the same SER. In addition, for some conditions, SER is less than 10^{-6} for both proposed systems when SNR is greater than 19dB. Moreover, the rate factors of these two proposed system vary from 0.55 to 0.96.

Chapter 6

Conclusion and Future work

6.1 Conclusion

In this thesis, two synchronization and channel estimation methods for single-input communication systems based on different training sequences are discussed. We have also developed a synchronization and channel estimation scheme for centralized multiple-input communication systems. In addition, two VTR OFDM-based communication system architectures are presented.

6.1.1 Semiblind Frequency-Domain Timing Synchronization and Channel Estimation

In chapter 2, we have proposed unit vectors in the high dimensional Cartesian coordinate system as the preamble, and then propose a semiblind frequency-domain timing

synchronization and channel estimation scheme for single-input OFDM systems. We have also developed a fine time adjustment algorithm to find the actual position of the first arrival path in different channel models and derived a scheme to choose the threshold. Based on a simple threshold without any pre-simulation and theoretical derivation, the proposed fine time adjustment algorithm outperforms conventional schemes even at very low SNR. Although the computational complexity in the proposed algorithm is higher than those in conventional methods, simulation results show that the proposed approach has excellent timing synchronization performance under several channel models at SNR smaller than 6dB. In addition, for an LDPC coded SISO OFDM system, our proposed approach has better BER performance than conventional approaches for SNR varying from 5dB to 8dB.

6.1.2 Optimized Joint Timing Synchronization and Channel Estimation

In chapter 3, a training-sequence-based joint timing synchronization and channel estimation for single-input communication systems is proposed. Based on the MMSE criterion, we also developed a fine time adjustment algorithm to find the actual position of the first arrival path in different channel models. Simulation results show that the proposed approach has excellent timing synchronization performance under several channel models at low SNR which is smaller than 1dB. Moreover, for an LDPC coded 1x2 SIMO OFDM system with MRC, a comparison BER of less than 10^{-5} can be

achieved using our proposed approach when SNR exceeds 1dB.

6.1.3 Optimized Joint Timing Synchronization and Channel Estimation with Multiple Transmit Antennas

A joint timing synchronization and channel estimation scheme for communication systems with multiple transmit antennas based on a well-designed training sequence arrangement is proposed in chapter 4. The proposed approach has excellent coarse timing and frequency synchronization performance at low SNR. In addition, a generalized M-L channel estimation scheme is presented. Based on the generalized ML estimation scheme, different CIRs from all transmit antennas can be obtained at each receive antenna. From the simulation results, the proposed approach has excellent timing synchronization performance under several channel models at SNR smaller than 1dB. In addition, the proposed approach has excellent channel estimation performance in 2×2 and 3×3 MIMO systems.

6.1.4 Variable Transmission Rate Communication Systems via Network Source Coding

In chapter 5, two VTR-OFDM systems that exploit network source coding schemes are presented, and the system performance characteristics of these two proposed VTR-OFDM systems are evaluated. For the proposed VTR-SISO-OFDM system, we employ the concept of a network with intermediate nodes to develop a 3-stage encoder/decoder,

and the proposed encoder provides three different coding rates from 0.5 to 0.8. The transmission rate is adjusted by selecting the bit stream from the output at different stages with different mapping functions in the encoder; however, how to choose an appropriate mapping function is important for the system performance. In addition, the cardinalities of the side information also affect the system performance. The larger the codebook size, the less gain in SNR to obtain better system performance. Therefore, a trade-off between higher transmission rate and better system performance is necessary. As for the proposed VTR-MB-OFDM system, correlated sources are simultaneously transmitted using different transmission rates. Different switch configurations provide us with various transmission rates and distinct system performance. Two sources are encoded by different coding rates from 0.25 to 0.5. Compared with a traditional uncoded OFDM system, the proposed VTR-OFDM systems have at least 1 to 4 dB gain in SNR to achieve the same SER in an AWGN channel.

6.2 Future Research Directions

Future research could be directed towards: (1) joint timing synchronization and channel estimation in distributed MIMO communication systems and (2) timing synchronization and channel estimation in amplify-and-forward relay networks.

6.2.1 Joint Timing Synchronization and Channel Estimation in Distributed MIMO Communication Systems

Due to hardware considerations or cost limitations, multiple antennas placed on a single device may be impractical for some wireless applications. Thus, in order to utilize spatial diversity, sparsely spaced single antenna devices can cooperate to construct a distributed MIMO systems as shown in Fig. 6.1. In Fig. 6.1, τ_{ij}, $\mathbf{h}_{ij}$, and v_{ij} represent timing offset from the ith transmit antenna to the jth receive antenna, CIR from the ith transmit antenna to the jth receive antenna, and CFO from the ith transmit antenna to the jth receive antenna, respectively. Since transmit antennas are sparsely distributed in space, different transmit-receive links have unequal timing offsets and CFOs because of diverse propagation delays and distinct carrier frequency oscillator pairs. This makes synchronization even more difficult in distributed MIMO systems than in centralized MIMO systems. In addition, accurate channel estimation algorithm is also needed in order to ensure better system performance. In distributed MIMO systems, most studies always perform timing synchronization and channel estimation in a separate way; however, errors in timing synchronization can affect the performance in channel estimation [85, 86, 87]. Special training sequence arrangements can be developed to solve the synchronization and channel estimation issues in distributed MIMO communication systems.

In this thesis, we have explored the timing synchronization and channel estimation for a centralized MIMO communication system in chapter 4. Therefore, we can further

investigate the problem in distributed MIMO communication systems.

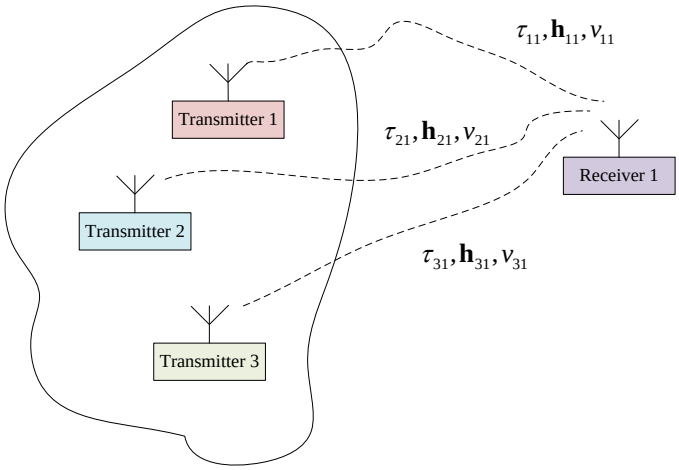

Figure 6.1: A typical distributed multiple-input single-output communication system model.

6.2.2 Timing Synchronization and Channel Estimation in Amplify-and-Forward Relay Networks

Cooperative communications is a new paradigm to make communicating nodes help each other, and cooperative communications can be generally categorized into amplify-and-forward (AF) relay and decode-and-forward (DF) relay [88]. For AF cooperative communication systems as shown in Fig. 6.2, most of the existing works assume perfect timing synchronization, and timing synchronization in AF cooperative communication

systems is much more complicated than that in DF cooperative communication systems. In Fig. 6.2, S, R, and D represent source, relay, and destination, respectively. Four parameters are shown in Fig. 6.2, where f_i means the channel from S to R_i, τ_i denotes the timing offset in f_i, g_i is the channel from R_i to D, and α_i represents the timing offset in g_i. Most studies utilized the iterative ML scheme to find $f = \{f_i,\ \forall i \in [1, K]\}$, $g = \{g_i,\ \forall i \in [1, K]\}$, and the fractional timing offset which is $res[\frac{\tau+\alpha}{T_s}] = \{res[\frac{\tau_i+\alpha_i}{T_s}],\ \forall i \in [1, K]\}$, where $res[\cdot]$ means the residual function and T_s is the symbol duration [89, 90]. In addition, superimposed training strategies for channel estimation that allow the destination node to obtain the f and g separately are proposed [91, 92, 93]. In the future, we can investigate this interesting problem and try to figure out a novel way to obtain f, g, τ, and α without using any iterative scheme.

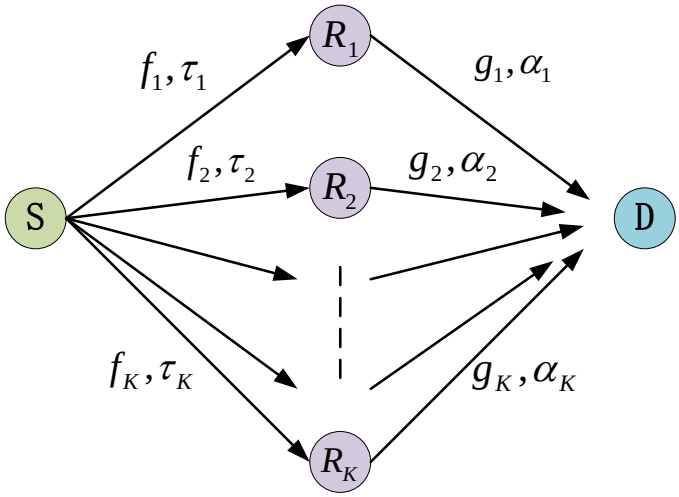

Figure 6.2: A typical amplify-and-forward relay network.

References

[1] Wikipedia, "5th generation mobile networks," accessed: 20 August 2013. [Online]. Available: http://en.wikipedia.org/wiki/5G

[2] J. G. Proakis, *Digital communications.* McGraw Hill, 2000.

[3] G. L. Stüber, *Principle of mobile communication.* Kluwer Academic Publishers, 2000.

[4] A. Goldsmith, *Wireless communications.* Cambridge University Press, 2005.

[5] T. M. Cover and J. A. Thomas, *Elements of information theory.* Wiley, 2006.

[6] K. Sayood, *Introduction to data compression.* Morgan Kaufmann, 2006.

[7] R. G. Gallager, *Low-density-parity-check codes.* M.I.T. Press, 1963.

[8] S. Lin and D. J. Costello, *Error Control Coding.* Prentice-Hall, Inc., 2004.

[9] W. Ryan and S. Lin, *Channel codes: classical and modern.* Cambridge University Press, 2009.

[10] J. I. Montojo and L. B. Milstein, "Channel estimation for non-ideal OFDM systems," *IEEE Transactions on Communications*, vol. 58, no. 1, pp. 146–156, 2010.

[11] U. Reimers, "Digital video broadcasting," *IEEE Communications Magazine*, vol. 36, pp. 104–110, 1998.

[12] Wikipedia, "Digital audio broadcasting," accessed: 20 August 2013. [Online]. Available: http://en.wikipedia.org/wiki/Digital_Audio_Broadcasting

[13] Wikipedia, "Asymmetric digital subscriber line," accessed: 20 August 2013. [Online]. Available: http://en.wikipedia.org/wiki/Asymmetric_digital_subscriber_line

[14] Wikipedia, "Very-high-bit-rate digital subscriber line," accessed: 20 August 2013. [Online]. Available: http://en.wikipedia.org/wiki/Very-high-bit-rate_digital_subscriber_line

[15] Wikipedia, "Wi-Fi," accessed: 20 August 2013. [Online]. Available: http://en.wikipedia.org/wiki/Wi-Fi

[16] Wikipedia, "Wireless local area network," accessed: 20 August 2013. [Online]. Available: http://en.wikipedia.org/wiki/Wireless_LAN

[17] Wikipedia, "WiMAX," accessed: 20 August 2013. [Online]. Available: http://en.wikipedia.org/wiki/WiMAX

[18] Wikipedia, "4th generation mobile networks," accessed: 20 August 2013. [Online]. Available: http://en.wikipedia.org/wiki/4G

[19] Wikipedia, "Orthogonal frequency-division multiplexing," accessed: 20 August 2013. [Online]. Available: http://en.wikipedia.org/wiki/Orthogonal_frequency-division_multiplexing

[20] H. Sari, G. Karam, and I. Jeanclaude, "Transmission techniques for digital terrestrial tv broadcasting," *IEEE Communications Magazine*, vol. 33, pp. 100–109, 1995.

[21] L. J. Cimini, J. C. Chuang, and N. R. Sollenberger, "Advanced internet services," *IEEE Communications Magazine*, vol. 36, pp. 150–159, 1998.

[22] R. van Nee and R. Prasad, *OFDM wireless multimedia communication.* Artech House, 2000.

[23] L. Hanzo, M. Münster, B. J. Choi, and T. Keller, *OFDM and* MC-CDMA *for broadband multi-user communications,* WLAN*s and broadcasting.* Wiley, 2003.

[24] Y. Li and G. L. Stüber, *Orthogonal frequency division multiplexing for wireless communications.* Springer, 2006.

[25] O.-S. Shin, A. M. Chan, H. T. Kung, and V. Tarokh, "Design of an ofdm coorperative space-time diversity system," *IEEE Transactions on Vehicular Technology*, vol. 56, no. 4, pp. 2003–2015, 2007.

[26] Y. S. Cho, J. Kim, W. Y. Yang, and C. G. Kang, *MIMO*-OFDM *wireless communications with* MATLAB. Wiley, 2010.

[27] *Multi-band OFDM Physical Layer Proposal for IEEE 802.15 Task Group 3a*, IEEE 802.15 Task Group, 2003.

[28] J. Balakrishnan, A. Batra, and A. Dabak, "A multi-band ofdm system for uwb communication," in *Proceedings of IEEE Conference Ultra Wideband System Technology*, 2003, pp. 354–358.

[29] M. Speth, S. A. Fechtel, G. Fock, and H. Meyr, "Optimum receiver design for wireless broad-band systems using OFDM – Part I," *IEEE Transactions on Communications*, vol. 47, no. 11, pp. 1668–1677, 1999.

[30] M. Speth, S. Fechtel, G. Fock, and H. Meyr, "Optimum receiver design for OFDM-based broadband transmission – Part II: A case study," *IEEE Transactions on Communications*, vol. 49, no. 4, pp. 571–578, 2001.

[31] S. Tung, "Multiterminal source coding," Ph.D. dissertation, Cornell University, 1978.

[32] Q. Zhao, "Network source coding: theory and code design for broadcast and multiple access network," Ph.D. dissertation, California Institute of Technology, 2003.

[33] C. Shannon, "A mathematical theory of communication," *Bell Systems Technical Journal*, vol. 27, pp. 379–423,623–656, 1948.

[34] D. Slepian and J. Wolf, "Noiseless coding of correlated information sources," *IEEE Transactions on Information Theory*, vol. IT-19, no. 4, pp. 471–480, 1973.

[35] H. Yamamoto, "Wyner-ziv theory for a general function of the correlated sources," *IEEE Transactions on Information Theory*, vol. IT-28, no. 5, pp. 1788–1791, 1982.

[36] R. Ahlswedw, N. Cai, S.-Y. Li, and R. Yeung, "Network information flow," *IEEE Transactions on Information Theory*, vol. IT-46, no. 4, pp. 1204–1216, 2000.

[37] A. Orlitsky and J. Roche, "Coding for computing," *IEEE Transactions on Information Theory*, vol. 47, no. 3, pp. 903–917, 2001.

[38] H. Feng, M. Effros, and S. Savari, "Functional source coding for networks with receiver side information," in *Proceedings of the Allerton Conference on Communication, Control, and Computing*, 2004, pp. 1419–1427.

[39] T. Ho, M. Médard, R. Koetter, D. Karger, M. Effros, J. Shi, and B. Leong, "A random linear network coding approach to multicast," *IEEE Transactions on Information Theory*, vol. 52, no. 10, pp. 4413–4430, 2006.

[40] M. Effros, "Network source coding: A perspective," *IEEE Information Theory Society Newsletter*, vol. 57, no. 4, pp. 15–23, 2007.

[41] R. W. Yeung, *Information theory and network coding.* Springer, 2008.

[42] T.-L. Kung and K. K. Parhi, "Frequency domain symbol synchronization for ofdm systems," in *Proceedings of IEEE Conference on Electro/Information Technology*, 2011, pp. 1–5.

[43] T.-L. Kung and K. K. Parhi, "Semiblind frequency-domain timing synchronization and channel estimation for OFDM systems," *EURASIP Journal on Advances in Signal Processing*, vol. 2013, no. 1, 2013.

[44] T.-L. Kung and K. K. Parhi, "Optimized joint timing synchronization and channel estimation for OFDM systems," *IEEE Wireless Communications Letters*, vol. 1, no. 3, pp. 149–152, 2012.

[45] T.-L. Kung and K. K. Parhi, "Optimized joint timing synchronization and channel estimation for communications systems with multiple transmit antennas," *EURASIP Journal on Advances in Signal Processing*, vol. 2013, no. 139, 2013.

[46] T.-L. Kung and K. K. Parhi, "Performance evaluation of variable transmission rate OFDM systems via network source coding," *EURASIP Journal on Advances in Signal Processing*, vol. 2013, no. 12, 2013.

[47] T. M. Schmidl and D. C. Cox, "Robust frequency and timing synchronization for OFDM," *IEEE Transactions on Communications*, vol. 45, no. 12, pp. 1613–1621, 1997.

[48] H. Minn, M. Zeng, and V. K. Bhargava, "On timing offset estimation for OFDM systems," *IEEE Communications Letters*, vol. 4, no. 7, pp. 242–244, 2000.

[49] H. Minn, V. K. Bhargava, and K. B. Letaief, "A robust timing and frequency synchronization for OFDM systems," *IEEE Transactions on Wireless Communications*, vol. 2, no. 4, pp. 822–839, 2003.

[50] H. Minn, V. K. Bhargava, and K. B. Letaief, "A combined timing and frequency synchronization and channel estimation for OFDM," *IEEE Transactions on Communications*, vol. 54, no. 3, pp. 416–422, 2006.

[51] "IEEE std 802.11: Wireless LAN Medium Access Control (MAC) and Physical Layer (PHY) specifications," IEEE 802.11 Task Group, 2007.

[52] C.-L. Wang and H.-C. Wang, "On joint fine time adjustment and channel estimation for OFDM systems," *IEEE Transactions on Wireless Communications*, vol. 8, no. 10, pp. 4940–4944, 2009.

[53] H. Abdzadeh-Ziabari and M. G. Shayesteh, "Robust timing and frequency synchronization for OFDM systems," *IEEE Transaction on Vehicular Technology*, vol. 60, no. 8, pp. 3646–3656, 2011.

[54] Y. Mostofi and D. C. Cox, "A robust timing synchronization design in OFDM systems-part II: high-mobility cases," *IEEE Transactions on Wireless Communications*, vol. 6, no. 12, pp. 4340–4348, 2007.

[55] J. J. van de Beek, M. Sandell, and P. O. Börjesson, "ML estimation of time and frequency offset in OFDM systems," *IEEE Transactions on Signal Processing*, vol. 45, no. 7, pp. 1800–1805, 1997.

[56] T. Lv, H. Li, and J. Chen, "Joint estimation of symbol timing and carrier frequency offset of OFDM signals over fast time-varying multipath channels," *IEEE Transactions on Signal Processing*, vol. 53, no. 12, pp. 4526–4535, 2005.

[57] R. Mo, Y. H. Chew, T. T. Tjhung, and C. C. Ko, "A joint blind timing and frequency offset estimator for OFDM systems over frequency selective fading channels," *IEEE Transactions on Wireless Communications*, vol. 5, no. 9, pp. 2604–2614, 2006.

[58] S. Ma, X. Pan, G.-H. Yang, and T.-S. Ng, "Blind symbol synchronization based on cyclic prefix for OFDM systems," *IEEE Transaction on Vehicular Technology*, vol. 58, no. 4, pp. 1746–1751, 2009.

[59] T. Fusco and M. Tanda, "Blind synchronization for OFDM systems in multipath channels," *IEEE Transactions on Wireless Communications*, vol. 8, no. 3, pp. 1340–1348, 2009.

[60] A. Charnes, E. L. Frome, and P. Y. Yu, "The equivalence of generalized least squares and maximum likelihood estimates in the exponential family," *Journal of the American Statistical Association*, vol. 71, no. 353, pp. 169–171, 1976.

[61] R. Neal, "http://www.cs.utoronto.ca/ radford/ftp/ldpc-2006-02-08/."

[62] Y.-C. Wu, K.-W. Yip, T.-S. Ng, and E. Serpedin, "Maximum-likelihood symbol synchronization for IEEE 802.11a WLANs in unknown frequency-selective fading channels," *IEEE Transactions on Wireless Communications*, vol. 4, no. 6, pp. 2751–2763, 2005.

[63] P.-Y. Tsai, H.-Y. Kang, and T.-D. Chiueh, "Joint weighted least-squares estimation of carrier-frequency offset and timing offset for OFDM systems over multipath fading channels," *IEEE Transactions on Vehicular Technology*, vol. 54, no. 1, pp. 211–223, 2005.

[64] M.-H. Cheng and C.-C. Chou, "Maximum-likelihood estimation of frequency and time offsets in OFDM systems with multiple sets of identical data," *IEEE Transactions on Signal Processing*, vol. 54, no. 7, pp. 2848–2852, 2006.

[65] H.-T. Hsieh and W.-R. Wu, "Maximum likelihood timing and carrier frequency offset estimation for OFDM systems with periodic preambles," *IEEE Transactions on Vehicular Technology*, vol. 58, no. 8, pp. 4224–4237, 2009.

[66] J.-W. Choi, J. Lee, Q. Zhao, and H.-L. Lou, "Joint ML estimation of frame timing and carrier frequency offset for OFDM systems employing time-domain repeated preamble," *IEEE Transactions on Wireless Communications*, vol. 9, no. 1, pp. 311–317, 2010.

[67] C.-L. Wang and H.-C. Wang, "A optimized joint timing synchronization and channel estimation scheme for OFDM systems," in *Proceedings of IEEE Vehicular Technology Conference*, 2008, pp. 908–912.

[68] C.-L. Wang and H.-C. Wang, "A low-complexity joint timing synchronization and channel estimation scheme for orthogonal frequency division multiplexing systems," in *Proceedings of IEEE International Conference on Communications*, 2006, pp. 5670–5675.

[69] E. G. Larsson, G. Liu, J. Li, and G. B. Giannakis, "Joint symbol timing and channel estimation for OFDM based WLANs," *IEEE Communications Letters*, vol. 5, no. 8, pp. 325–327, 2001.

[70] J.-H. Wen, G.-R. Lee, J.-W. Liu, and T.-L. Kung, "Joint frame synchronization and channel estimation scheme using regression method in OFDM systems," in *Proceedings of IEEE International Wireless Communications, Networking and Mobile Computing*, 2007, pp. 164–167.

[71] D.-C. Chang, "Effect and compensation of symbol timing offset in OFDM systems with channel interpolation," *IEEE Transactions on Broadcasting*, vol. 54, no. 4, pp. 761–770, 2008.

[72] G. G. Raleigh and J. M. Cioffi, "Spatio-temporal coding for wireless communications," *IEEE Transactions on Communications*, vol. 46, no. 3, pp. 357–366, 1998.

[73] A. L. Moustakas and S. H. Simon, "Optimized multiple-input single-output (MISO) communication systems with general Gaussian channels: nontrivial covariance and nonzero mean," *IEEE Transactions on Information Theory*, vol. 49, no. 10, pp. 2770–2780, 2003.

[74] G. L. Stüber, J. R. Barry, S. W. Mclaughlin, Y. Li, M. A. Ingram, and T. G. Pratt, "Broadband MIMO-OFDM wireless communications," *Proceedings of the IEEE*, vol. 92, no. 2, pp. 271–294, 2004.

[75] T. Pollet, M. van Bladel, and M. Moeneclaey, "BER sensitivity of OFDM systems to carrier frequency offset and Wiener phase noise," *IEEE Transactions on Communications*, vol. 43, pp. 191–193, 1995.

[76] A. N. Mody and G. L. Stüber, "Synchronization for MIMO OFDM systems," in *Proceedings of IEEE Global Communications Conference*, 2001, pp. 509–513.

[77] N. D. Long and H. Park, "Joint fine time synchronization and channel estimation for MIMO-OFDM WLAN," in *Proceedings of IEEE International Symposium Intelligent Signal Processing and Communications systems*, 2004, pp. 463–467.

[78] H.-C. Wang and C.-L. Wang, "A new joint time synchronization and channel estimation scheme for MIMO-OFDM systems," in *Proceedings of IEEE Global Communications Conference*, 2006, pp. 1–5.

[79] C.-L. Wang and H.-C. Wang, "Optimized joint fine timing synchronization and channel estimation for MIMO systems," *IEEE Transactions on Communications*, vol. 59, no. 4, pp. 1089–1098, 2011.

[80] P. Stoica and O. Besson, "Training sequence design for frequency offset and frequency-selective channel estimation," *IEEE Transactions on Communications*, vol. 51, no. 11, pp. 1910–1917, 2003.

[81] R. Zhang and L. Hanzo, "Multiple-source cooperation: From code-division multiplexing to variable-rate network coding," *IEEE Transactions on Vehicular Technology*, vol. 60, no. 3, pp. 1005–1015, 2011.

[82] A. Wyner and J. Ziv, "The rate-distortion function for source coding with side information at the decoder," *IEEE Transactions on Information Theory*, vol. IT-22, no. 1, pp. 1–10, 1976.

[83] T. Berger, *Multiterminal Source Coding.* Springer-verlag, 1978.

[84] J. C. Kieffer, "A method for proving multiterminal source coding theorems," *IEEE Transactions on Information Theory*, vol. IT-27, no. 5, pp. 565–570, 1981.

[85] F. Guo, D. Li, and L. Cai, "A novel timing synchronization method for distributed MIMO-OFDM system," in *Proceedings of IEEE Vehical Technology Conference*, 2006, pp. 1933–1936.

[86] Y. Cheng, Y. Jiang, and X.-H. You, "Preamble design and synchronization algorithm for cooperative relay systems," in *Proceedings of IEEE Vehical Technology Conference*, 2009, pp. 1–5.

[87] H.-C. Wang and C.-L. Wang, "A compact preamble design for synchronization in distributed MIMO-OFDM system," in *Proceedings of IEEE Vehical Technology Conference*, 2011, pp. 1–4.

[88] K. J. R. Liu, A. K. Sadek, W. Su, and A. Kwasinski, *Cooperative Communications and Networking*. Cambridge University Press, 2008.

[89] X. Li, C. Xing, Y.-C. Wu, and S. C. Chen, "Timing estimation and resynchronization for amplify-and-forward communication systems," *IEEE Transactions on Signal Processing*, vol. 58, no. 4, pp. 2218–2229, 2010.

[90] A. A. Nasir, H. Mehrpouyan, S. D. Blostein, S. Durrani, and R. A. Kennedy, "Timing and carrier synchronization with channel estimation in multi-relay cooperative networks," *IEEE Transactions on Signal Processing*, vol. 60, no. 2, pp. 793–811, 2012.

[91] F. Gao, B. Jiang, X. Gao, and X.-D. Zhang, "Superimposed training based channel estimation for OFDM modulated amplify-and-forward relay networks," *IEEE Transactions on Communications*, vol. 59, no. 7, pp. 2029–2039, 2011.

[92] S. Zhang, F. Gao, and C.-X. Pei, "Optimal training design for individual channel estimation in two-way relay networks," *IEEE Transactions on Signal Processing*, vol. 60, no. 9, pp. 4987–4991, 2012.

[93] S. Zhang, F. Gao, Y.-H. Yi, and C.-X. Pei, "Study of segment training based individual channel estimation for two-way relay network," *IEEE Communications Letters*, vol. 17, no. 2, pp. 401–404, 2013.